CHARACTERIZATION AND FUNCTIONAL STUDIES OF ELECTROSPUN/SPRAYED COMPLEXES LOADED WITH PHYTOCHEMICALS

by

ZHENYU LIN

A dissertation submitted to the

School of Graduate Studies

Rutgers, the State University of New Jersey

In partial fulfillment of the requirements

For the degree of

Doctor of Philosophy

Graduate Program in Food Science

Written under the direction of

Qingrong Huang

And approved by

_____

_____

_____

_____

New Brunswick, New Jersey

MAY 2018

ABSTRACT OF THE DISSERTATION

Characterization and Functional Studies of Electrospun/Sprayed Complexes Loaded with Phytochemicals

by ZHENYU LIN

Dissertation Director:

Qingrong Huang

At the era of high civilization, people are facing elevating amount of negative environmental impacts like polluted air or water, increased UV irradiation, carcinogens and many more. These impacts may lead to accumulation of oxidative stresses in our body which further trigger inflammations and even cancers. Fortunately, researchers found many bioactive phytochemicals could act against these oxidative stresses thus achieve multiple health benefits. However, many of them are not stable, prone to oxidation and heat during storage or productions. Besides, a large number of them have problems in water solubility and absorption. In order to overcome these barriers, various types of delivery systems are developed to encapsulate and protect the phytochemicals, to increase their solubility, bioaccessibility and bioavailability.

Nano emulsions may be the most popular delivery systems and are able to significantly increase the solubility of beneficial phytochemicals. Nevertheless, they also came with some disadvantages like emulsion breakage, low encapsulation efficiency, etc. Besides, production of nano emulsion also require large amount of

mechanical energy input like high pressure homogenization. Addition of preservatives to the nano emulsions also caused some health concerns.

In this research, a novel lipid delivery system called electrosprayed lipid-polymer complex (ELPC) was established. ELPC was fabricated by electrospinning technique for atomizing phytochemicals and other formulation components without high energy consumption or generating noticeable heat. Unlike most of the routine electrospinning process, ELPC was prepared without toxic organic solvents or components that was highly applicable in the real world. More importantly, ELPCs are able to generate self-assembled emulsions when they are in contact with water. Since the ELPCs could be stored in dry condition and able to generate emulsions at the moment of application, they are immune to environmental impacts like ambient temperature fluctuation, physical shocks or bacterial contamination that are fatal to routine emulsions.

ELPC was substantiated to achieve effective topical skin delivery of water-insoluble phytochemicals with the ability of anti-oxidation and tyrosinase inhibition, which was quantified by Franz-cell diffusion and visualized by confocal laser microscopy. The self-assembled nano emulsions generated from ELPCs have mean diameters around 300-400 nm by measured by dynamic light scattering. Cellular uptake of phytochemical loaded ELPC emulsion was proven effective against B16F10 melanoma cells. In addition, ELPC could also be adopted as an effective oral delivery system for phytochemicals. Digestion profile and characteristics of the edible ELPC was examined by USP-4 dissolution tester and an *in vitro* lipolysis assay, which had indicated successful digestion of the ELPC system and improved release of phytochemical comparing to the control. Afterwards, a Caco-2 monolayer membrane transport assay was carried out and proved effective transport of phytochemicals from the digested ELPC through the artificial intestinal monolayer to be able to enter the blood stream.

ACKNOWLEDGEMENT

I want to express my great appreciation to Dr. Qingrong Huang in Rutgers University Food Science department for his generous and non-stopping support during my five-year long research carrier. He provided me knowledges on food nanotechnology; inspired me on developing a new delivery system for bioactive phytochemicals and many other aspects. Thanks to Dr. Huang's great help, I had acquired the national scholarship support from China Scholarship Council. Dr. Huang was very nice and easy going, he gave me many suggestions on my research and carrier planning, and also enlightened my doctoral study life.

Secondly, I want to appreciate the great help from my lab mates. Without them my research could hardly be done smoothly. Here I want to specially thanks Dr. Jun Li from the Food Science department of South China Agricultural University. She had high enthusiasm in research and generously taught, helped many of my experiments like anti-oxidation assays, enzyme kinetics and conducting the research on visualizing skin delivery of phytochemicals. My view on the food and cosmetic science was largely broaden by her. Her energetic spirits also driven my research in a much faster pace. Besides, I also want to appreciate the generous help from Huijuan Zheng and Neil Wang in my MTT and XRD experiments, and thanks to other lab mates that gave me so much help.

Last but not least, I want to appreciate my dearest parents and relatives who provided me support on my life and study expenses. I want to thank Rutgers University to offer me an opportunity for promoting my life towards a doctoral degree and thank China's Scholarship Council for greatly supporting my doctoral studies.

TABLE OF CONTENTS

LIST OF TABLES

LIST OF ILLUSTRATIONS

Introduction

Bioactive phytochemicals have gained tremendous public attention because of their well-acknowledged health benefits like anti-inflammation, oxidative free radical scavenging, anti-cancer and more. Phytochemicals not only attract food supplement industry but also cosmetic field since they are potent in overcoming skin problems like UV-damage, freckles, acnes and other inflammatory symptoms related with oxidative stress. Interdisciplinary studies between food nutraceuticals and cosmetic science has attached great significance to the market.

Nevertheless, many of the phytochemicals are not readily applicable for the skin. It is because our protective barrier----stratum corneum (SC) blocks most of the phytochemicals from entering the epidermis. SC is a relatively thick, highly compact and layered matrix of lipids, proteins and water. Its characteristic "brick & concrete" structure blocks or retards the entry of many drug crystals and nutraceuticals. Facing the harsh situations inside SC, amphiphilic vehicles are desired for phytochemical delivery promotion. As a consequence, the real challenge on achieving the therapeutic effects of the phytochemicals is the proper design of delivery systems to overcome the SC barrier. Emulsions, organo-gels, solid lipid nano particles are typical examples of these vehicles. Here in this project, electrospun (E-spun) complexes were adopted as novel delivery systems for phytochemicals, which has the advantages like huge surface area and high affinity to the skin.

Based on these rationales, I hypothesize that the formulated E-spun complexes can facilitate phytochemicals to penetrate the SC barrier and reach the targeted cells or organs in the epidermis to achieve their bioactive functions.

`

To verify the hypothesis, four research objectives are listed below to characterize the general properties of the formulated E-spun complexes and more importantly, to examine their ability and mechanism of drug release and delivery *in vitro*.

1. Fabrication of formulated E-spun complexes loaded with phytochemicals

First of all, electrospun complexes are fabricated under a high voltage power supply, through which the solvents could be vaporized and finally leaving countless strands of solid nano scale polymer fibers. At the same time, the dissolved nutraceuticals and other functional components are entrapped in the nano fibers. Optimization of the e-spun conditions are performed. This include adjusting electric field strength and other physical parameters, formulating the polymer solution blend by determining the polymer concentration and solvent systems, tuning the quantity and type of surfactants, oil phase, etc.

2. Morphological observation and physical characterizations of the E-spun complexes

Morphological observation and other characterization measures are crucial for understanding the basics of E-spun fiber films. Morphological information is helpful to explain how the nutraceuticals are released from the polymer nano fibers and also how the E-spun fibers interacting with the skin. In addition, examining the molecular interactions between varied chemicals inside the E-spun film and acquiring crystalline information of the loaded nutraceutical are valuable to help understanding the detail mechanisms of nutraceutical delivery and interactions between the complex ingredients.

3. Examination of the delivery performance of the e-spun nano fiber films

Immersion dissolution and Franz-cell topical delivery assays are carried out to yield the delivery efficacy of the nutraceutical loaded E-spun complexes. Immersion dissolution directly yields the release characteristics of the E-spun films in aqueous

`

environment. Franz-cell experiments evaluate the nutraceutical delivery efficacy against mimic or pig skin, which are closely related to realistic conditions.

4. Functional studies of the E-spun complexes

To further acquire the nutraceutical delivery information of the formulated E-spun films and better sustain the hypothesis, cell studies are adopted in this research. Cellular uptake, MTT experiments are performed to investigate the drug transport from the formulation to the tissues. Confocal microscopy is adopted to visually prove the entry of nutraceuticals into the skin tissues and reach the target cells.

`

Chapter I: Characterization and Functional Studies of Quercetin-Loaded Electrospun Cellulose Acetate Fiber Mat with Varied Fiber Diameter Scales

1. Background

Herbal extracts like carotenoids, polyphenols, phytoestrogens, plant sterols are common seen phytochemicals on the current dietary supplement market. Many of them could achieve therapeutic effects, having certain physiological benefits or protection against diseases. They could potentially improve sub-healthy conditions, against aging and increase vitality. Study results demonstrated that nutraceuticals have promising effect against diabetes, arthrosclerosis, cardiovascular diseases, cancer, Alzheimer, inflammatory problems, etc.[1] Some other researchers focused on the use of phytochemicals to inhibit oxidative damages to the bioactive molecules in our skin tissues caused by UV irradiation and internal Reactive Oxidative Species (ROS).[2] ROS are able to attack biomacromolecules, expend the endogenous antioxidants inside our body, interrupt normal physiological processes and cause sub-healthy conditions. Nevertheless, phytochemicals especially antioxidants, are able to intervene and even block this harmful process by quenching oxidative radicals, restoring native bioactive macromolecules and having other beneficial physiological actions.[3]

For example, carotenoids as nutraceuticals contribute a part of golden yellow tone to our skin with some photo-protection effect against UV damage. Lycopene, one of the carotenoids, is able to significantly reduce erythema triggered by ultraviolet light, which further against skin aging.[4] In addition, carotenoids had demonstrated ability to inhibit certain types of cancer, which was supported by many experimental evidences. The International Cancer Research Data Bank had investigated about 324 cancer research papers related to carotenoids and several relevant papers in the 1979 issue of

`

Federation Proceedings together demonstrated that various carotenoids can reversibly suppress or postpone the malignant behavior of transformed cells; regress human skin keratosis processes; delay the appearance of transplanted tumors, etc.[5]

For another example, green tea polyphenols are broadly acknowledged phytochemicals potent of achieving anti-oxidative health benefits. The catechin families are well-known effective quenchers against a series of potent oxidative free radicals.[6] Green tea polyphenols might have encouraging potential against various types of cancers. Researchers had investigated biomarkers of DNA oxidative damages in animal models consuming green tea components. It was reported that green tea administration to lab mice displayed inhibition effect of lung adenomas that suppressed the increase of 8-OH-dGuo levels (the most frequently used biomarker for DNA oxidation damage evaluation) in mouse lung DNA.[7] Tea polyphenols were also reported to quench xanthine oxidase-generated oxidative free radicals in human cell studies[8] and against inflammation related oxidases in human colon cells.[9] Tea polyphenols act against the activation of NF-kB and AP-1 which was found to be extensively related to inflammatory diseases and cancer progression.[10] Other evidences also demonstrated green tea's preventive effect against multiple types of cancers.[11-12]

Besides cancer prevention and inhibition, green tea components were also found to be potent against varied types of chronic diseases. Their anti-inflammatory properties contributed in acting against anti-cardiovascular diseases.[13-14] Suggested by animal studies, green tea polyphenols may benefit in regulating or restoring normal blood pressure and glucose, maintaining coronary and heart health.[15] In addition, they are also reported to have therapeutic effects like potential cholesterol-lowering effects,[16] protection against degenerative diseases,[11] anti-arthritic,[17] synergism with antibiotics,[18]

`

anti-angiogenic,[19] anti-viral,[20] anti-fungal,[21] neuroprotective effects against Alzheimer's, Parkinson's diseases[22] , memory regression,[23] and more.

Tea polyphenols also has shown remarkable preventive effects against some skin photo-damage conditions like photo-carcinogenesis and photo-toxicity.[24] EGCG demonstrated potent protective effect against UV damages. It was reported that EGCG significantly reduced dermal lipid peroxidation to nearly three folds in animal models and skin cell cultures after 18 hours of UV irradiation treatment. It was also reported to act against excessive expression of inflammation related collagen secretion mRNA triggered by UV irradiation in cell culture experiments.[25]

Quercetin (3, 3, 4′, 5, 7-pentahydroxyflavone) is a highly representative flavonoid compound. It was ubiquitously found in fruits and vegetables, especially onion and the peel of apple.[26] Quercetin possesses multiple benefits like against oxidative free radicals,[27] metal-chelating,[28] against coronary heart disease,[29] anti-viral, [30]anti-proliferation and cancer,[31] etc. It is potent against inflammatory signaling pathways and related enzymes. Studies have shown quercetin was capable of depressing the cyclooxygenase and lipoxygenase pathways which are critical for inflammatory activities.[32] Besides, quercetin was demonstrated to inhibit activation of NF-κB pathway which controls many genes involved in inflammation.[33] It was effective against carrageenan triggered inflammation model in rats.[34]

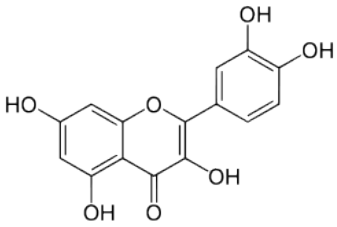

Quercetin chemical structure

Quercetin in Electrospun fiber mat

Figure 1. Quercetin

`

Moreover, topically applied quercetin was reported to be potentially effective against skin problems caused by direct UV irradiation or related inflammation. Quercetin suppressed inflammatory signaling substance production in skin cell studies against UV exposure.[35] It is promising against oxidative damages under UV to cell membrane lipids that may lead to skin cancers and acceleration of skin aging.[36-37] The naturally-originated property and multiple beneficial aspects of quercetin make it highly suitable for skin applications against inflammatory skin symptoms, such as reddish, acnes and others. A major cause of these symptoms is sebaceous gland malfunctioning. When sebaceous gland has inflammation or under oxidative stress triggered by environmental factors (UV-B, humidity, temperature fluctuation, oxidation, bacterial infection, etc.), it would secret over dose of skin lipid and inflammatory substances that cause swelling and inflammation sebaceous glands. Skin quality change, Acnes and even hair loss can happen due to this type of sebaceous glands malfunctioning.

Nevertheless, the topical protective benefits of quercetin were rather difficult to achieve due to its poor water/oil solubility and large particle sizes. Quercetin was reported to have a water solubility of 3.60μg/mL[38] and a low octanol-water partition coefficient.[39] The low lipophilicity and poor water solubility properties of quercetin greatly decrease the compatibility between quercetin and epidermal tissue and retard its topical delivery performance. Consequently, quercetin was hampered from reaching the UV damaged or inflammatory sites in the epidermis area to achieve functional effects.[40-41]

Besides the nature of quercetin that raised difficulties in topical delivery, the barrier protective effect of our skin further reduced the rate of drug transport. Skin is the largest organ in our body with huge surface area. The skin envelops our entire body and it is one of the key aspects in identifying individual human beings. Skin protects the body

`

from injury and is largely responsible for limiting body fluid from escaping and external fluids from penetrating. At the same time, skin is able to communicate, respond and adapt to the outside environment.[42] Besides, our skin is important in acting against bacterial infection, UV irradiation and foreign substances. It also functions in regulating body temperature, removing our body waste, secreting substances that attract or repel others, etc.

Our skin appeared as a layered structure matter. Generally, the skin is constituted by epidermis and dermis. A layer rich in fat tissue below the dermis is called the subcutaneous layer. The most outside rough layer of our skin is called stratum corneum (SC), which was made of multi-layered "dead skin" material----an extensive matrix of keratin protein. In between this material, there are various types of dermal lipids that further protects our skin from water loss. The distribution and inter-relation between these lipids and keratin are like "mortar" and "brick" in a wall. This model is well accepted to represent the internal environment of SC. In detail, the mortar stands for intercellular spaces filled with lipids while the bricks stand for the relatively hydrophilic corneocytes.[43-44]

The SC has excellent barrier properties against invasion of topical substances and also loss of internal water and body heat. As a result, the available topical delivery routes are rather limited. There are generally three routes considered for topical delivery: intercellular route through the lipids; skin appendages; intracellularly.[43] The efficiency of the pathway utilizing skin appendages is rather low. The intracellular route is the most direct one however topical drugs need to penetrate right through the thick and dense keratin structures and also some intercellular lipids, which actually poses the highest difficulty for topical drug delivery although it looks like the shortest way. As a result, the intercellular pathway utilizing the skin lipids is the most common one for

`

topical drug delivery.[45] The SC blocks most of the substances that was applied above it, which significantly increased the difficulty in topical application formulation designs.

The epidermis also contains melanocytes, which contribute to the various skin tone of human being because of a polymeric compound melanin produced by them. Melanin is a dark brown to black color compound and is effective against UV irradiations that protect our skin cells from sun burn or cancer. However, melanin is also a largescale polymer that decomposes or metabolize in a fairly slow pattern. If overproduction of melanin occurred, it was also challenging to reduce or remove it, like the pigmented spots on our skin.

Right underneath the epidermis there lays the dermis. It is a rather hydrophilic environment of fibrous and elastic tissue rich in elastic proteins that support our skin structure and make it highly flexible. The dermis area has massive amount of blood vessels where absorption of drug could take place. The dermis interacts and responds to the environment in various ways such as contraction of hair follicles when chilled or scared and adjustment of blood vessels flows for body temperature maintenance. Sweat glands and sebaceous glands are the two major glands in the dermis. Sweat glands produce sweat to transfer water, salts, and other compounds out of the body. They are also important in cooling down our body especially during sports or staying in high temperature environment. Sebaceous glands generate a series of lipids (sebum) which helps us against water loss, environmental impacts, etc.[46]

According to the complex structure and barrier properties of epidermis, there are several parameters that are utilized to represent the possible aspects related to the drug permeation. Fick's law could be used to describe passive diffusion process of topical drug delivery. Permeability coefficient K_p is a combined factor that describes both drug and barrier properties, which could be further developed as the following. As long as

`

the major delivery pathway property (the intercellular lipids) is a relatively stable concept, the factors we actually concern with significance to the topical delivery is the drug loading concentration (C_v) and the vehicle or formulation properties (K_m)

$$J = K_p C_v$$

$$J = \left(\frac{DK_m}{L} \right) C_v$$

Fick's law

By understanding the basics of Fick's law of diffusion, topical delivery enhancement strategies are made to optimize the factor C_v and K_m. The very first factor to concern should be the soluble drug concentration, which is the driving force for the topical drug delivery. However, we should notice the C_v refers to effective drug content that is soluble on the way to the deeper skin. Excessive chunks of drug particles or those drugs not successfully loaded in the vehicle generally do not help to push the topical delivery and also wasted the drug chemicals. In addition, constructions of the vehicle and optimized formulations have significant impact on the partition coefficient factor Km and could markedly enhance topical delivery performance of the drug.[47]

Various strategies to enhance transdermal drug delivery were studied to enhance the factor C_v (concentration variation), K_m (partition coefficient) concluded from the Fick's law. Changing the skin barrier property is one of the most common strategies, which reversibly modify the intercellular lipid arrangements to influence the partition coefficient. Hydration is the safest way for increasing permeation. Hydration alters the solubility of the drug and also making the SC less compact and creating hydrophilic gaps to enhance topical delivery. Another frequently applied method to modify intercellular lipid barrier is chemical penetration enhancers that disordering or partially fluidizing the intercellular lipids in the SC. Amphiphilic compounds like various

`

surfactants, general organic solvents like Dimethyl Sulfoxide (DMSO) and alcohols, also some aliphatic hydrocarbons are able to locally dissolve some dermal lipids, creating tiny porous zones that increase the total surface area for drug contact. Some of them can interact or dissolve some keratins to enhance skin permeability. Another important strategy that affects both C_v and K_m is modifying the drug properties directly or formulating the drugs into proper vehicle systems. Prodrugs as derivatives of the drug modified with better solubility and intercellular lipid compatibility in the SC may help to increase the partition coefficients. Complexation into polymers and encapsulation into nano-scale lipid-based vehicles may also be effective strategies to cover the solubility/lipid compatibility weakness of the drug. The nano-encapsulating vehicles together with the drug are designed to better pass through internal barrier gaps and reach deeper area of the skin to release the drug to take effect. [45]

Aging of skin is a concept known to almost everyone, which stands for loss of the appealing appearance, texture and functions of the skin tissues over time. Nevertheless, photoaging is not so familiar to the people as the general aging of skin. Most of them regard skin aging as totally intrinsic, but the fact is that extrinsic factors like daily UV irradiation also “contribute” plenty to the skin aging. Formation of wrinkles, smoothness or texture changes, disorder of skin tones are possible outcomes of photoaging, which could happen even during early stage of life.

UV irradiation from the sunlight is able to directly damage our skin. 95% of the sunlight UV is UV-A with the wavelength ranging from 315-400nm. The high abundance and energy of UV-A allow it to penetrate deeper of the skin into the dermis, which contribute more to the alterations in the cellular component and damaging the collagen, elastin and fibrillin proteins in the deep dermis. Loss or dysfunction of these important structural proteins of the dermal connective tissue would cause deforming or

`

collapsing of the skin, which appear as wrinkles and loss of smoothness of the skin. Therefore, wrinkle formation and skin aging was actually not necessarily related to the age of people. For the UV-B with the wavelength of 280-315nm, though it has much weaker energy, it is actually more dangerous than UV-A since it is rather reactive with DNA that is genotoxic and carcinogenic. It reaches the epidermis of your skin causing skin reddening, sunburn and possibly skin cancer.[48-49]

Besides direct UV irradiation, the UV-generated reactive oxygen species (ROS) can also deplete our intrinsic antioxidant like glutathione and SOD as defense systems of the skin. ROS can be activated by UV or generated intrinsically and damage skin biomolecules to cause DNA cleavage, dermal lipid oxidation, dermal protein denaturation.[50] Inflammatory pathway activation, induction of matrix metalloproteinases as well as mutations of mitochondrial DNA caused by UV induced ROS have been identified, which displayed the high inflammatory potential of UV-generated ROS.[51]

Nanoscale delivery systems are attractive for dermal applications due to their small particle sizes and large surface area for optimal skin penetration and protection of active ingredients. They may pass through the tiny pores and gaps in the epidermal intercellular lipid route and also accumulate in cutaneous appendices. Based on these advantages, nano delivery systems of varied types have been extensively studied.[45]

Loading of drugs into vesicles in nanometer size range is an acknowledged technique for the optimizing drug stability, enhancing absorption performance and intracellular drug transfer.[52] The most common atomization technique is nano emulsion. Nano emulsions are homogeneous matrix of droplets of a certain type of polarity dispersing in a continuous substance phase with an adverse type of polarity, which is in a thermodynamically equilibrium state. The most common case of nano emulsion is

`

ultrafine lipid droplets dispersing in continuous water phase. Their droplet sizes are small and suitable for design of topical delivery systems to overcome the barriers in the skin delivery route.[53] At the same time, lecithin added in most of the emulsions is a permeation enhancer for many topical drugs.[54]

Comparing to nano emulsions, electrospun delivery system is a relatively novel approach for topical delivery enhancement. Electrospinning is a powerful and efficient technique for producing up to nano-scale fine substances. It is versatile in encapsulating multiple types of phytochemicals with highly tunable fiber properties like alignment, fiber diameters and more that are related with drug delivery properties. Electrospinning utilize high voltage electrostatic force to charge and accelerate the polymer molecules in the solution towards a grounded metal collector. The solvents are evaporated under electric field and the solute polymer is stretched into ultra-fine fibers under the electrostatic repulsion force against the surface tension of the solvent.[55] Once the diameters of polymer fibers hit microns or even nanometer scale, they will achieve some attractive functional characteristics like huge surface area to volume ratio, largely increased affinity to skin surface which provides much more effective topical drug delivery zone.

E-spun nano films are composed of countless amount of super fine fibers, scale from microns to hundreds of nanometers. As a result, the E-spun films has huge amount of surface area available for dermal drug delivery, though it appears similar to a piece of fabric cloth. The superfine fibers have great affinity to the skin through static force, which not only in touch with your skin surface but also in close contact with the numerous furrows on the skin, which further increase the sites for drug delivery. Besides, during the delivery process, the film fibers are in contact with water and a great number of nano-sized pores will be generated on the fibers that also increase drug

`

release rate. In addition, nutraceuticals loaded in the fiber mat are not in a crystal form but amorphous form, which further assist the delivery of nutraceuticals.

Electrospun cellulose acetate (CA) fiber mat is a potential vehicle (facial mask type) to assist topical delivery. It offers large surface contacting area against human skin, which increases effective drug-delivery zone. Moreover, swelling and porous characteristics of E-spun CA fibers can facilitate drug delivery. In this study, e-spun CA fiber mats were fabricated by applying a strong electric field to the acetic acid solution of CA loaded in a needle. Solvent pumped out of the needle was squeezed and evaporated under the strong electric field, leaving solid CA polymer fibers to be collected on the cathode.

The electrospun fiber films are fortified with varied penetration enhancers to promote skin absorption of phytochemicals. The penetration enhancers are usually compounds that temporarily altered the skin lipid compositions or local structures for increasing the passage of certain types of drugs.[43] Here, Tween 80 and lecithin as chemical penetration enhancers were incorporated in the formulation for phytochemical delivery.

`

2. Experimental

2.1 Materials

Cellulose acetate (average Mn ~30,000 Da, 39.8 wt. % acetyl content) and Tween® 80 was purchased from Sigma Aldrich (MO, USA). Quercetin dihydrate (90%) was purchased from VWR Scientific (Seattle, WA, USA). Glacial acetic acid was purchased from Amresco (OHIO, USA). Strat-M® Membrane for transdermal diffusion testing was purchased from EMD Millipore (MA, USA)

2.2 Fabrication of quercetin-loaded electrospun CA fiber films loaded with varied diameters

In this research, quercetin loaded electrospun CA films were prepared in two different formulations in order to achieve variations in fiber diameters. CA and quercetin were dissolved in pure glacial acetic acid or 85% acetic acid aqueous solution in order to achieve different diameter scales. CA concentration was fixed at 20% while the mass ratio of quercetin over CA was 1%, 5% and 8%. All the polymer solutions contain 6% Tween 80 to assist dissolution. A blank CA acetic acid solution without quercetin was also prepared as a control for later experiments. Polymer solutions were filled into syringes, being loaded on a syringe pump and then electrospun under an electric field of 15 kV/10 cm at room temperature 20°C. Fiber mats were collected for two hours with feeding rate at 0.8mL per hour controlled by a syringe pump.

2.3 Characterization of quercetin-loaded CA electrospun films

Morphology of quercetin-loaded CA electrospun films was yield by Scanning Electron Microscope (SEM) while a Cryo-SEM system was also utilized to examine

`

the porous surface morphology of CA fiber films while immersing in buffered dissolution medium to assist in demonstrating the release mechanism of quercetin. X-Ray Diffraction (XRD) was adapted to examine quercetin crystalline status and while Fourier transform infrared spectroscopy (FTIR) examined molecular interaction within the quercetin-CA fiber mats.

2.4 Release profile of quercetin-loaded CA electrospun fiber films

2.4.1 Preparation of buffered mediums for dissolution assay

Buffered mediums were prepared to mimic the human skin conditions. Phosphate buffered saline (PBS) 1X was chosen with the pH adjusted to pH 5.5 to represent the typical human skin surface conditions for the general immersion release assay (medium A). Another release medium was also prepared with PBS 1X and 1% Tween 80 while the pH was adjusted to 7.4 to mimic the human dermis environment for the Franz-cell transdermal diffusion assay (medium B).

2.4.2 Release profile and topical delivery of quercetin in vitro

General release of the CA electrospun films loaded with quercetin were evaluated by an immersion dissolution experiment while the topical delivery profiles of the films were tested against Strat-M® membranes that mimicked and predicted human skin diffusion characteristics. For the general immersion dissolution, a small piece of the electrospun film (300mg) was casted into 10mL of medium A. Dissolution process was carried out for one hour with seven time intervals (0, 3, 6, 10, 20, 40, 60 minutes). At each interval, 0.3mL dissolution media was withdrawn and filtered through 0.2μm

`

nylon filters then assayed by HPLC with the detection wavelength at 370nm. 0.3mL medium A was recovered to dissolution media immediately after each sampling. Immersion dissolution experiments were carried out in triplicates.

In vitro topical release profiles of quercetin loaded CA electrospun films were carried out with Franz diffusion cells vertical type(PermeGear, Inc., Hellertown, PA, USA) with 0.81 cm^2 skin contact area and a 5mL receptor. The receptors of the Franz-cells were filled with medium B to mimic human dermis conditions at 37 ± 0.1 ◦C with 600 rpm agitation. Strat-M® membranes were then mounted on the receptors to represent human skin epidermis. After that, 20mg of the quercetin loaded CA electrospun films was put into each donor cell and the films were wet by 0.1mL deionized-water. The donor cells were sealed with Parafilm® to prevent the films from drying. Franz-cell diffusion process was carried out for four hours with three time intervals (1, 2, 4 hours). The topically delivered quercetin in the Strat-M® membranes was shred into small pieces and extracted by 10mL of methanol for thirty minutes. 1mL of the extracted solution was fed to the HPLC to assay quercetin content at the detection wavelength of 370nm. The quercetin concentration results were then back calculated to yield the amount of topically delivered quercetin from the electrospun CA films at different time points. All the Franz-cell assays for the electrospun films are carried in triplicate.

2.5 Statistical analysis

All the quercetin content and *in vitro* release profile data presented were carried out in duplicates or triplicates. Microsoft® Excel 2007 and Origin 2016® assisted the calculation and analysis of mean values and standard deviations. Statistical variation significance was based on confidence level lower than 0.05 calculated with SPSS 22.0.

`

3. Results and discussions

3.1 Morphology of quercetin loaded electrospun CA films fabricated in varied scales

General appearances of the quercetin loaded electrospun CA films in varied scales are shown in Fig 15. Under the same lighting and camera conditions, the electrospun film made with 85% acetic acid (nano scale fiber) appears glossier. This feature might be related to the more organized intermolecular arrangements or higher degree of crystallinity in the electrospun film made with glacial acetic acid (micron scale fiber) that will be discussed later in the article.

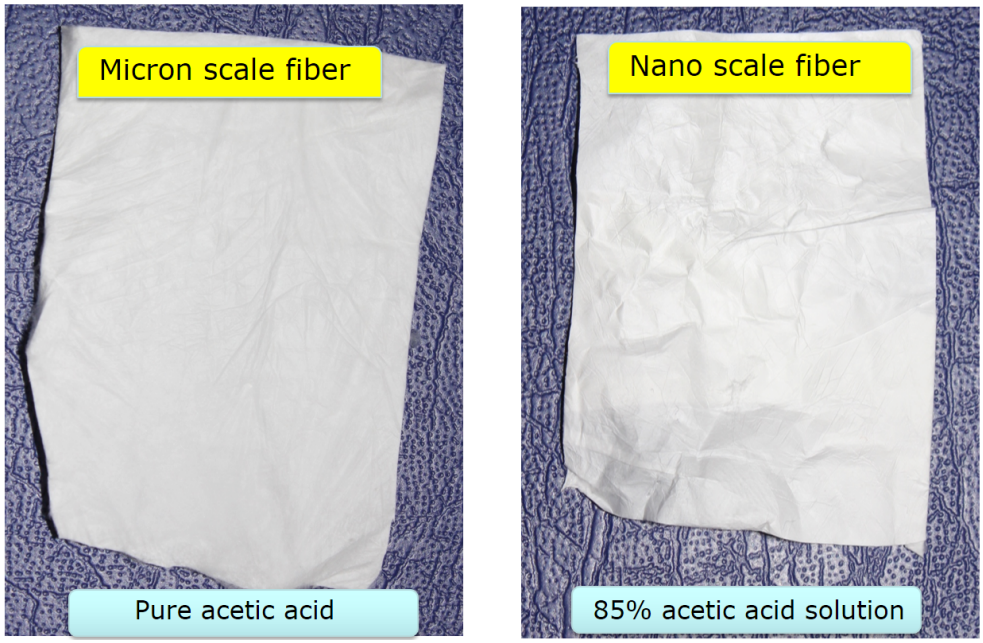

Figure 2. Overall appearances of quercetin loaded CA electrospun films in varied scales

`

3.2 SEM examination

SEM images of the electrospun CA films loaded with 5% quercetin prepared with varied formulations are shown below. Large variation of fiber diameter was observed. Fiber diameter was significantly reduced in films prepared with 85% acetic acid solution. This variation in diameter scales was considered mostly related to the change in the conductivities between pure glacial acetic acid and acetic acid aqueous solution. Increase in acetic acid concentration would result in harder dissociation of acetic acid that lowers the charge densities----the driving force of electrospun fiber formation. The less charge densities there are, the less the polymer would be "squeezed" so that the fiber diameter will increase dramatically.[56]

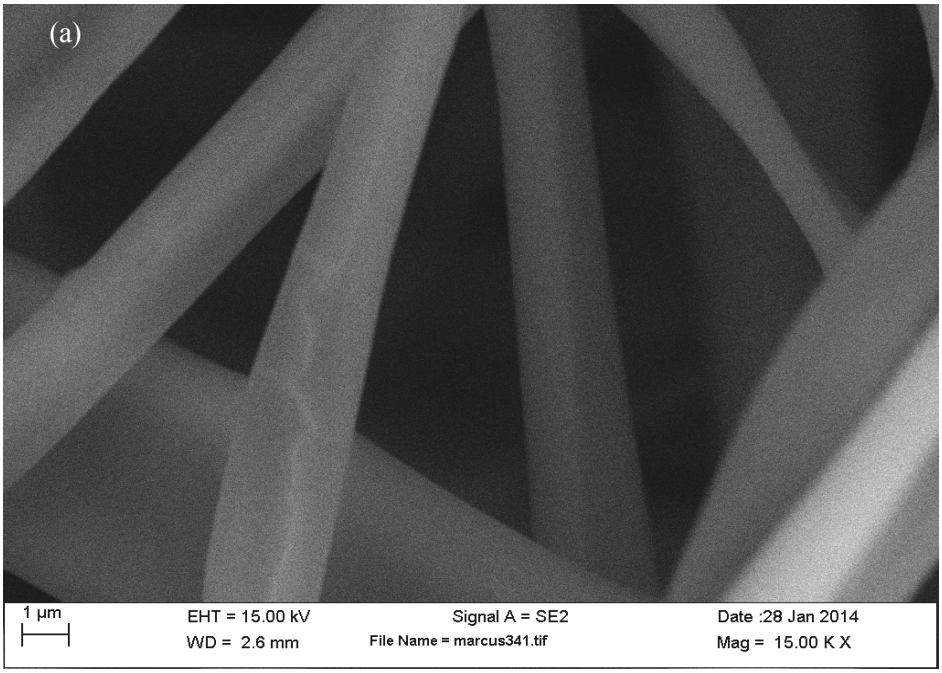

`

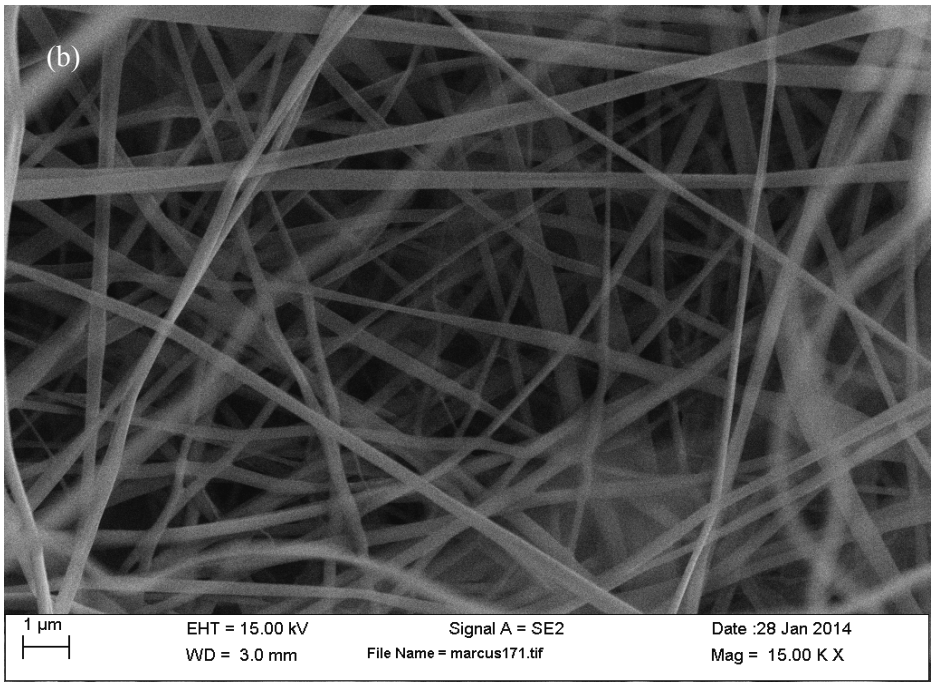

Figure 3. SEM images of electrospun film with glacial acetic acid(a) and 85% acetic acid (b)

3.3 Diameter distribution

Film Fiber diameter distribution data corresponded to micron and nano scale fibers are shown in figure. 4. Average fiber diameter of micron scale fibers was demonstrated to be nearly ten folds of the size of nano scale fibers, which quantitatively supported the theory that acetic acid concentration (charge density) in the formulation had a strong positive correlation with electrospun film fiber diameters.

`

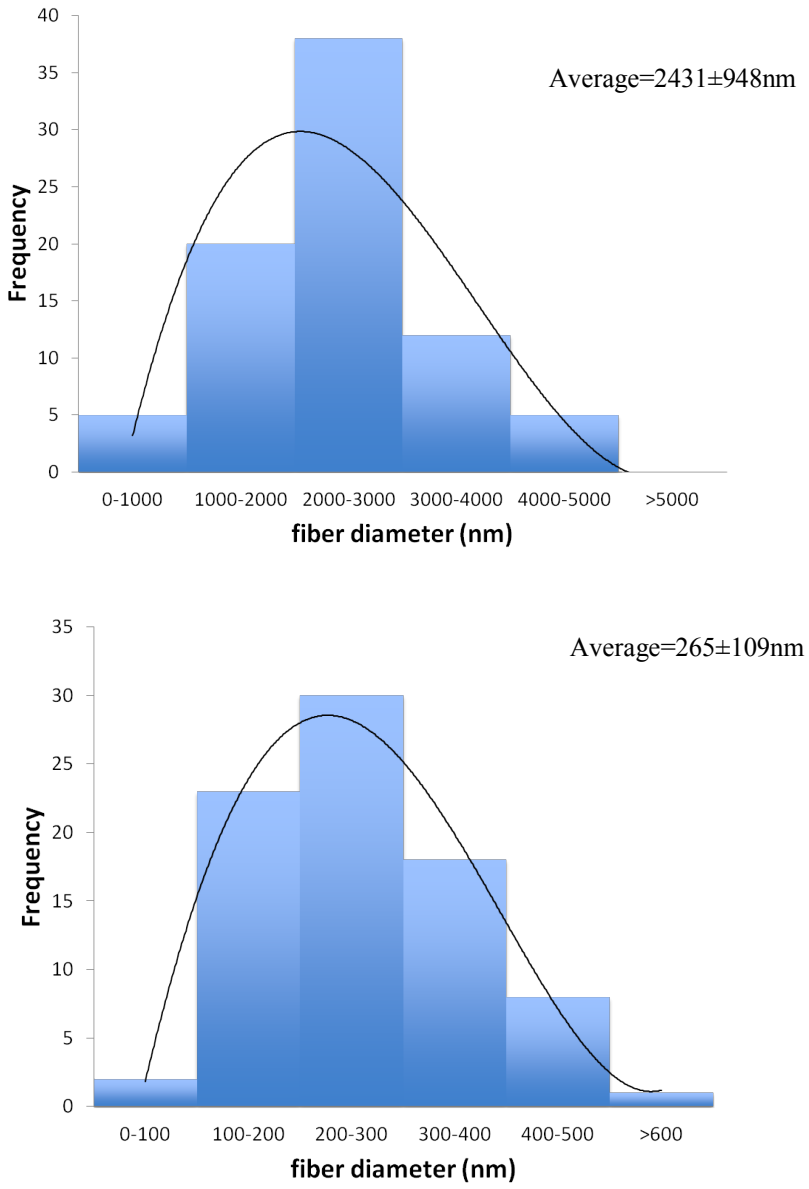

Figure 4. Diameter distribution of electrospun films

3.4 Cryo- SEM examination

Cryo-SEM images of the electrospun films in both scales are displayed below. Cryo-SEM is the electron microscope where the sample is studied in vacuum and cryogenic temperatures conditions that offer a frozen appearance of the water-containing samples. Here in the images, electrospun films are preserved in the state during dissolution. Porous surface structure formation of electrospun CA fibers was believed for the first

`

time to be discovered. These nano-scale pores were not observed in regular SEM images, which confirmed they were appeared during dissolution process while the swelling of electrospun fibers occurred. It was majorly believed that swelling effect of CA electrospun fibers contribute the most to the elevation of total surface area and enhancement of topical drug delivery. Nevertheless, this discovery reminds us that the formation of nano-scale pores also plays an important role in drug release from electrospun CA fibers.

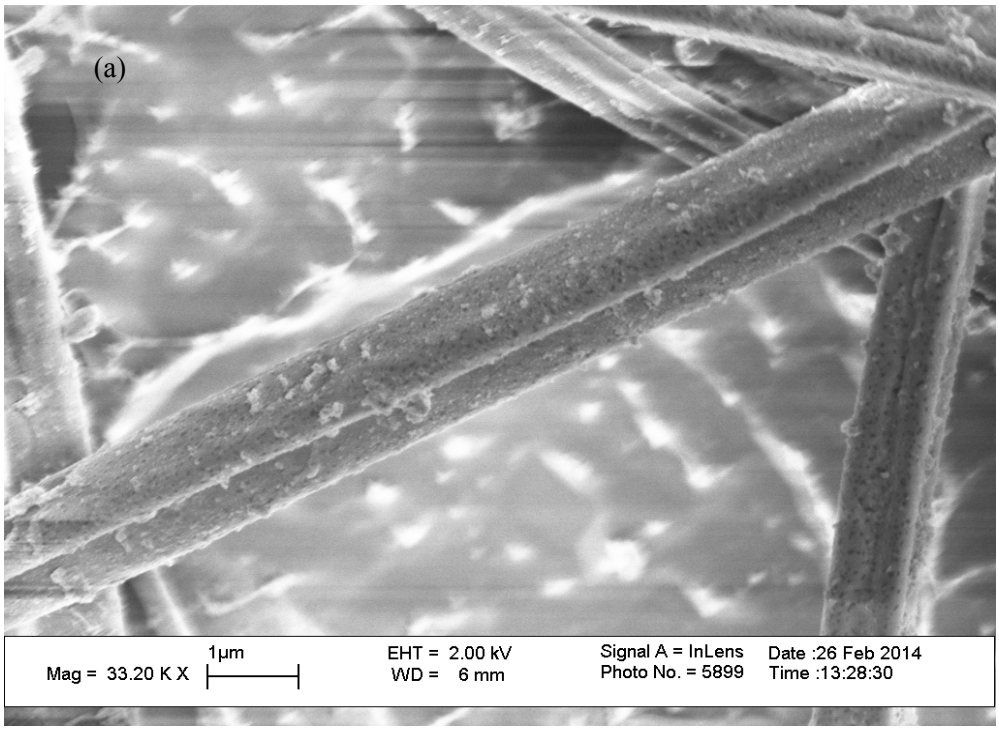

Figure 5a. Cryo-SEM image of micron scale electrospun film

`

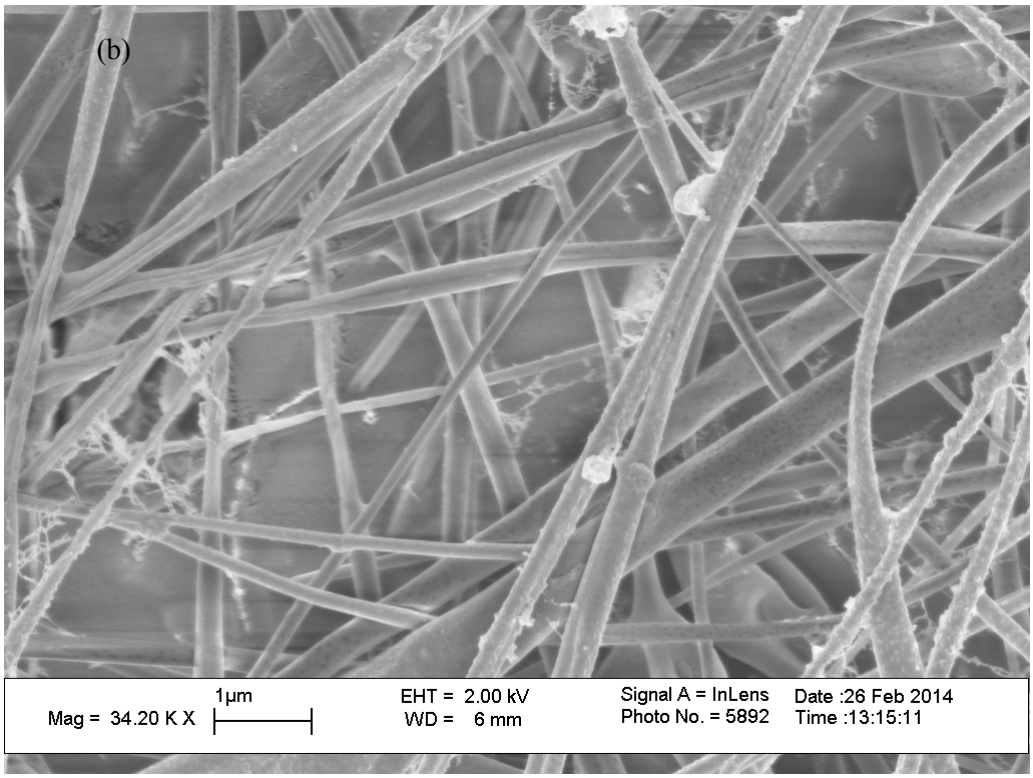

Figure 5b. Cryo-SEM image of nano scale electrospun film

3.5 Physical characterizations

3.5a XRD examination

The crystalline information of CA in different status, including micron scale fiber, nano scale fiber and raw powder, are shown in fig. 6. Raw powdery CA exhibited certain degree of crystalline structure with diffraction angle of 2θ at 8.5, 10.5, 13.5 & 18.0 degrees. Comparing to raw powdery CA, the blank electrospun CA films without quercetin displayed two diffraction haloes which proved an amorphous status for CA in the electrospun films. However, the nano scale electrospun film did exhibit higher crystallinity signal than the micron scale film.

`

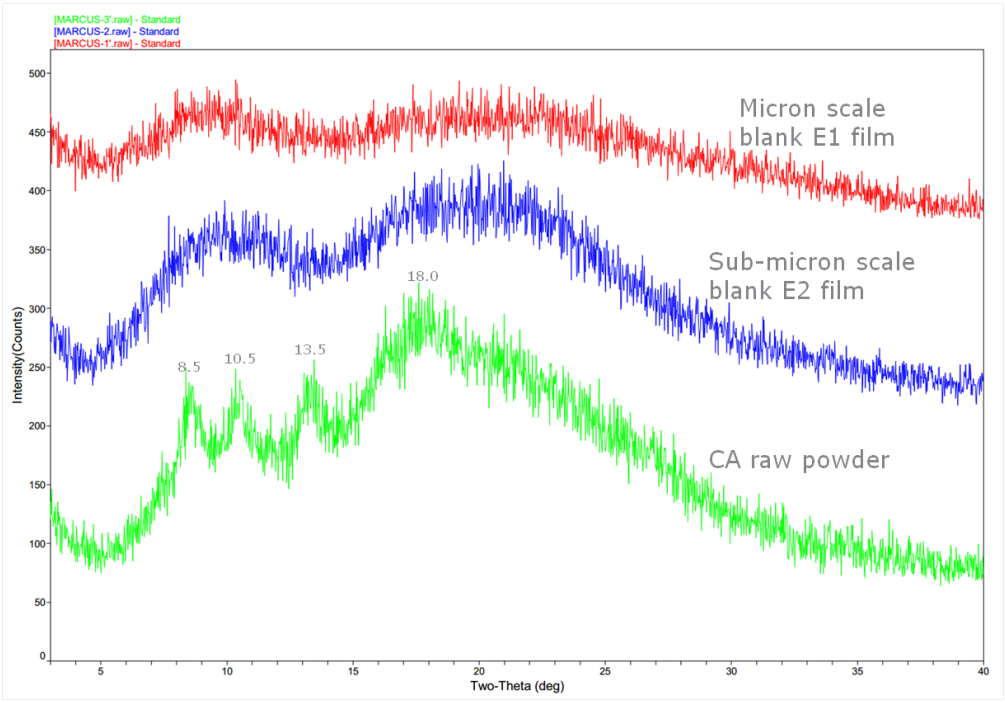

Figure 6. XRD patterns of CA in varied status

The XRD data of raw quercetin and quercetin-loaded electrospun fiber films are shown in fig. 7. The raw quercetin dihydrate is a yellowish powdery crystal substance under polarized light microscope.[57] Raw quercetin exhibited characteristic peaks with diffraction angle of 2θ at 10.7◦, 12.4◦, 15.87◦, 27.40◦ and more. This XRD pattern indicated a highly crystalline nature of quercetin. However, the characteristic diffraction peaks of crystalline quercetin are absenting in all the quercetin loaded electrospun CA films. These results implied that quercetin in the fiber mats is not crystalline.

`

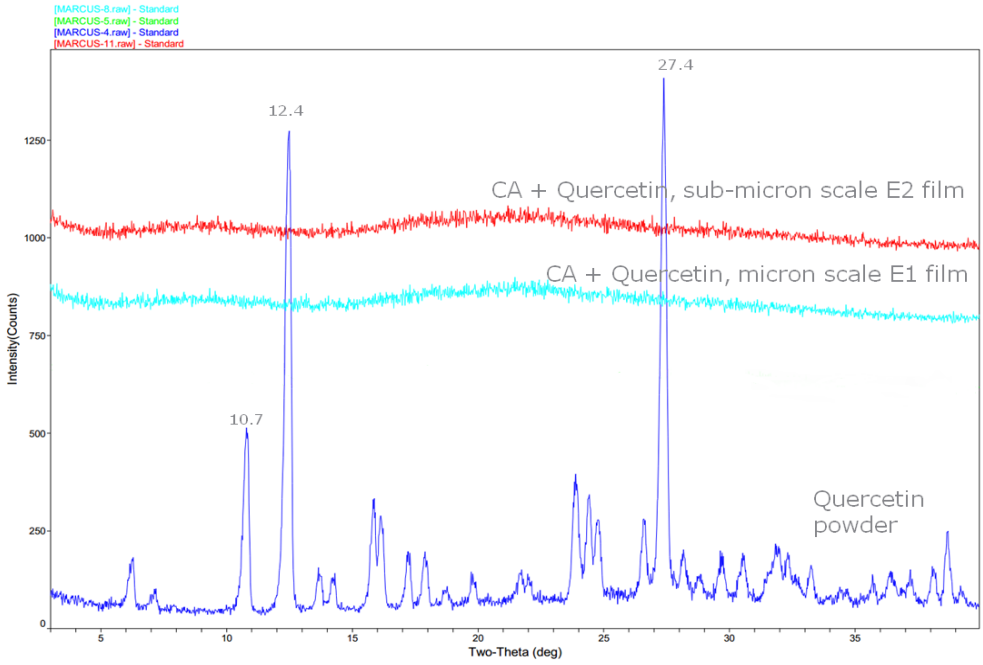

Figure 7. XRD patterns of raw quercetin and quercetin loaded electrospun films

3.5b FTIR examination

The FTIR spectrum of raw quercetin and quercetin-loaded electrospun fiber films are shown in figure 8. From the IR spectrum of quercetin, characteristic peaks at wavenumber 1437, 1518, 1605 representing for the stretching of cyclobenzene skeleton in the quercetin molecule was observed; 1267 for stretching of aryl ether (C ring) 1383 for phenol O-H bending,1318 for C-H bond in Aromatic hydrocarbon and other characteristic patterns under wavenumber 1000 were also displayed. However, these specific signals are hardly found in the patterns of quercetin loaded electrospun. It is suggested that van der Waals' force and other hydrophobic interactions stabilized and yield a homogeneous nano-composite structure of quercetin and cellulose acetate within the electrospun film.[57]

`

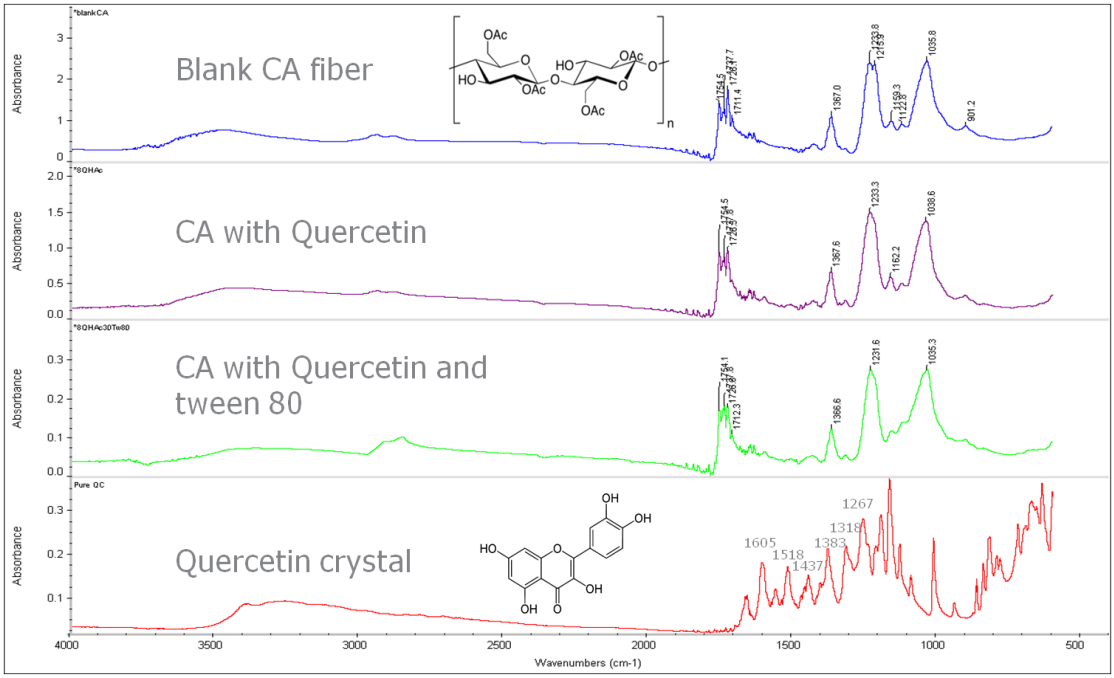

Figure 8. FTIR patterns of raw quercetin, blank and quercetin loaded electrospun CA films

3.6 in vitro drug release profiles

3.6a Immersion dissolution assay

Practically, the very first step of releasing quercetin from the electrospun fiber to achieve therapeutic effect was to immerse the film in an aqueous environment which swelled, interrupted and weakens the interactions between quercetin and the CA matrix, under the help of Tween 80 as a dissolution enhancer which allows quercetin to be compatible with aqueous environment. Therefore, an immersion dissolution assay is able to demonstrate the general release performance of the quercetin-loaded electrospun CA films.

`

The immersion dissolution data are shown below. All the fiber films contained 5% of quercetin loading and 6% Tween 80 to assist dissolution. From the profile of immersion dissolution of the first 10-20 minutes, performance of both micron and nano scale fiber films appear to be similar. From 40 minutes on, nano scale fiber film started to outperform the micron scale and the difference of quercetin dissolution was also increasing. Throughout the whole process, E-spun fibers exhibited significant better dissolution performance than raw quercetin ($P<0.05$).

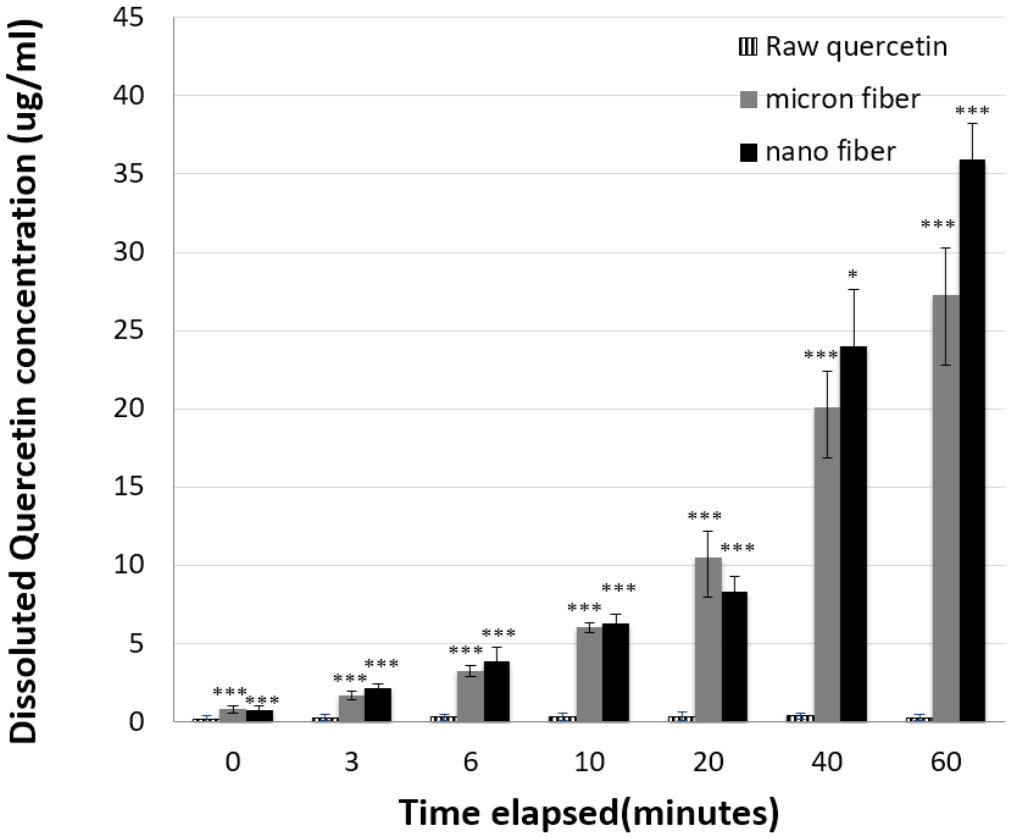

Figure 9. Immersion dissolution profiles for micron scale fibers, nano scale fibers and raw powdery quercetin as control (*: $P<0.05$, **: $P<0.01$, ***: $P<0.001$, comparing to the control)

`

3.6b Franz-cell diffusion assay

Topical delivery performance of quercetin loaded electrospun CA films was evaluated by Franz-cell diffusion assay on the Strat-M® membranes to mimic the human skin environment. The accumulated quercetin within the membrane after topical delivery process was extracted with methanol and brought to HPLC for quantitative assay. The quercetin content in the receptor cell, which simulated the dermis environment, was also examined to observe penetration effects.

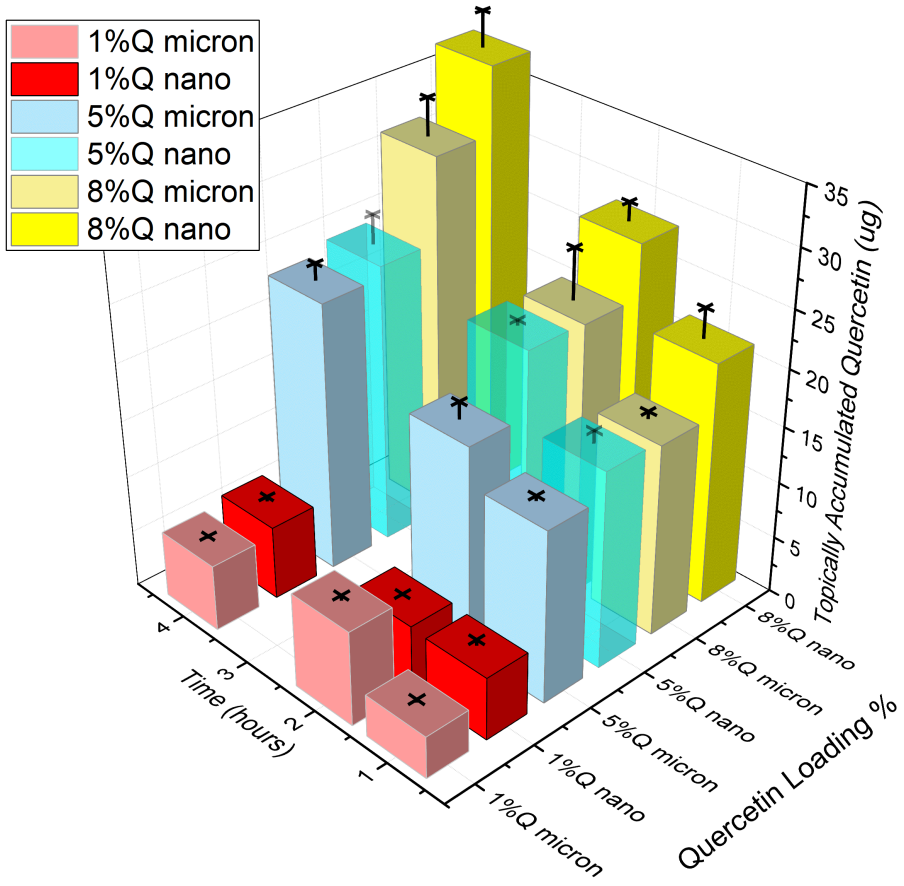

Figure 10. Cross-comparison of topical delivery performance for fibers with varied scales and quercetin content

`

In the topical delivery results, nano scale fibers had slightly higher performance in most of the experiments (5 out of the 9 comparison groups with $P < 0.1$ variations). Although nano scale fibers possessed only one tenth of the fiber diameters with much larger total surface area, they did not outperform the micron scale fibers so dramatically. Besides, quercetin was not detected in the receptor cells of the Franz diffusion kit in most of the experiments (or under quantification limits), meaning that penetration of quercetin can be neglected for the electrospun quercetin CA film topical delivery.

`

4. Conclusion

Quercetin is a compound with strong anti-oxidative activity and potent against UV irradiation induced peroxidative damage to the skin liposomal membranes.[36] However it did not perform well against skin inflammation triggered by sunlight damage.[41] The reason for that is the poor skin absorption of quercetin, which was related to its low water and lipid solubility. In this study, electrospun CA films successfully introduced quercetin into the Strat-M® mimic skin membranes. This was demonstrating the electrospun CA films have a strong potential in "recovering" the functional properties of quercetin to act against UV damage to the skin. This study also demonstrated the difference in release performance between electrospun fibers fabricated in micron scale and sub-micron scale (ten-fold variation) for the first time. Results implied that the sub-micron scale (265±109nm) electrospun fibers only slightly outperform the regular micron scale electrospun fibers. Considering the processing speed reduction (ingredient dissolving process and film collection were apparently slower and harder) in electrospinning the nano scale fiber formulations, it was not cost-effective. So far there are plenty of research efforts paid to the reduction of fiber diameter; however, the actual improvements with diameter-reduction was sometimes overestimated. More efforts should be paid to establish the detail relationship between fiber-diameter reduction and drug release/topical delivery performance to increase the cost effectiveness and achieve practical benefits. Besides, numerous nano-size pores were found on the surface of electrospun CA films with the help of Cryo-SEM, which was an interesting clue for understanding the mechanisms of drug released from electrospun CA fibers and might promote the development of computer simulation of electrospun drug release.

`

Chapter II: Topical Delivery of Carnosic Acid through a Novel Self-Assembled Nano-Emulsion Generated from Electrosprayed Lipid-Polymer Complex

1. Background

Nano-encapsulation of bioactive compounds is a hot topic in recent decades because it helps to address some critical problems come up during the application of bioactive compounds effectively. These problems are usually related to the stability, solubility, absorption and bioavailability of the bioactive compounds. Nano-encapsulation usually offers a shell-like mechanism to protect the bioactive compounds from oxidation, degradation and other environmental impacts. Within multitudinous types of nano-encapsulation strategies, nano emulsion is a widely applied encapsulation technique. However, emulsion systems came with several disadvantages in production and application. Breaking of emulsions may happen through ambient temperature fluctuation, microorganism digestion, Ostwald ripening and other impacts. To avoid these situations, high-shear and high-pressure homogenization were broadly applied in most of the emulsion productions. These high-power homogenization processing can significantly reduce the mean diameter of dispersed phase and reduce the surface free energy of the droplets, thus increases the stability of emulsions. However, these high-energy input systems largely increase the production cost and may potentially degrade the functional ingredients put into the emulsion formulations. Moreover, although nano-emulsions are thermodynamically much more stable than regular emulsion, they are still prone to some other environmental impacts like bacterial degradation and phase-separation in long-term storage. As a result, preservatives are frequently added to emulsion products, some of which may potentially pose adverse impacts towards

`

human health. Besides, efforts and costs were usually invested in optimizing formulations for better nano-emulsion product stability.

Self-assembling nano-emulsion generated from Electrosprayed/Electrospun Lipid-Polymer Composite (ELPC) has high potentials in addressing the problems of conventional emulsion mentioned above. ELPC products are generally films or particles containing numerous amount of nano to micron scale polymer particles/fibers loaded with drugs, phytochemicals, flavor compounds or other functional ingredients. ELPC products are in dry state for storage while capable of generating self-assembling nano-emulsions when they are in contact with sufficient amount of water. As a result, ELPC products are way less prone to microbiological impacts due to its dry state property comparing to aqueous emulsions. Preservatives are even not necessary for ELPCs. The functional ingredients encapsulated inside the ELPCs can also last significantly longer since ELPC products can be vacuum-packaged to avoid photo-degradation and oxidation.

EPLCs are fabricated through electrospinning/spraying. Electrospinning/spraying were techniques utilizing high-voltage electric field to rapidly evaporate volatile solvents and generate up to nano-scale particles/fibers from various types of polymer solutions. During this process, the high-voltage generator was just adopted to maintain an electric field with negligibly low electric current. Therefore, as atomization approaches, electrospinning/spraying are significantly more efficient than conventional approaches that involves large amount of thermal and kinetic energy input. In addition, the solvents being evaporated during the electrospinning processing could be collected and recycled through proper designing of the machineries. This move greatly eliminates the environmental concern of electrospinning processing and makes it more mature and cost-effective for an alternative atomization approach. However, in possession of

`

multiple advantages, electrospraying/spinning techniques are still not widely adopted in the world of industry. One of the major reasons was that it belongs to a "dry-atomization" technique. The products of routine electrospinning are mostly dry films or powder of confined types of polymers. Addition of other ingredients for electrospinning researches was mostly targeted at tuning solvent system polarity, solubility for higher drug loading, lower particle/fiber diameters, core/shell properties, etc. In order to contribute to the modern industry of atomization processing, studies on ELPC is highly necessary for the electrospinning research field.

In this research, an ELPC consisting of cellulose acetate, medium train triglyceride (MCT) and carnosic acid was fabricated with the capability of creating self-assembling nano-emulsion once the particles contacts with water molecules. Certain amounts of oil phase, emulsifiers together with the polymer were dissolved in glacial acetic acid. Cellulose acetate was frequently studied in the field of electrospinning. It was low cost, compatible with our skin (one of the fabric materials in the clothes) and most importantly, it has a property of swelling which was very useful in drug deliver. Carnosic acid was an active phytochemical with multiple health benefits like anti-oxidation, anti-inflammation and also an attractive potential—inhibition of tyrosinase activity and skin whitening. Carnosic acid loaded ELPC was characterized in various approaches in this project and was expected to boost the topical delivery of carnosic acid.

Carnosic acid is a famous phenolic diterpene antioxidant readily found in some *Lamiaceae* family plants like sages, rosemary and basil[58], which are spices frequently adopted in western cuisine. Carnosic acid content inside rosemary could be affected by genetics, seasons, maturity, locations and many other environmental factors. [59-60] Even the extraction techniques had significant impacts to the concentration figures. Carnosic

`

acid content in rosemary leaves was reported to be ranging from 1.8% to 3.5% by supercritical carbon dioxide extraction and about 0.4% to 1.2% by methanol extraction.[60-61] Carnosic acid majorly distributed in the leaves of rosemary and exhibit peak concentration in the spring season, the content in the stem was much lower than the leaves.[61] Interestingly, its concentration was found not related to the overall shape or dimension of rosemary[60] that the growers and consumers usually concerned when they cultivated or purchased the rosemary spice. However, carnosic acid was probably not considered a contributor to the overall flavor or aroma profile of rosemary (pine-like). [62-63]

Carnosic acid featured as a potent antioxidant. It was applied as preservative against lipid oxidation for various types of foods like vegetable oil[64], fish oil[65], lamb meat[66], dressings[67], etc. The phenolic hydroxyl groups play important roles in the antioxidative capability of carnosic acid, especially for the one near the carboxylic group since there would be higher electron density to reduce oxidative radicals. Moreover, carnosic acid has a unique characteristic that constitutes its high antioxidative potentials. It was able to be gradually oxidized to derivative forms while still remaining antioxidative properties (like carnosol and rosmanol demonstrated in figure.11.), which further increases its antioxidative efficacy. Rosmanol, an oxidized derivative of carnosic acid, was reported to be significantly more potent than commercially available synthetic antioxidants without adverse health concerns.[68]

`

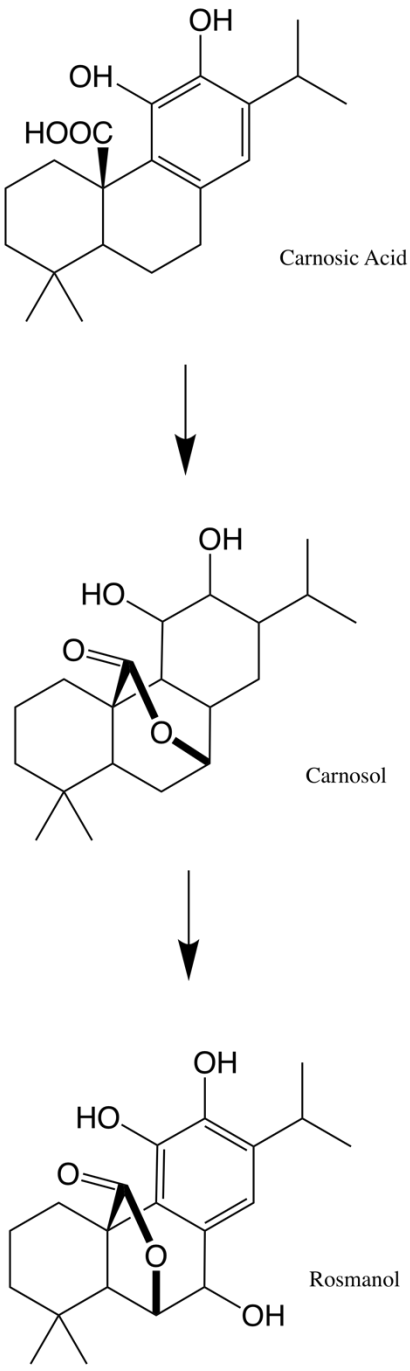

Figure 11. An example of carnosic acid oxidation

`

Carnosic acid possesses multiple health benefits that are more or less related to its potent antioxidative properties. For instances, carnosic acid was frequently reported to benefit in lipid/glucose metabolic problems like obesity, steatohepatitis, diabetes and more. Zhao et al. reported that carnosic acid supplementation achieved over 90% reduction of blood insulin elevation, over 80% reduction of weight gain for mice administered with high-fat diet. Dose dependent effect was also observed (over 80% weight reduction for 0.224% w/w carnosic acid diet comparing to over 50% for 0.112% w/w group), indicating the key role of carnosic acid in these metabolic related benefits.[69] Apparent weight gain reduction, hepatosteatosis and blood lipid level suppression was also observed in high fat diet treated mice ($P < 0.05$) supplemented with only 0.02% of carnosic acid in the diet.[70] Some other results also demonstrated the effect of weight gain reduction and lipid metabolism inhibition of carnosic acid.[71-73] Other health beneficial potentials were frequently discovered like acting against multiple types of cancer in cell and animal studies (colon[74], leukemia[75], breast[76], liver[77] and more), cardiovascular protection[78], neuron protection[79], against Alzheimer disease[80], etc. Most of these health benefits were related to the anti-oxidative and anti-inflammatory characteristics of carnosic acid.[81]

`

2. Experimental

2.1 Materials

Cellulose acetate (average Mn ~30,000 Da, 39.8 wt. % acetyl content) and Glacial acetic acid were purchased from Sigma Aldrich (MO, USA). Fresh pig shoulder skin was purchased from local supermarket. Medium Chain Triglyceride was a kind gift from Stepan® Company (Neobee 1053). Lecithin PC75 was purchased from American Lecithin Company. Carnosic acid was purchased from Wuling Yangguang Biotechnology Co., Led.

2.2 Fabrication of the Electrosprayed Lipid-Polymer Composite

Cellulose acetate 5% (w/v), MCT 10% (w/v), PC-75 lecithin 10% (w/v) and 1%(w/v) carnosic acid were dissolved in glacial acetic acid all together to create a polymer blend solution for electrospraying. This solution was loaded into 3ml syringes to be loaded onto a syringe pump for feeding at a constant speed of 2ml/hour during the fabrication process. An electric field was applied to both the syringe tips (positive end) and a piece of aluminum foil (negative end). The distance between the foil and the tips was 15cm and the electric field was set at 18KV. The electrosprayed products were placed in the fume hood for 12 hours to evaporate the solvent residues and then kept within desiccators to avoid contact with moisture before further characterizations.

`

2.3. Morphology and Physical characterizations

The morphology of the electrosprayed ELPC particles were examined with field emission scanning electron microscope (FESEM) S-3000N (Hitachi, Japan). Average size of the ELPC solid particles (n=100~200) were measured with FIJI (Fiji Is Just ImageJ) software.[82] A BIC 90 Plus particle size analyzer with Brookhaven BI-9000AT digital correlator (Brookhaven Instrument Corporation, New York, NY, USA) dynamic laser light scattering system (DLS) was applied to determine the hydrodynamic droplet diameter of the self-assembled emulsions generated from the ELPCs. A D/M-2200T automated system (Ultima+, Rigaku) was adopted to analyze the crystalline information of the ELPC material matrix. A Nicolet™ Nexus 670 with a Smart MIRacle™ horizontal Attenuated Total Reflectance accessory ATR-FTIR system (Thermo Fisher Scientific, Madison, WI) was utilized for examining interactions and functional group related information of the chemicals inside ELPCs.

2.4. Functional characterizations

2.4.1 ORAC Anti-oxidation activity of carnosic acid

ORAC (oxygen radical absorbance capacity) is an assay measuring the ability of scavenging oxidative free radicals thus capable of evaluating the anti-oxidative potential of chemicals. 2,2′-Azobis (2-amidinopropane) dihydrochloride (AAPH) is adopted as the source of oxidative free-radical in this assay while Trolox (6-hydroxy-2,5,7,8-tetramethylchroman-2-carboxylic acid) is selected as a reference of anti-oxidative ability. Sodium Fluorescein is a fluorescent probe sensitive to oxidative attack and it is utilized as an indicator of the scavenging capability for oxidative free radicals.[83]

`

In this assay, a phosphate buffered saline (PBS) was utilized to maintain the reaction environment. 4.275g of K_2HPO_4 and 1.02g of KH_2PO_4 were dissolved in 500mL DI water with pH adjusted to 7.4. 119 mmol/L AAPH (1.614g dissolved in 50mL PBS buffer solution), 0.96 μmol/L Sodium Fluorescein (0.16g dissolved in 500ml PBS, then dilute 1000 times) were prepared. 50μmol/L Trolox solution was prepared by dissolving 0.3129g Trolox in 25mL methanol then dilute 1000 times. It was further diluted to 3.125, 6.25, 12.5 and 25μmol/L as gradient concentrations for establishing a standard curve for quantification of Trolox. The same concentration gradients were also applied to prepare Vitamin C as a negative control and to the carnosic acid as samples. The experiment was carried out in the UV 96-well plate reader to detect the amount of fluorescence from the Sodium Fluorescein during the reactions. The reaction environment within the reader was kept at 37 °C with the excitation wavelength set at 485nm and the emission at 528nm. Fluorescence signal was detected at a 4.5-minute interval for totally 2.5 hours.

Relative intensity of the AAPH and each sample was plotted against the elapsed time on the experiment as figure 26 displayed. The relative intensity equals to the fluorescence intensity of sodium fluorescein added with samples plus AAPH divided by that of the sodium fluorescein without AAPH added (AAPH-). The differential area between the AAPH+ curve and the curve for sample at a certain concentration was integrated by Origin software. A standard curve for the differential area against sample concentration was plotted to determine a linear region for ORAC value calculation. Finally, the ORAC value would be defined as: The specific differential area for each sample divided by the specific differential area for Trolox at the same molarity. [84]

`

2.4.2 In vitro tyrosinase inhibitory assay of carnosic acid

Carnosic acid and its derivatives were capable of anti-oxidation and anti-inflammation. The anti-oxidative properties of carnosic acid could also be applied against some oxidases, like tyrosinase---an oxidase responsible of producing melanin through oxidizing L-tyrosine and to L-DOPA and L-DOPA-quinone, which would be further oxidized and polymerized to the big molecule melanin. As a series of dark color polymers, melanin exists in the melanocytes in our skin responsible of the pigmentation of our skin. However, over or unwanted production of melanin causes skin problems like age spots, hyperpigmentation, lentigines and melasma. Melanin is fairly stable which requires relatively long time for metabolism and removal. As a result, prevention of melanin production by inhibiting the tyrosinase activity was an important strategy for skin whitening and treating skin problems related with overproduction of melanin.

In this research, tyrosinase inhibition activity of carnosic acid was evaluated through a previously reported method with slight modifications.[85] 0.2M PBS buffer was used to maintain the reaction pH at 6.8 with appropriate ionic strength. 0.01M L-DOPA solution and 100 Units/ml mushroom tyrosinase solution was prepared with the above PBS buffer. Carnosic acid sample solution was prepared by dissolving 6mg carnosic acid with 2ml DMSO then dilute to 10ml by PBS to make a 600μg/ml stock solution. The stock solution was then diluted to 60, 30, 15, 7.5, 3.75μg/ml to form the sample solutions. Kojic acid, a compound broadly used in cosmetic industry for tyrosinase inhibition and skin whitening functions, was prepared in PBS at the same series of concentration to be a reference compound. The reaction was conducted in a 96-well plate reader with UV absorbance set at 475nm to monitor the content of L-DOPA. For the overall background, each well was filled with 40μL PBS plus 160μL L-DOPA solution. For the negative control, each well was filled with 20μL PBS, 160μL L-DOPA

`

and 20μL tyrosinase solution. For the sample background, each well was filled with 20μL PBS, 160μL L-DOPA and 20μL sample solution of gradient concentrations. For the reaction sample, 160μL L-DOPA, 20μL tyrosinase solution and 20μL sample solution of gradient concentrations was added. The plate was then incubated at 30℃ for 30 minutes within the plate reader and the absorbance at 475nm was read. The enzyme activity was expressed as 0.001 elevations in the OD value at 475nm. Percentage of enzyme inhibition was defined as:

$[(\text{Absorbance}_{\text{Control}^-} - \text{Absorbance}_{\text{Overall Background}})]/(\text{Absorbance}_{\text{Control}^-} - \text{Absorbance}_{\text{Sample Background}})$

The % inhibition (reaction rate) will then be plotted against each corresponding carnosic acid/kojic acid sample concentration that followed Michaelis-Menten kinetics in order to yield K_m, V_{max} and also analyze the IC50 value (concentration for 50% activity inhibition) assisted with IBM SPSS Statistics software.

2.4.3 Circular Dichroism (CD) examination of conformational changes of tyrosinase interacted with carnosic acid

Circular Dichroism (CD) is an important and sensitive measure for evaluating the structural information of many chiral biomolecules, just like the secondary structure situations of various proteins. When plane/linear polarized UV light is shone to the chiral protein molecule, it would become circularly polarized light spinning perpendicularly (left or right handed) to the direction that the light spreads. Protein molecules have UV absorption properties due to the conjugated system of aromatic rings in the tyrosine, tryptophan and phenylalanine residues. And, because of the asymmetric nature of the chiral molecules that leads to differences in local refractive

`

index, proteins will have varied degree of UV absorption between clockwise and counter clockwise circularly polarized light. This variation in absorption can be plotted against a range of UV wavelength that the protein molecule absorbs, which is called a circular dichroism plot. Based on the mechanisms explained above, the CD pattern displays the specific special conformation characteristics of the secondary structure of protein molecules. Changes happen to the secondary structures of proteins could be demonstrated in the CD curves. Therefore, it is helpful for studying interactions between protein and other substances.

In this research, CD was adopted to study the interactions between carnosic acid and tyrosinase. It demonstrates the structural changes of tyrosinase that assists to understand the mechanism of the enzyme inhibition activities of carnosic acid. An Aviv Model 420 Circular Dichroism Spectrometer was utilized to examine the CD spectra of tyrosinase before and after interacting with carnosic acid. A 0.2M PBS buffer solution was used to maintain the whole interaction environment pH at 6.8. 1000 unit/ml concentration of tyrosinase buffered solution was adopted as the control for the CD study. 50μM carnosic acid buffered solution was prepared by diluting a 0.1mM carnosic acid DMSO solution to 50μM with the 0.2M PBS buffer mentioned above. A 50μM kojic acid buffered solution was prepared as a reference for tyrosinase inhibition activity. 0.3mL of sample solution (0.2M PBS for the control) and 0.3mL of the enzyme solution prepared as described above was mixed and pipetted into each cuvette (0.1cm path length cells) for CD detection. Nitrogen purge was turned on 20 minutes prior to igniting the UV lamp. 190–260 nm Far UV range wavelength was selected for the CD examinations.

`

2.4.4 Topical delivery of carnosic acid by ELPCs

Dermal intake of the carnosic acid from the ELPCs was evaluated by an *ex vivo* topical delivery assay on pigskins. Vertical Franz diffusion cell was adopted for this assay, which has an orifice diameter of 9mm and a 5mL receptor chamber. Pig shoulder skin was freshly purchased from local supermarkets. As soon as the skin arrived in the lab, subcutaneous fat of the pig shoulder skin was carefully scarped and removed in a fast pace without hurting the dermal tissue. The de-fat pigskin was chopped into small pieces that completely covers the orifice of the Franz-cells and then stored at -80◦C. 1X PBS buffer at pH 7.4 with 1% Tween 80 was prepared as the medium loaded within the receptor to mimic the subcutaneous environment. The Franz-cells were heated by circulating water flow to keep the diffusion environment at 37 ◦C and the medium was constantly agitated at 600 rpm. For each experiment, the donor cells were filled with 10mg ELPC powder with 5% carnosic acid as samples or with 1ml MCT oil containing the same 500μg carnosic acid as the control.

To carry out the diffusion assay, the receptor chamber would be firstly loaded with the PBS-tween media prepared as above. Then, pieces of frozen pigskin were thawed in 1X PBS buffer at pH 7.4 for 15 minutes to activate the skin. The thawed skin was being installed above the receptor cells. In the end, the donor cells were filled with proper quantity of samples then the assay was started right away. The topical delivery assay was carried out for up to six hours. The time intervals were designed as 0.5, 1, 2, 4, 6 hour(s). Each chopped piece of pigskin was used only once for each time interval of experiment. At the time interval, the pigskin was removed from the Franz-cells and being flushed under a strong current of water for twenty seconds and the surface of the skin was thoroughly wiped with Kimwipes™ (Kimberly-Clark™ Professional) to remove residues not delivered into the skin.

`

After the experiment, the pieces of pigskin were further chopped into tiny pieces and placed into 10mL of ethanol heated to 70◦C for thirty minutes to extract the carnosic acid out. Then, the extraction solvent would then be analyzed by HPLC to detect the topically delivered content of carnosic acid.

2.4.4a HPLC detection of carnosic acid

Detection of the carnosic acid amount in the extractions was being carried out by an Agilent 1100 series HPLC with DAD detector and auto-sampler installed. A reverse phase C18 column (ZORBAX SB-C18, 4.6*250mm, 5-micron particle size) was utilized for the separation and identification of carnosic acid. The mobile phase was designed to run isocratically at 0.8 mL/minute with the composition of 70% acetonitrile and 30% of DI water with 0.1% of phosphoric acid added for reduction of tailing and better elution. The injection volume was 20 μL and the samples were filtered by 13mm 0.22μm Nylon Syringe filters (ArkBio Group Inc.) before HPLC examination. The examination UV wavelength was set at 230nm. 210nm was also observed to ensure identification of the correct peak of carnosic acid.

`

2.4.5 Visualization of ELPC's Topical delivery effect through confocal laser scanning microscopy (CLSM)

In this research, both the ELPC and the skin matrix would be stained with different fluorescent dyes in order to visualize the distribution of topically delivered drug and the depth of formulation penetration. For this experiment, the ELPC were specially prepared. The MCT within the formulation for electrospraying the ELPC was added with 0.01% Nile Red by weight[86] and then being electrosprayed together. The ELPC containing Nile Red would then be applied onto the pigskins using Franz diffusion cells as described before for a range of time intervals including 0.5, 1, 2, 4, 6 hour (s). After diffusion, the pigskin would be washed with a strong current of water for twenty seconds and thoroughly wiped clean to remove the excessive formulations.

In order to be easily visualized by confocal microscopy, a cryo-sectioning process was applied to the pigskins after topical delivery. After the Franz diffusion, the round center part of cleaned pigskin where the ELPC contacted with would be cut out. Then, the center of skin was vertically cut in the middle with sharp scissors to expose the inside of the skin. The half-piece of pigskin with smoother section was kept aside for later use. A cryo-sectioning specimen mold (Tissue-Tek® Cryomold®, 25mm*20mm*5mm) was utilized to fill with O.C.T compound (Optimal Cutting Temperature Embedding Medium) for freezing the skin specimen properly. After filling the compound, small pieces of dry ice were put underneath the mold to begin freezing. At this moment, tweezers were used to carefully hold the edge of skin specimen; to let the section facing outwards and slowly soaked into the O.C.T compound to avoid air bubbles. The section surface should be fully immersed. The piece of cut skin was hold within the mold stably until the O.C.T compound medium was completely frozen by the dry ice, then store the whole piece at -20◦C overnight.

`

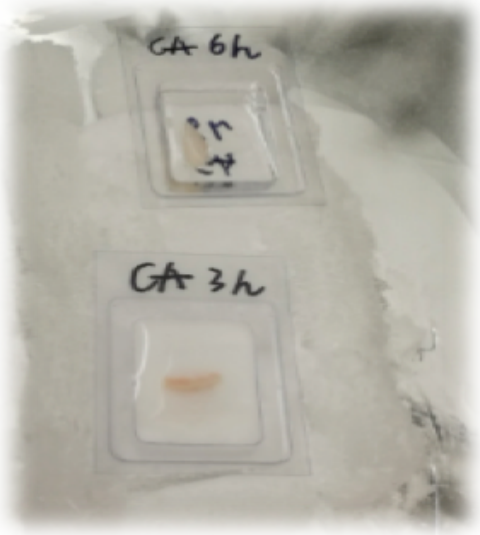

Figure 12. Skin specimen soaked in the O.C.T medium (top) and frozen (bottom) in the mold

The molded frozen skin pieces with O.C.T medium would be carried to a cryo slicing machine to be cryo-sectioned in order to fabricate slices of vertically cut pigskin with 10μm thickness. The thin slices had to be placed onto positively charged glass slides (VWR VistaVision™ HistoBond® Adhesive Slides) to be fixed properly for the imaging work later.

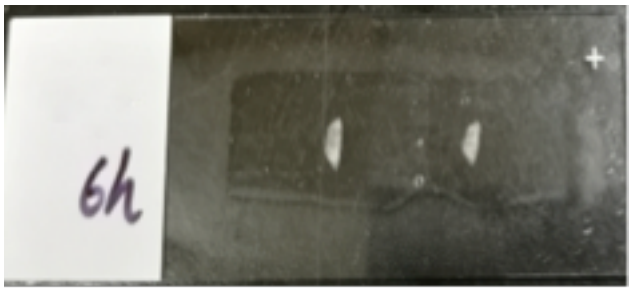

Figure 28. Two pieces of 10μm pigskin slices fixed onto positively charged slides

`

The thin slices of pigskin would then be processed for staining. They were firstly incubated in paraformaldehyde solution (prepared by dissolving 40mg/mL paraformaldehyde in PBS 1X solution at pH 7.4 stirring overnight at 60◦C) for 15 minutes for the fixation of the tissue. Then, carefully wash away the fixation solution by dipping PBS 1X solution on top of each skin for several times. Make sure the dipping was gentle so that the slices were not flushed away or flipped over. Secondly, DAPI dye solution (10µg/mL DAPI dissolved in PBS 1X at pH 7.4) was utilized for staining the nuclei area of the cells within the skin tissues. The duration for DAPI staining was about 10-15 minutes and then the dye was washed away by gently dipping with PBS 1X again. After staining, the slices should be transferred to the facility of confocal microscopy imaging in a short time.

The confocal laser scanning microscopy utilized in this experiment is Zeiss LSM 710 with computer driven X-Y stage and multiple routine laser lines plus an additional 594 nm HeNe laser. The LSM 710 equipped with a DAPI, a Cy3 and a GFP fluorescence filter. The controlling program was Zen 2.1. The ultrathin slices of pigskin after fixation and staining processing were quickly brought to this CLSM for examination. 405nm and 633nm laser beams were tested and selected for the detection of DAPI and Nile-Red dyes independently without interfering over channels. Laser power of 405nm was set to 2.0 while for 633nm it was set to 49.5 in order to obtain best effects of visualization. Pinhole was set to 64.2 units to scan 17.9µm of section. For the DAPI channel, gain was set to 575 units while for the Nile Red channel the gain was 776.

`

2.4.6 Melanoma cell culturing

In order to observe the delivery carnosic acid by ELPC from a cellular level of view and to assist evaluating the skin whitening potential of the ELPC-carnosic acid formulation, a melanoma cell-line study was adopted. B16F10 mouse melanoma cell-line (CRL-6475™) was ordered from ATCC® (American Type Culture Collection). The culturing media was DMEM (Dulbecco's Modified Eagle's Medium) with 10% fetal bovine serum and 100 IU/ml of penicillin and 100 mg/ml of streptomycin (Gibco™, Thermo Fisher Scientific, USA). The cell incubation environment was controlled at 37◦C with 5% CO_2. Culturing medium was changed about every two days when medium turns pale yellow. As the cell growth reached about 80% confluence counted by hemo-cytometer, the cells would be treated with trypsin, transferred and seeded in new flasks for future utilizations. [87]

2.4.7 Cell viability MTT assay

To investigate the melanoma cytotoxicity under the effect of carnosic acid or carnosic acid loaded ELPC, a Methyl Thiazol Tetrazolium bromide (MTT) colorimetric assay, which utilized cellular oxidoreductase in the mitochondria of living cells to reduce the MTT dye to formazan, a compound with purple color that was linearly related to the quantity of the normal functioning cells.[88-89] The assay was conducted with the B16F10 mouse melanoma cell-line in a 96-well plate. Each utilized well was filled with culture medium containing 1×10^4 cells to be seeded and kept at 37◦C for a whole day. After that, discard the DMEM from the wells and use PBS 1X buffer to clean. Then, each sample well was filled with the culturing medium again added by 100 μL DMSO solution of carnosic acid with a series of concentration gradient (DMSO was diluted to less than 0.5% to avoid toxicity to the cells). For the wells of control, only

`

0.5%DMSO was added to the medium. After 37◦C incubation for 24 hours, again discard the DMEM and clean with PBS. Then, 100 μL 0.5 mg/mL MTT solution (in RPMI 1640 media) was applied to all the experiment wells and the plate was set at 37◦C for 2 hours. After MTT treatment, the solution in each well was removed and washed thoroughly with PBS buffer. 100 μL DMSO was then applied to dissolve formazan. Finally, the plate was fed to the microplate reader (Bio-Tek) to shake for 20 minutes and read the absorbance at 570nm (490nm as reference). Experiments were carried out in triplicates. Cell viability was defined as the percentage of the sample's absorbance result divided by that of the control (background deducted).

2.4.8 Observation of cellular uptake of carnosic acid from ELPC through confocal laser microscopy

Here the confocal laser microscopy was utilized again to further examine the B16F10 melanoma cellular uptake of carnosic acid released from ELPC over time. The melanoma cells were firstly cultured as previously mentioned and then seeded on 20mm round cover glasses (CELLTREAT® SCIENTIFIC PRODUCTS) with quantity of $1*10^5$ cells/ml and placed into 12-well plates. In order to visualize the cellular uptake process, a lipophilic fluorescence dye, coumarin-6, was added to the polymer blend to fabricate fluorescent ELPC in a concentration of 0.01% by weight of the dry materials. Then, 0.1g of this fluorescent ELPC was put into 0.9mL of cell culture medium to generate a self-assembling nano emulsion loaded with carnosic acid and coumarin-6 dye. This emulsion was further diluted with culture medium by 500 times to ensure the coumarin-6 and carnosic acid amount are safe for the melanoma cells. Then the diluted emulsion-medium was added to the wells for 0.5, 1, 2, 4, 6 hours as the designed time interval for gradual cellular uptake observations. Another fluorescent dye, DAPI

`

(10μg/mL) was utilized for staining the nuclei area of the melanoma cells. At each time interval, all the medium in the wells were removed and DAPI solution was added to the wells. The treatment time for DAPI staining was about 30 minutes and then the dye was washed away with PBS 1X for three times to avoid excessive staining. The seeded glasses treated with emulsion and dyes were brought to confocal laser microscopy for examination. Addition of emulsion-medium to the cells should follow a reverse chronological order to let all the time interval finish at the same moment, which facilitated CLSM examination.

2.4.7 Statistical analysis

All the detection data presented were carried out in duplicates or triplicates. Origin® 2016 and Microsoft Office 2016 were utilized in the calculation of averages and standard deviations. IBM SPSS Statistics 22.0 was used for determining IC50 value and significant variation was considered with confidence level<0.05 by IBM SPSS independent T-tests.

`

3. Results and discussion

3.1 Morphology of carnosic acid loaded ELPC

3.1.1 Overall appearances

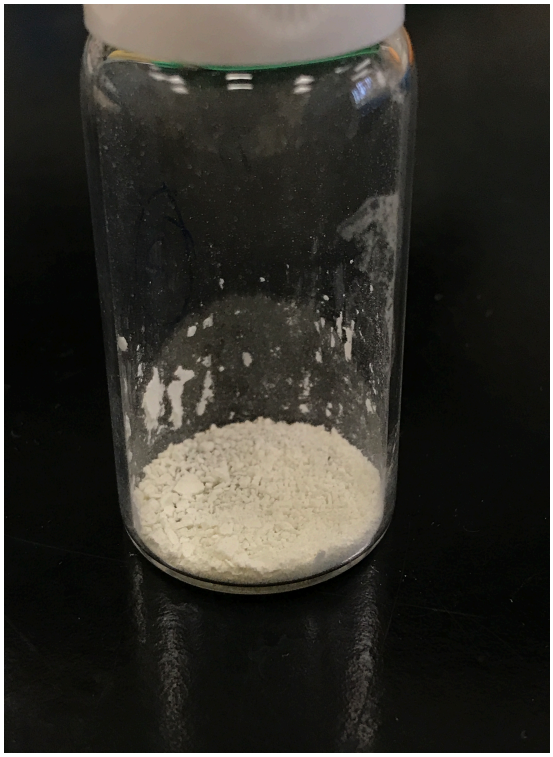

Figure 14. Powdery appearance of the carnosic acid loaded ELPC products (Bottle diameter=2.5cm)

`

3.1.2 Particle Morphology examined by SEM and particle size distribution

3.1.2a Control

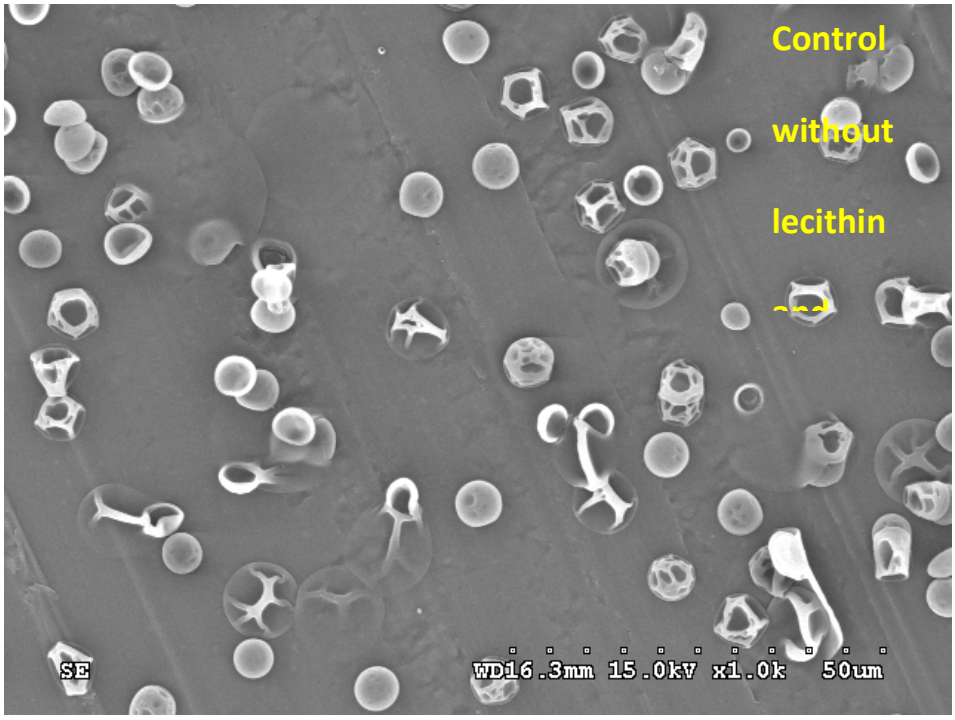

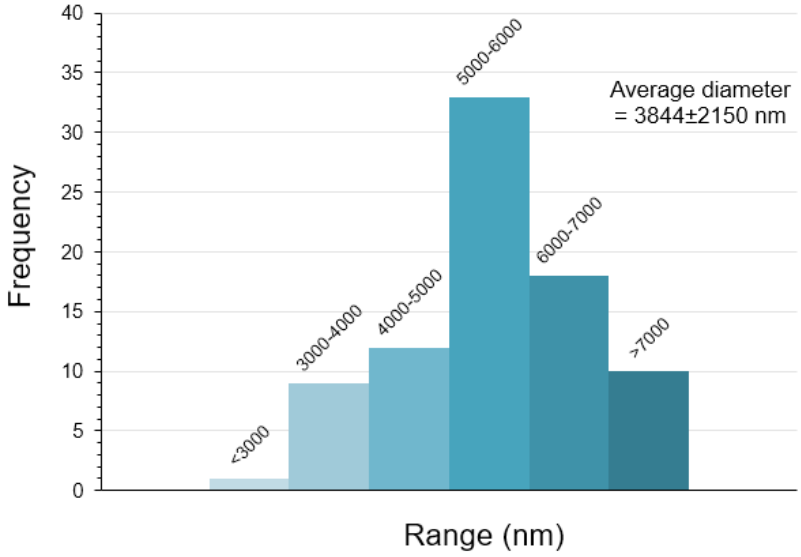

Figure 15. FESEM picture and particle size distribution of the carnosic acid loaded electrosprayed cellulose acetate as control

`

The carnosic acid loaded electrosprayed cellulose acetate (CA) particles sample was adopted as the control. The morphology of these particles was spheres with deep grooves and trenches on the surface. Many of the particles had bowl-like structure. These electrosprayed particles were much larger in diameters compared to electrospun fibers made with cellulose acetate in acetic acid solvent systems adopted in the previous chapter. Their diameters usually ranged from hundreds of nanometers to less than two microns. The particle size distribution chart demonstrated that the particles had relatively scattered sizes in a wide range from three to seven microns. About 40% of the particles were five to six microns large and the average diameter of all particles was 3844±2150nm.

3.1.2b Particles with lecithin

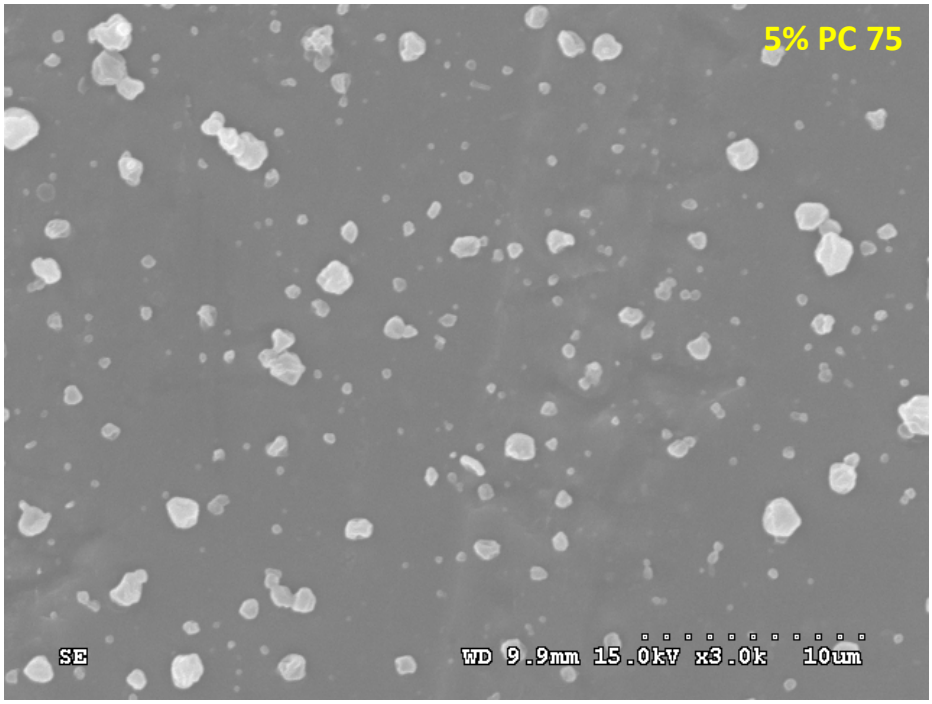

`

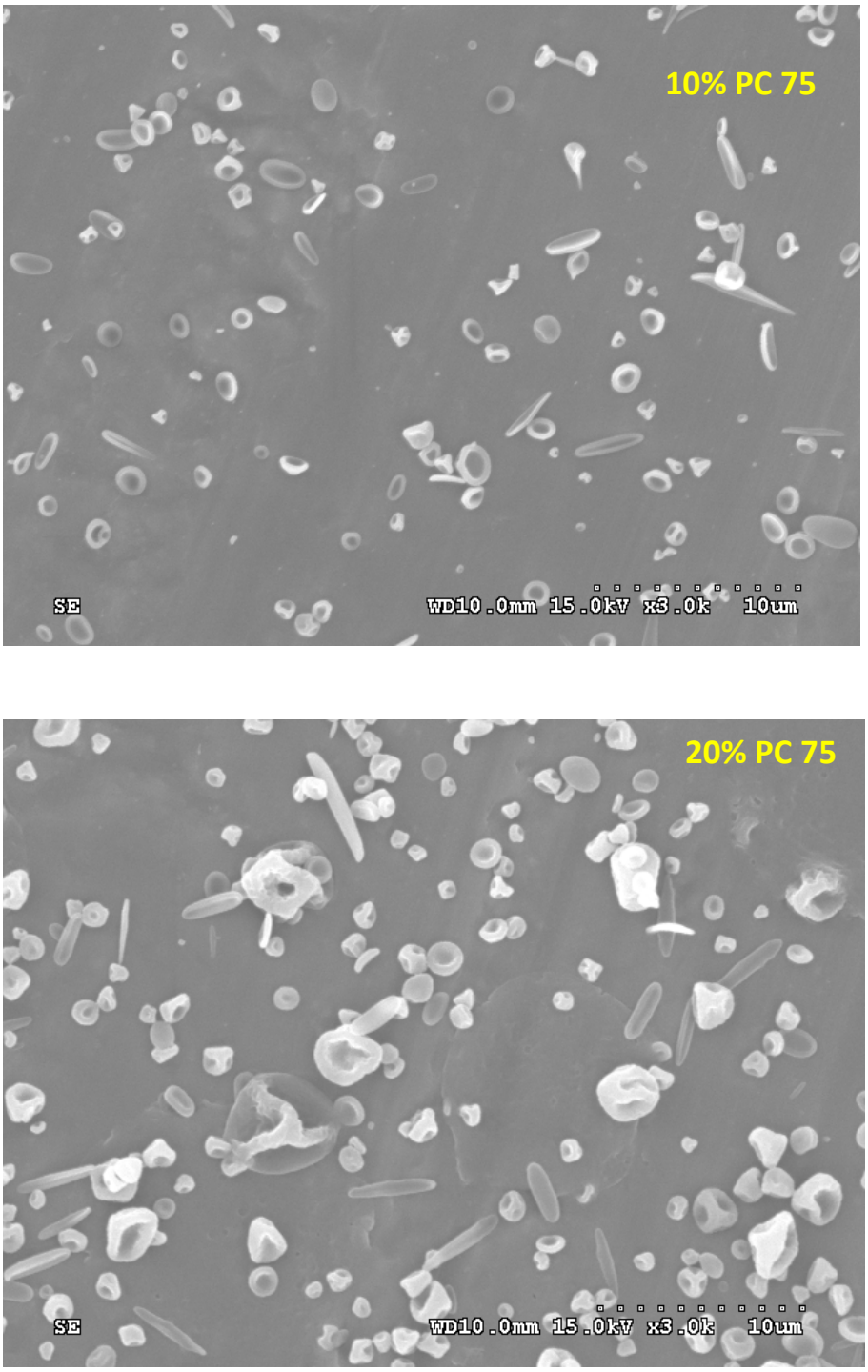

Figure 16. FESEM pictures of the carnosic acid loaded ELPC containing varied amount of lecithin (PC75), from 5% to 20%.

`

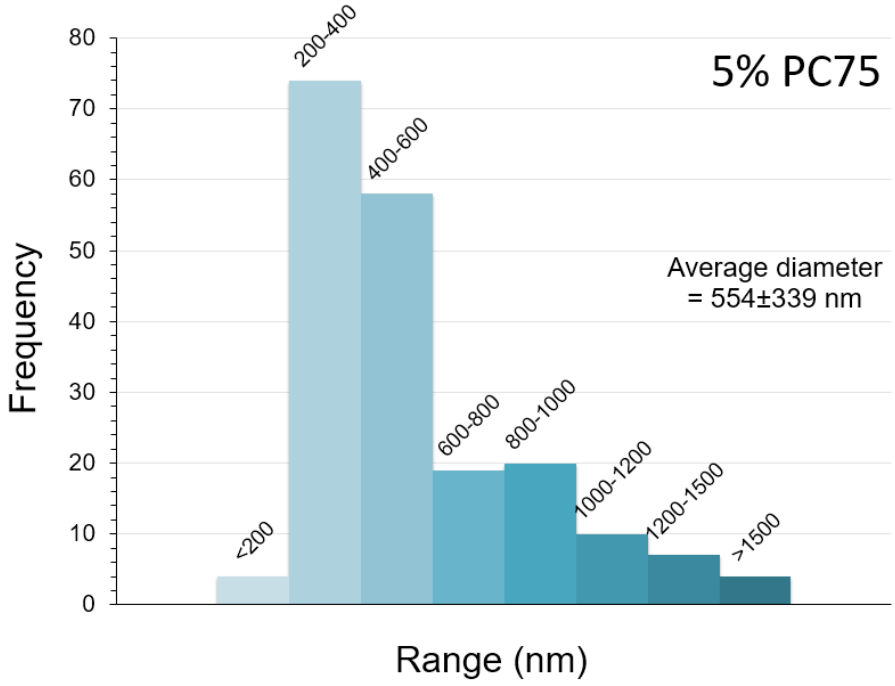
5% PC75
Average diameter
= 554±339 nm
Frequency
Range (nm)
<200
200-400
400-600
600-800
800-1000
1000-1200
1200-1500
>1500
0
10
20
30
40
50
60
70
80

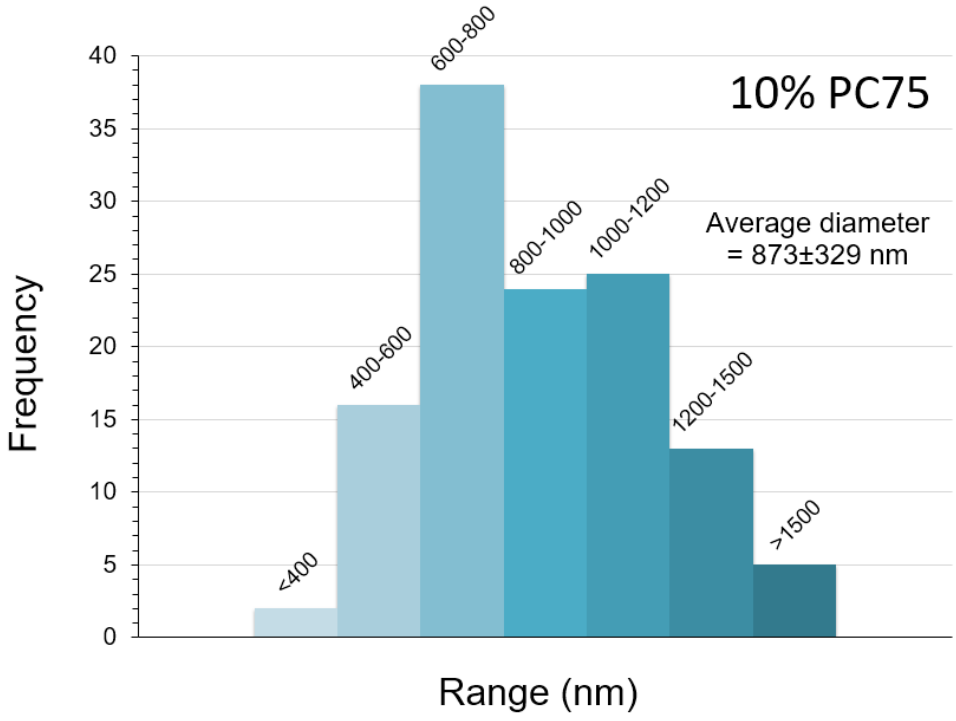
10% PC75
Average diameter
= 873±329 nm
Frequency
Range (nm)
<400
400-600
600-800
800-1000
1000-1200
1200-1500
>1500
0
5
10
15
20
25
30
35
40

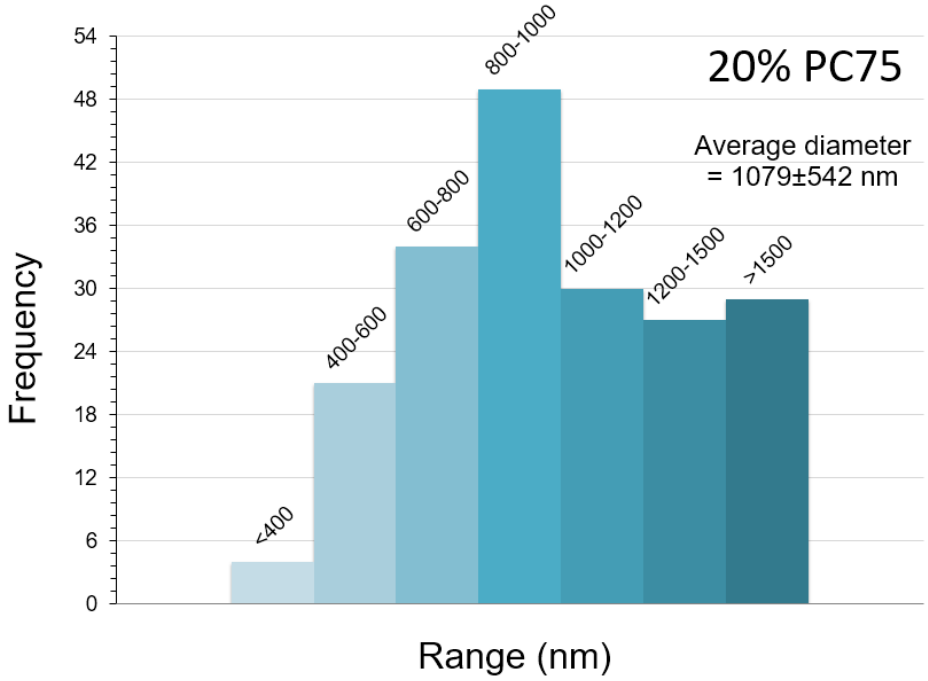

Figure 17. Average diameter and distribution of the carnosic acid loaded ELPC containing varied amount of lecithin (PC75), from 5% to 20%.

Comparing with the control, particles with lecithin had significantly smaller dimensions. Addition of 5%, 10%, 20% lecithin caused around 8, 5 and 3 folds reduction in average particle diameters. This was potentially caused by dramatic decrease in surface free energy by addition of lecithin as a surfactant. At the moment of electrospraying, micro droplets of cellulose acetate (CA)-acetic acid solution evaporated rapidly. Once the CA molecule left acetic acid and contacted with the open air environment, because CA was insoluble and incompatible with the components of open (nitrogen, oxygen, moisture, etc.), the polymer molecules would gather up and form large aggregates/crystals (average diameter ≈ 3.8μm) ----a typical form with lower total surface area, low surface energy and thermodynamically stable. Nevertheless, if lecithin was present within the micro droplets of CA polymer-acetic acid solution, it would be extensively involved in the interface between CA and air environment once

`

the acetic acid was evaporated by electrospraying. Lecithin molecules were more compatible with the open air especially the moisture; they also interrupt the process of CA molecule crystallization by embedding themselves extensively in-between the massive CA polymer molecule arrays. This property significantly reduced the particle-air interfacial free energy. Consequently, as long as the interfacial surface energy potential was largely decreased, the system could bear with much higher total surface area for the particles, in other words, dramatic reduction in particle sizes.

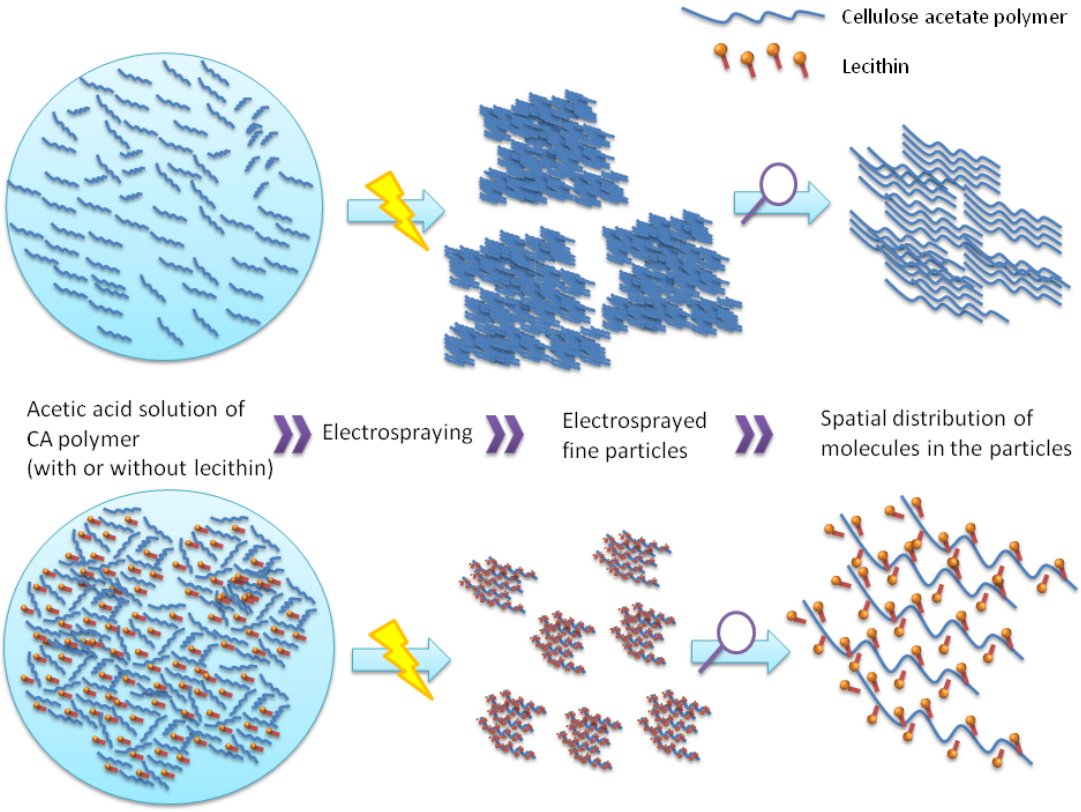

Figure 18. Schematic of electrospraying of CA polymer with or without lecithin

In addition, the detail surface morphology also changed with increasing addition of lecithin as a topical delivery enhancer. From both aspects of general appearance and particle size distribution, variations could be clearly observed. As displayed on figure 16., the ELPC particles with 5% lecithin were relatively irregular in shape with rough surfaces. The particle size distribution was highly focused. The particles were majorly

`

(over 50%) around 400nm with an overall particle diameter of 554±339 nm; the ELPC particles with 10% lecithin became a characteristic rounded, bowl-like shape with smoother surfaces. Besides the major bowl-like ones, rod-like particles began to form, which were possible to be nano-crystals of excessive lecithin. The particle size was increasing while the distribution was becoming scattered. More particles (about 20%) had the size of 600-800nm than other sizes, the overall diameter was 873±329 nm (60% larger than ELPC particles with 5% lecithin); as the amount of lecithin further increased to 20%, the ELPC particles was becoming much larger and denser than before. The larger bowl-like particles now had more grooves and dents on them. Rod-like particles was obviously increased in the ratio. The particle size distribution was even more scattered with about 75% particles larger than 800nm. The overall particle size was 1079±542 nm, which was almost double the size of the ELPC particles with only 5% lecithin.

3.1.2c Particles with MCT oil

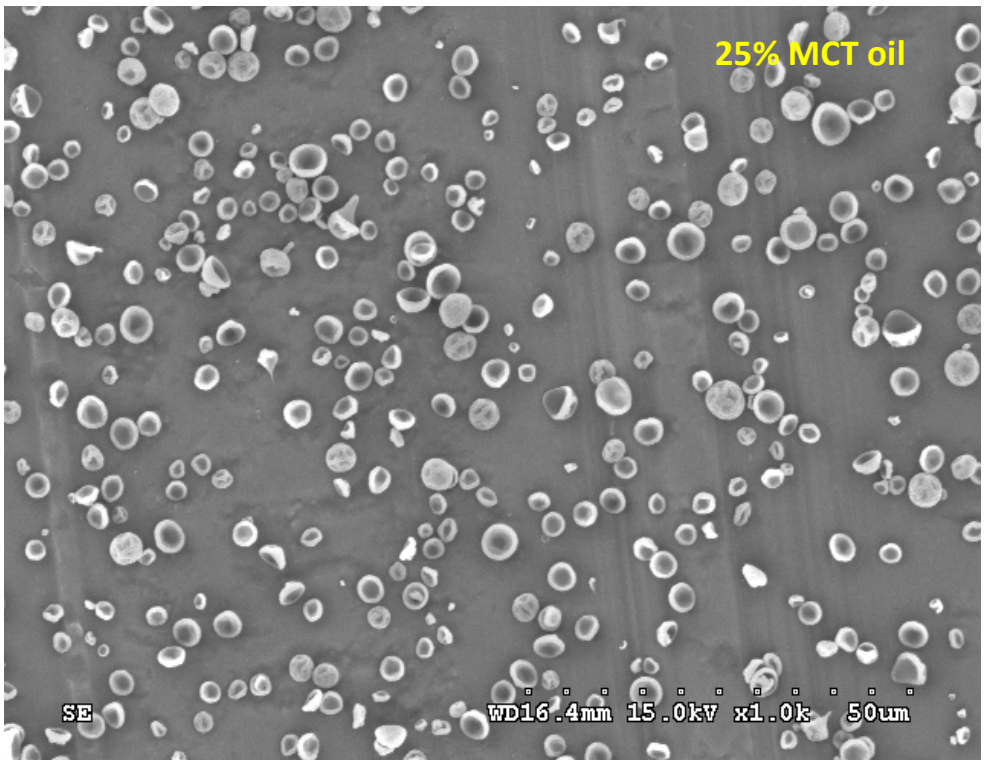

`

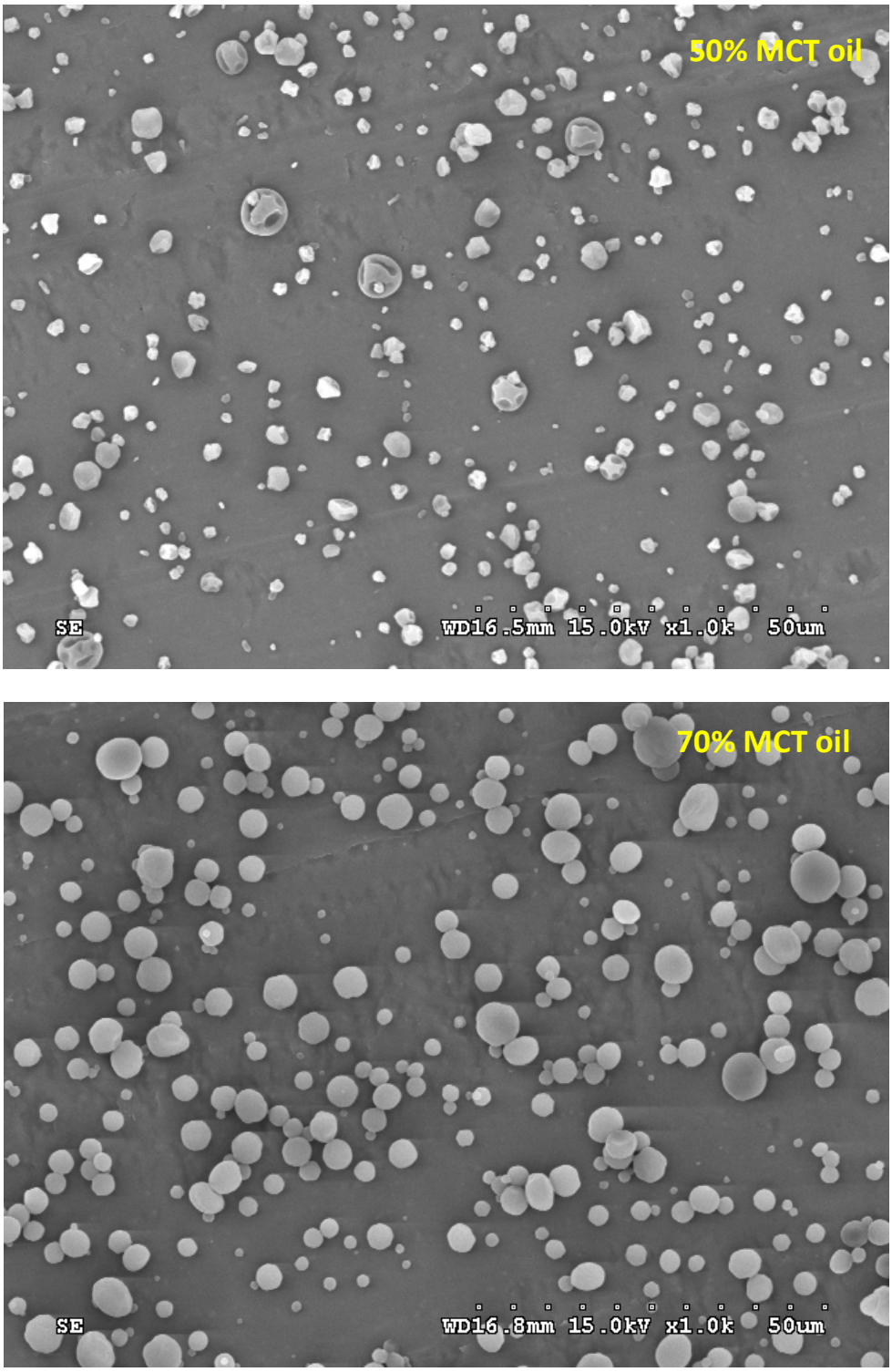

Figure 19. FESEM pictures of the carnosic acid loaded ELPC containing varied amount of lecithin (PC75), from 25% to 70%.

`

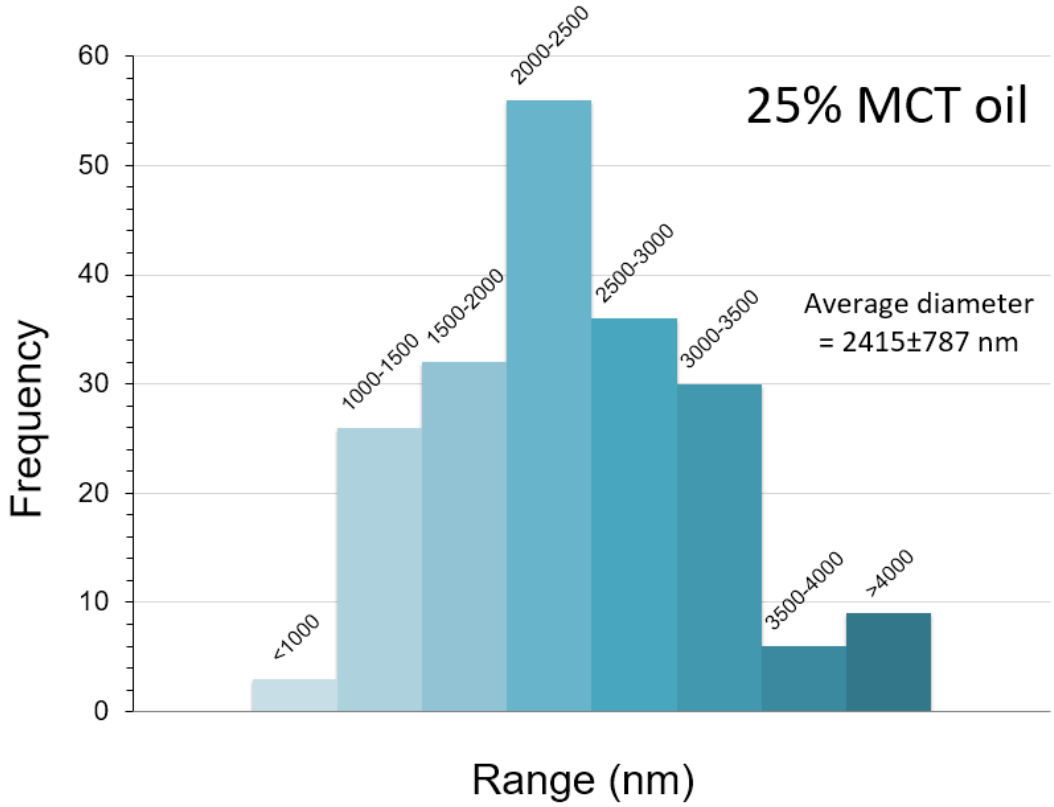
25% MCT oil
Average diameter
= 2415±787 nm
Frequency
Range (nm)
<1000
1000-1500
1500-2000
2000-2500
2500-3000
3000-3500
3500-4000
>4000
0
10
20
30
40
50
60

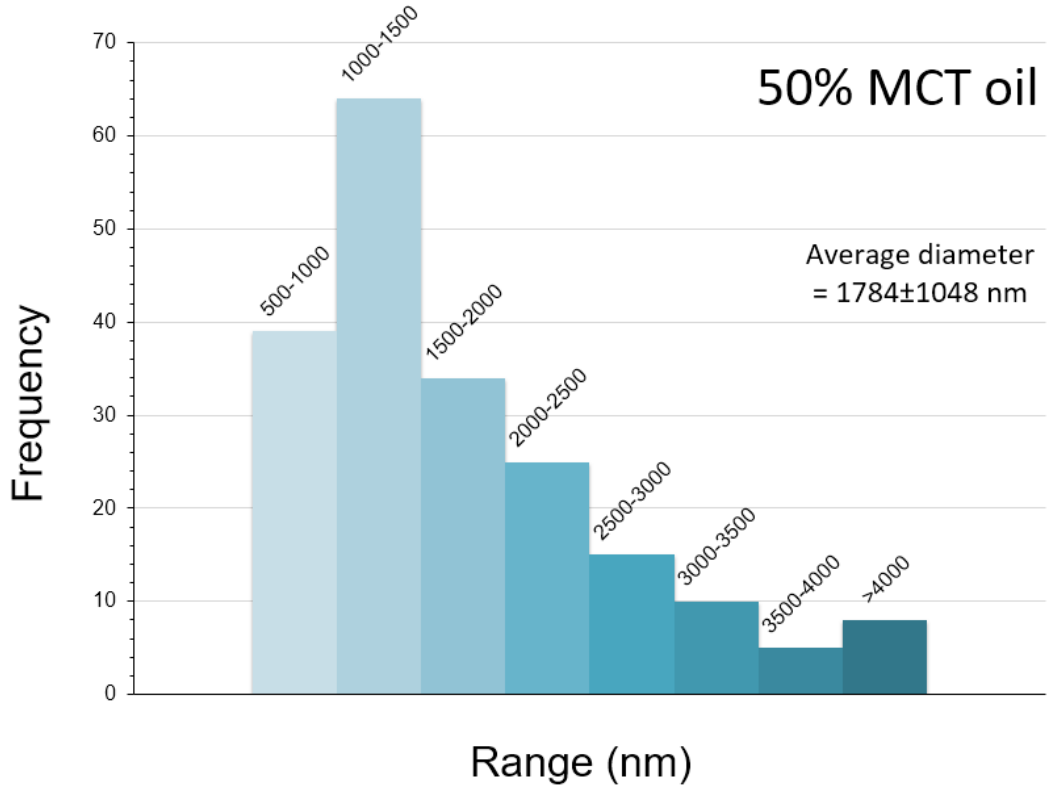
50% MCT oil
Average diameter
= 1784±1048 nm
Frequency
Range (nm)
500-1000
1000-1500
1500-2000
2000-2500
2500-3000
3000-3500
3500-4000
>4000
0
10
20
30
40
50
60
70

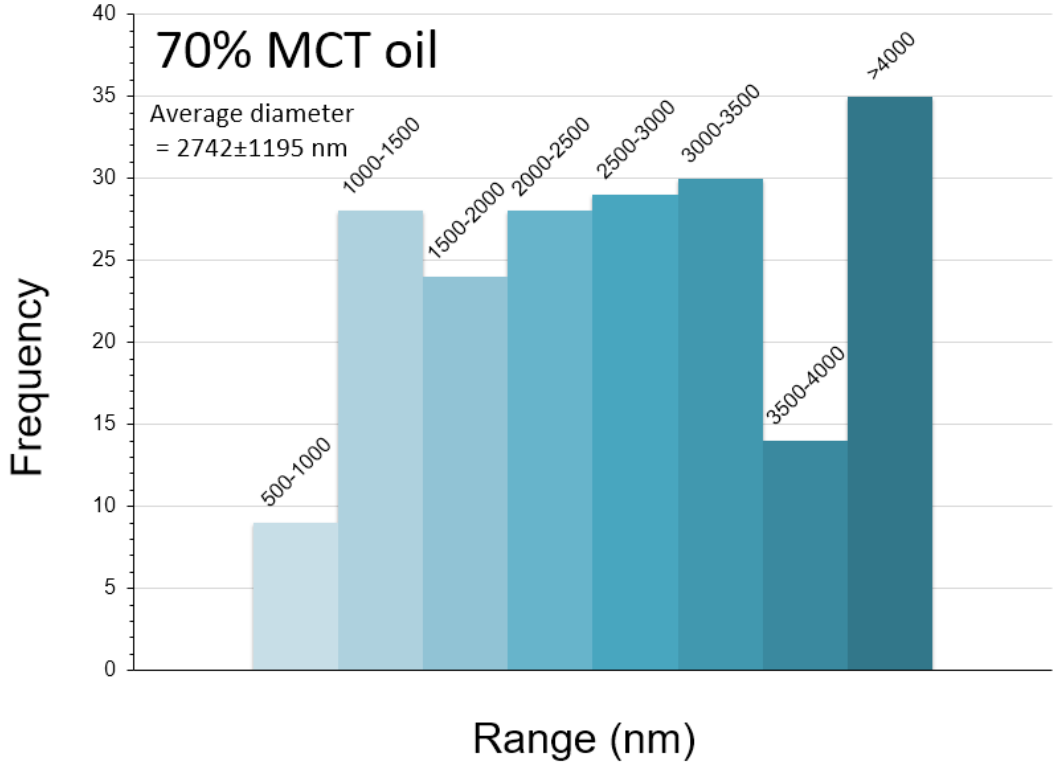

Figure 20. Average diameter and distribution of the carnosic acid loaded ELPC containing varied amount of MCT oil, from 25% to 70%.

For the electrosprayed CA particles incorporated with MCT oil, their overall particle sizes were apparently larger comparing to the lecithin group but still smaller than pure cellulose acetate without additives. This is potentially because the MCT oil molecules were also able to exist in-between the CA polymer molecules (hydrocarbon chain of MCT could interact extensively with the hydrocarbon backbone of the cellulose acetate) thus interrupts the crystallization process of CA. Nevertheless, MCT molecules were not as surface active as lecithin thus unable to reduce the surface energy and dimensions of the electrosprayed CA particles as much as lecithin did.

Unlike the situations in ELPC with lecithin, the particle sizes of MCT oil was not proportional to the increase of MCT oil content within the particles. For the particles with 25% MCT, most of them appear to have the rounded bowl-like morphology.

`

Particle dimension distribution was scattered with average particle size about 2.4μm. More than 25% of particles sized in the range of 2-2.5μm. For the particles with 50% MCT, an apparent reduction of particle size was observed. The data chart displayed that the diameter distribution was focused on 1-1.5μm with average particle diameter about 1.8μm. The SEM picture demonstrated that the typical rounded bowl-like shape was not found in these 50% MCT CA particles. They appear to be irregular but smaller chunks. For the particles with 70% MCT, their morphology underwent another dramatic change. All the grooves and trenches disappeared on the particles. They appeared to be perfect spheres with dimension increased to 2.7μm on average. The particle sizes was highly scattered in the range of about one to four microns.

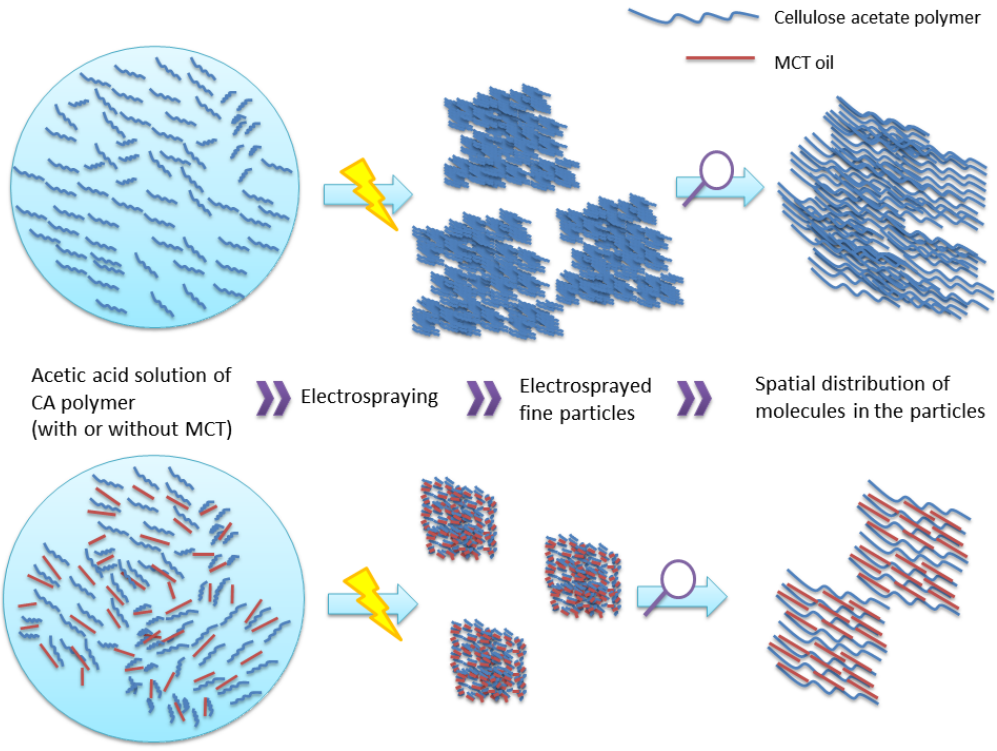

Figure 21. Schematic of electrospraying of CA polymer with or without lecithin

`

3.1.2d Droplet size analysis for the ELPC self-assembled emulsion

A self-assembled nano emulsion generated at the moment when ELPC contacted with water. The emulsion was a mixture of CA polymer molecules, nano droplets of MCT oil and lecithin micelles loaded with carnosic acid and some unchanged ELPC particles. The self-assembled emulsion was prepared by mixing one part of powdery ELPC into nine parts of water with gentle stirring for 5-10 minutes. Then the ELPC emulsion was diluted 5000 times before examination. Cuvettes with one-centimeter path length were used and the laser was set at 658 nm at the scattering angle of 90° for the DLS at 20°C. The result autocorrelation function has an R^2 of 0.9999 and the hydrodynamic radius was approximately 330nm.

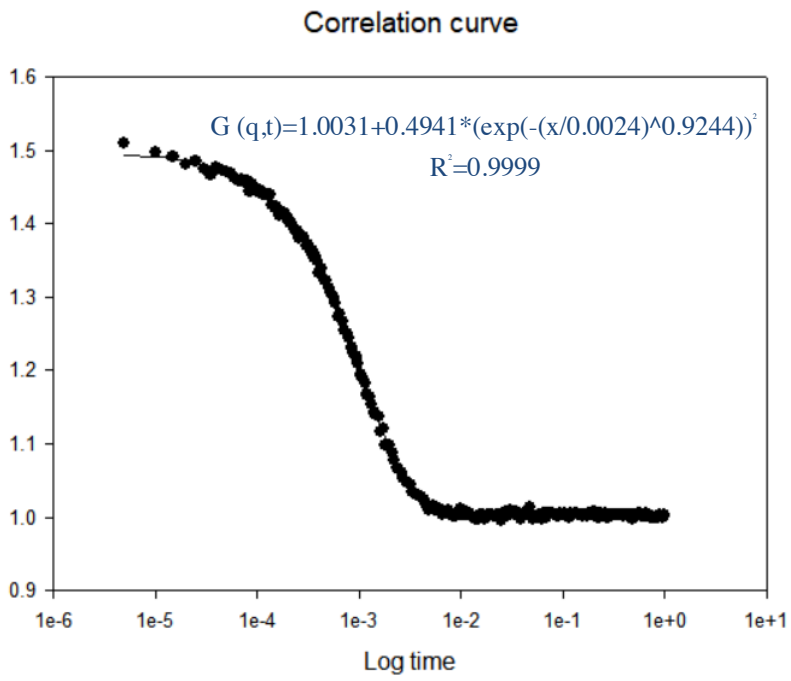

Figure 22. Autocorrelation curve and fitted function

`

3.2 Physical examination of the ELPC

3.2.1 XRD examination

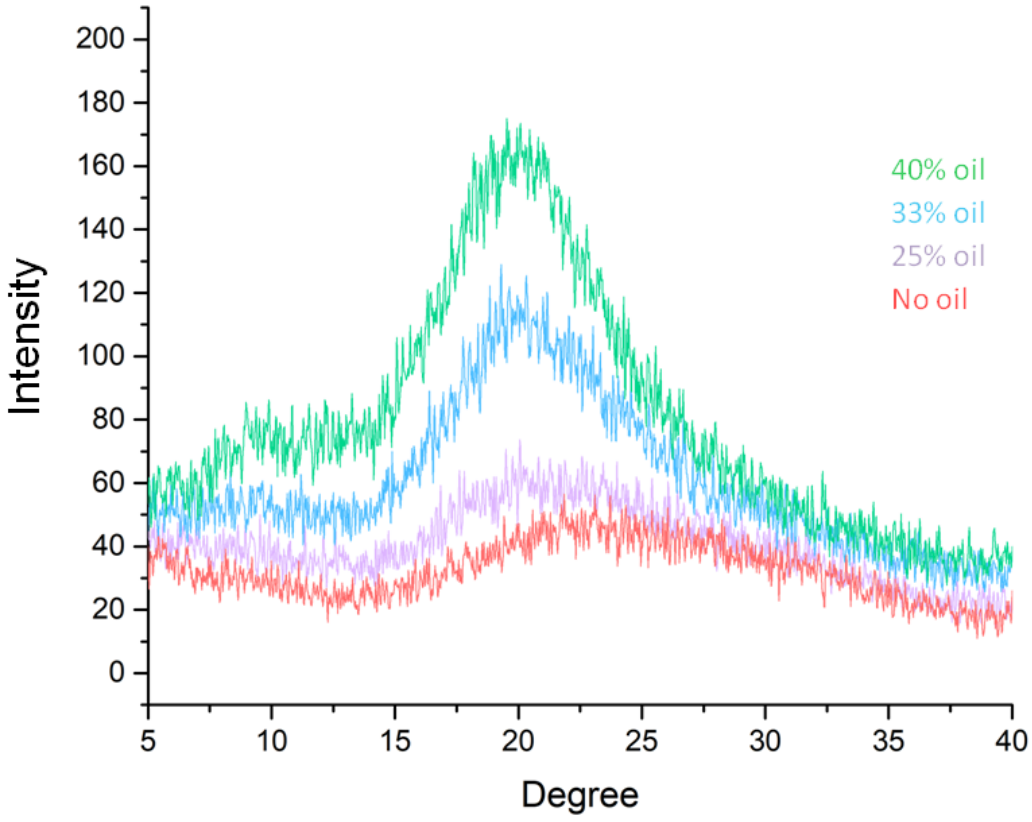

Figure 23. XRD patterns of ELPC with varied oil content

The crystalline properties of ELPC with a gradient content (0-40%) of MCT oil was examined and demonstrated in the figure. Thicknesses of all the ELPC sample pieces were controlled at around 50μm to avoid interferences from thickness variations. As mentioned in the previous project, pure CA powder would return XRD signal that had some sort of crystallinity observed at 8.5, 10.5, 13.5 & 18.0 degrees with diffraction angle of 2θ. The ELPC sample of pure CA only return signals with a large diffraction halo indicating the ELPC backbone was amorphous, which matches with the results studying CA electrospun materials in the previous project. Nevertheless, with addition

`

of oil phase, the crystallinity of ELPC began to change. Diffraction patterns in the chart clearly exhibited that the increase in crystallinity of ELPC was proportional to the elevation of incorporated MCT oil content, from 25% to 40%, with diffraction angle of 2θ at about 20 degrees. This clue indicated either the oil itself or the oil-CA matrix displayed some sort of crystalline structure in the detection range. However, considering MCT oil was in liquid state at room temperature which should be amorphous, these special XRD signals were more possibly generated from the structure of oil-CA matrix that was not reported before. In addition, crystalline pattern was not detectable for the carnosic acid loaded within the ELPC, which should have fairly strong signals. This suggested that the carnosic acid was in a highly amorphous state existing in the ELPC, the electrosprayed material was proved to be evenly fabricated without leaving chunks of residues of carnosic acid.

`

3.2.2 FTIR examination

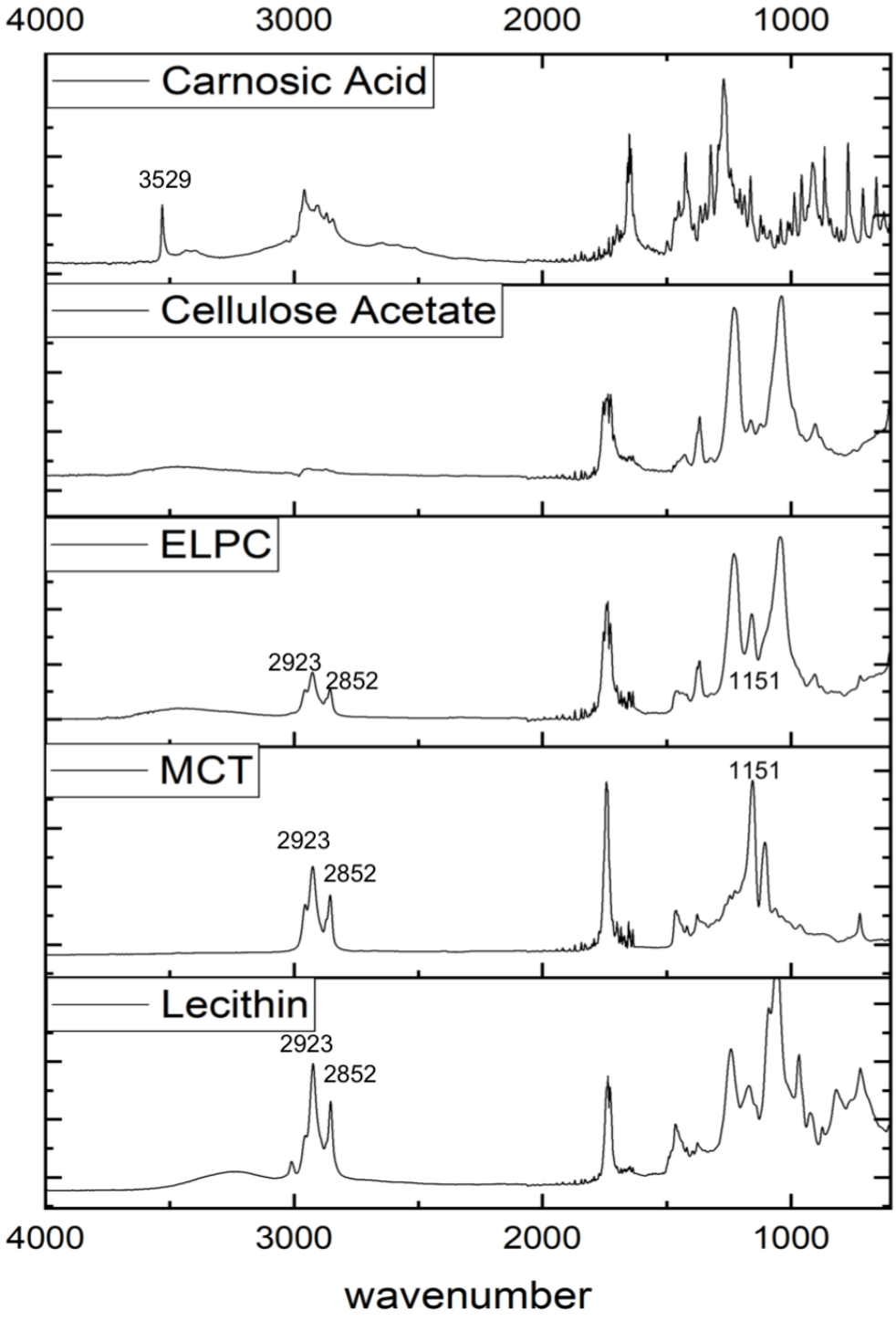

Figure 25. FTIR spectrums of ELPC and its components

`

Information on changes in functional groups situations for the ELPC was examined by FTIR. Carnosic acid crystal has a fingerprint pattern region at the wavenumber range from 400 - 1800 cm^{-1}. Nevertheless, these fingerprint signals disappeared in all the ELPC loaded with carnosic acid, which was the same as the previous research and other literatures reported.[90-91] Besides, carnosic acid molecules in crystalline state had a characteristic FTIR peak at 3529 cm^{-1} representing the free O-H stretch of the carnosic acid molecule. This signal was also not found in any of the ELPC FTIR spectrums. Together with the information provided by the XRD chart above, they manifested that carnosic acid molecules are evenly distributed and interacted with the massive cellulose acetate network within the ELPC instead of interacting with each other like in the carnosic acid crystals. Both lecithin and MCT oil were rich in aliphatic hydrocarbons, indicated by the strong FTIR peaks at 2923 and 2852 cm^{-1} for the alkyl C-H stretch on the spectrum above and as reported before.[92] These C-H stretch signals were found in the CA ELPC with lecithin and ELPC with lecithin plus MCT oil. The alkyl C-H stretch signal was prominently stronger for the ELPC with both lecithin and MCT than only with lecithin. These clues were potentially correlated with the fact that the lipids in the ELPC existed in some degree of crystalline form. Broad O-H stretch at the wavenumber 3200 - 3600 cm^{-1} was observed in the IR spectrum for lecithin PC75, nevertheless it was principally caused by moisture in the lecithin (can be eliminated by drying) but not intermolecular hydrogen bonding. However, this signal was significantly weakened when lecithin was incorporated within ELPC, implying that intermolecular hydrogen bonding was not a major interaction within the ELPC. Hydrophobic interactions and Van der Waals forces were dominant interactions inside the massive ELPC matrix.

`

3.3 Functional characterizations for the ELPC

3.3.1 ORAC Anti-oxidation activity of carnosic acid

The anti-oxidative capability of carnosic acid was expressed as equivalent ORAC value. Firstly, the assay was carried out on the reference compound Trolox. The relative intensity of Trolox with designed concentration gradient was plotted. The differential area between the two curves for each Trolox concentration and the AAPH+ was integrated and then plotted to be the standard curve for the anti-oxidative capability of Trolox which has an R^2 of 0.9961. Secondly, the assay was carried out on the sample compound carnosic acid. Again, the relative intensity of carnosic acid gradient concentration was plotted. The differential area was integrated and then plotted to be the calibration curve representing the anti-oxidative capability of carnosic acid. ORAC value for carnosic acid was calculated by differential area for carnosic divided by the specific differential area for Trolox at the same molarity. Finally, the ORAC equivalent value for CA was calculated as 6.34 ± 2.46 μM equivalent Trolox / μM carnosic acid.

3.3.2 In vitro tyrosinase inhibitory assay of carnosic acid

Tyrosinase inhibition activity was plotted against the increase of carnosic acid/kojic acid concentration as the figures demonstrated below. The IC_{50} inhibition value of kojic acid was calculated as 0.376mM while the IC_{50} for carnosic acid was 1.532mM, which means carnosic acid was effective in tyrosinase inhibition and skin whitening, but not as strong as the industrial standard. These properties were related to the potent antioxidant activity of carnosic acid.

`

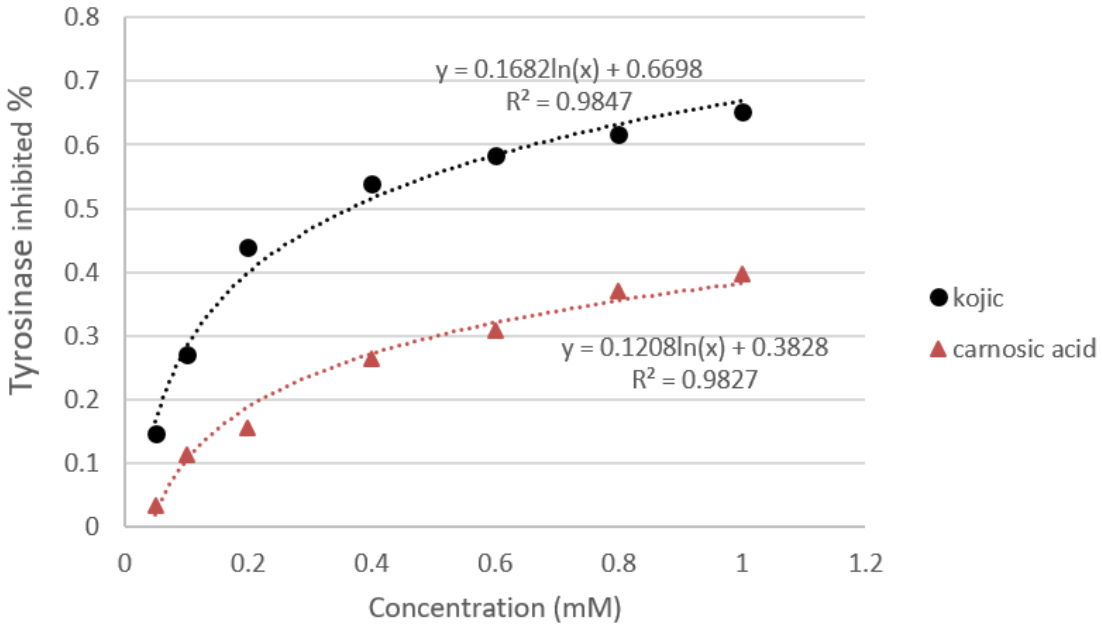

Figure 26. Tyrosinase inhibition activity of carnosic acid and kojic acid

In order to determine the type of enzyme inhibition for the carnosic acid-tyrosinase interaction, a Lineweaver-Burk plot was conducted. Through increasing the concentration of carnosic acid, the lines crossed at the same intercept of the Y-axis. The slope of the lines was increasing with the elevation of carnosic acid concentrations. These results mean that the Km was increased and the Vmax was unaffected accompanied with the increase of carnosic acid concentration, which implied that the enzyme inhibition type was competitive.

`

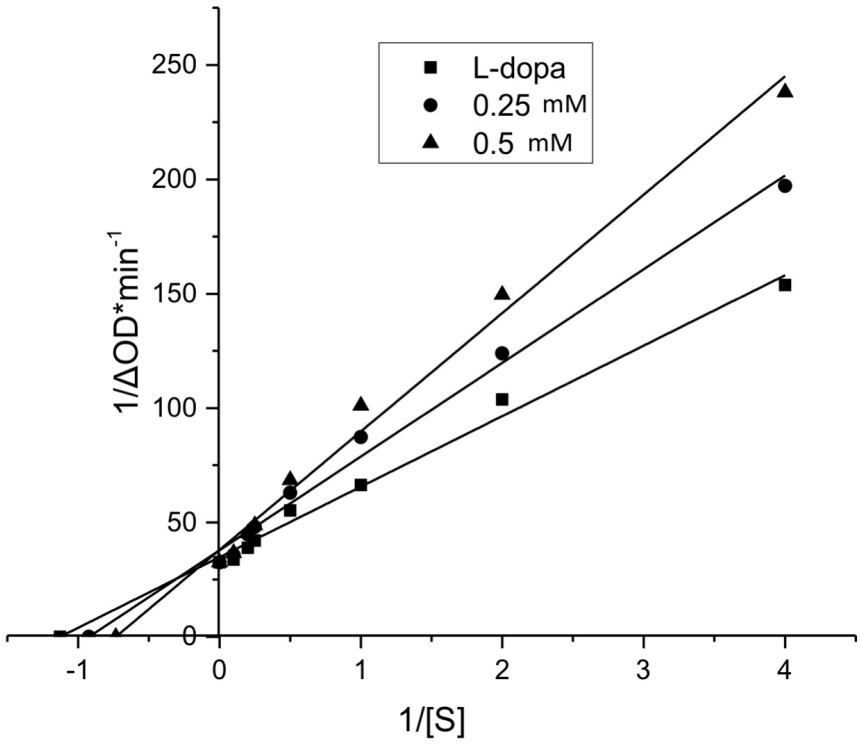

Figure 27. Lineweaver-Burk plot for DOPA oxidation with tyrosinase under the effect of carnosic acid at varied concentrations

3.3.3 Secondary structure observation for tyrosinase by circular dichroism

Secondary structure changes of tyrosinase before and after interacting with carnosic acid and the reference compound kojic acid was examined with far-UV circular dichroism. Negative bands at 208 and 222nm were observed for the tyrosinase samples, which was able to imply the structural information of α-helixes.[93] Both carnosic acid and kojic acid were able to reduce the signal intensity around these two characteristic bands without shifting, which manifested that the α-helix related structure was affected or decreased. Distribution of other secondary structure components including the amount of β-sheets, β-turns and other unordered structures (random coils) were analyzed by program CDSSTR reference set 4 (optimized for 190-240nm far UV region) offered by DichroWeb. [94-96]

`

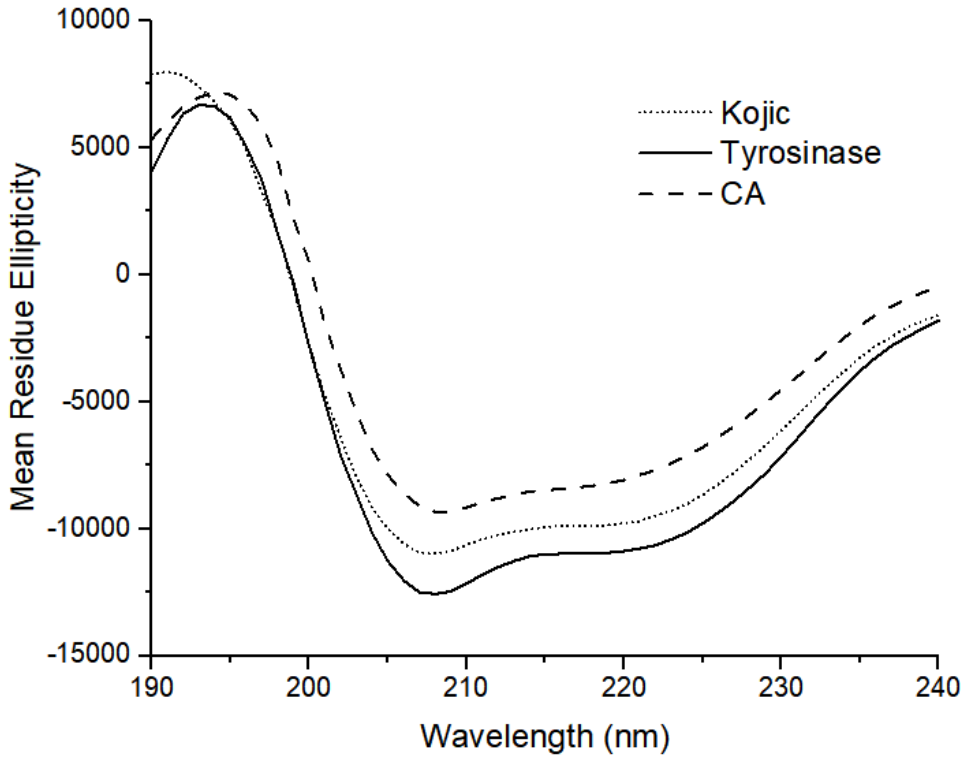

Figure 32. CD spectrums for tyrosinase before and after interaction with carnosic acid and kojic acid

	Tyrosinase	Kojic acid	Carnosic acid
Helix	35%	20%	17%
Strand	17%	23%	27%
Turns	22%	26%	25%
Unordered	28%	31%	31%

Table 1. Secondary structure element distribution for tyrosinase, tyrosinase with kojic acid and tyrosinase with carnosic acid[96]

`

By comparing to the free tyrosinase, the alpha helix structures decreased about 43% for the tyrosinase interacted with kojic acid and 51% with carnosic acid, which matched with the observations on the circular dichroism spectrums. In addition, carnosic acid caused a 59% increase in strands of the tyrosinase while 35% increase kojic acid. Carnosic acid and kojic acid turned large amount of the helical structure of tyrosinase into less ordered structures. Nevertheless, they did not cause significant increase in the unordered structure of tyrosinase, indicating that the structure disruption was not severe. These figures potentially implied that both carnosic acid and kojic acid inhibit the enzyme activity by interrupting amino acid H-bonding and thus changing the α-helixes to β-sheets, turns and other lower order secondary structures.

3.3.4 Franz-cell topical delivery assay

Topical delivery capability of the carnosic acid loaded ELPC was examined by the Franz-cell diffusion assay against pigskin. After diffusion, the surface-cleaned pieces of pigskin were extracted and carried to the HPLC for detection. Results were demonstrated in the figure below.

`

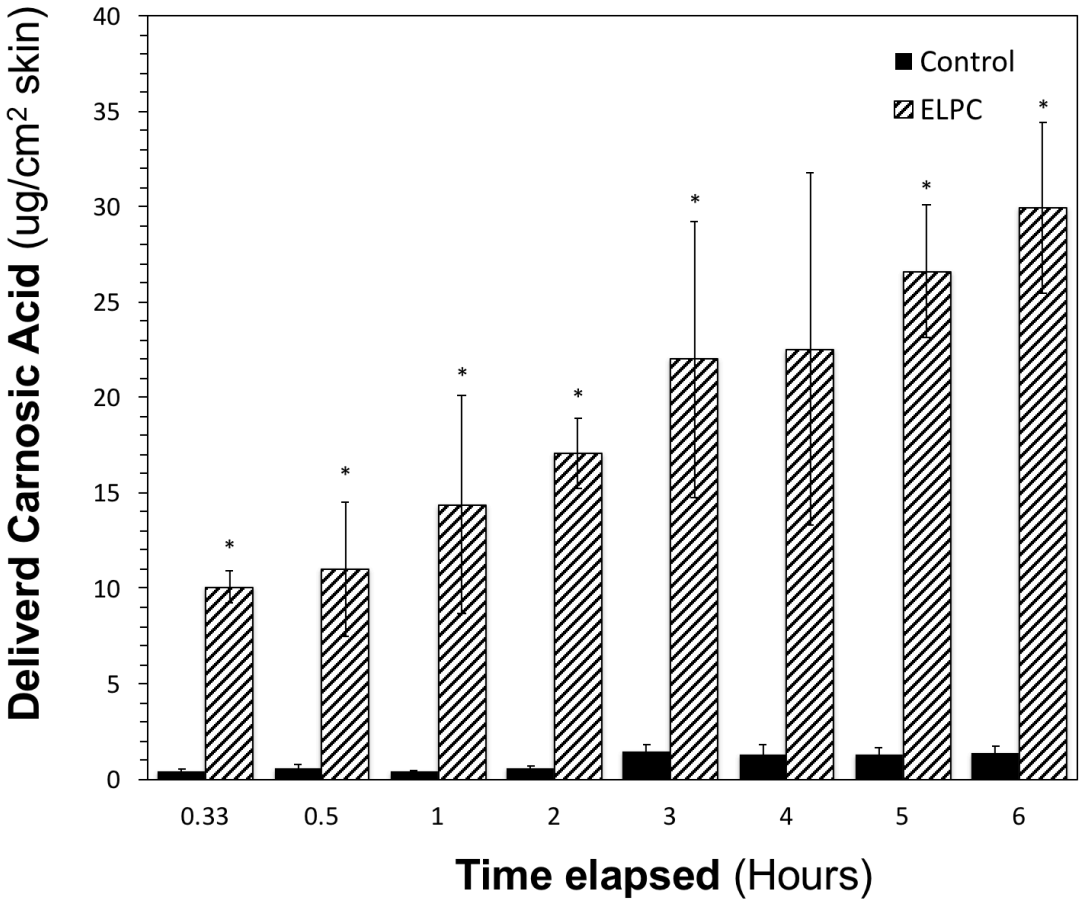

Figure 29. Topical delivery profile of carnosic acid loaded ELPC and the control (*: P<0.05)

From the chart of topical delivery profile, ELPC exhibited prominent performance in carrying carnosic acid into the pigskin. The EPLC was able to generate self-assembled nano emulsion with the moisture release from above the skin. This locally formed nano emulsion was able to carry the active compounds into the skin efficiently. The assay was arranged to stop at 6 hours without further data collection because pigskin as an animal tissue subjected to degradation over time. At the end of the assay, ELPC was able to deliver a total of 1.85μg/cm^2 skin of carnosic acid which significantly

`

outperformed the control carnosic oil solution. The topical delivery performance of ELPC was substantiated.

Kinetic models	Fitted equations	R^2
Zero order	$Q_{\%}=0.0043t+0.0128$	0.9799
First order	$\ln Q_{\%}=0.183t-4.2731$	0.9344
Hixon-Crowell	$(1-Q_{\%})^{1/3}=-0.0015t+0.9957$	0.9803
Higuchi	$\mathbf{Q_{\%}=0.013t^{1/2}+0.0048}$	**0.9837**
Korsemeyer-Peppas	$Q\%=0.0184t^{0.3679}$	0.9826

Table 2. Model fitting for the ELPC release profile of carnosic acid against pig skin

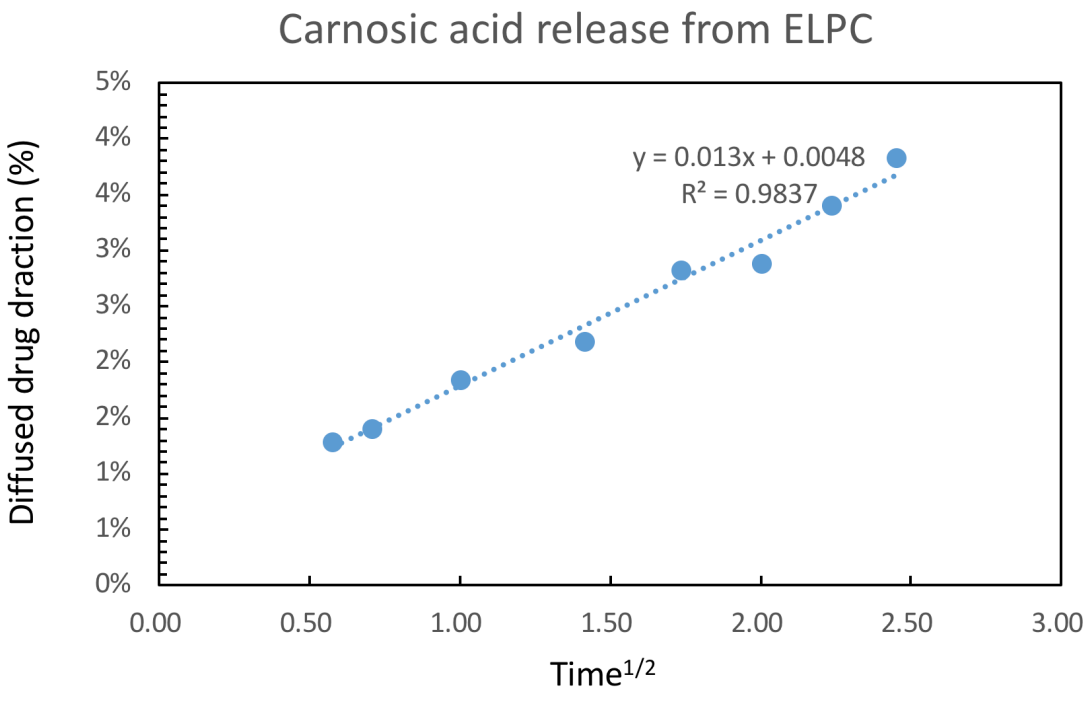

Figure 30. Carnosic acid release from ELPC against the square root of time, fitted with Higuchi model of drug diffusion

`

The topical delivery profile of ELPC was further fitted with several drug diffusion kinetic models. From the value of R square, we can see that this profile was closest to Higuchi model. In this case, the drug transport was driven by Fickian diffusion. Higuchi model is derived from Fick's law against the square root of time, it hypothesizes for the situations that the drug chemicals loaded in the formulation is much higher than its solubility of in target system. Higuchi model was effective in analyzing and predicting the drug transport amount over time for situations like transdermal patches, topical ointment films and similar systems and it is proven suitable here for describing the ELPC topical release of carnosic acid. [97-98]

3.3.5 CLSM visualization of ELPC toppical delivery

Franz-cell diffusion assay was able to accurately quantify the amount of carnosic acid deposited topically and inside the skin. Nevertheless, it was unable to discern where and how deep the active compound can reach inside the skin. It was important to determine the accumulation area and speed of the active compound loaded formulation because the carnosic acid had to be carried into the melanocytes in the basal cell layer (in between the epidermis and dermis) to start inhibiting tyrosinase activity, reducing the generation of melanin thus whiten the skin. Here are the CLSM pictures for the ELPC formulation distribution within the pigskin after the diffusion experiment.

`

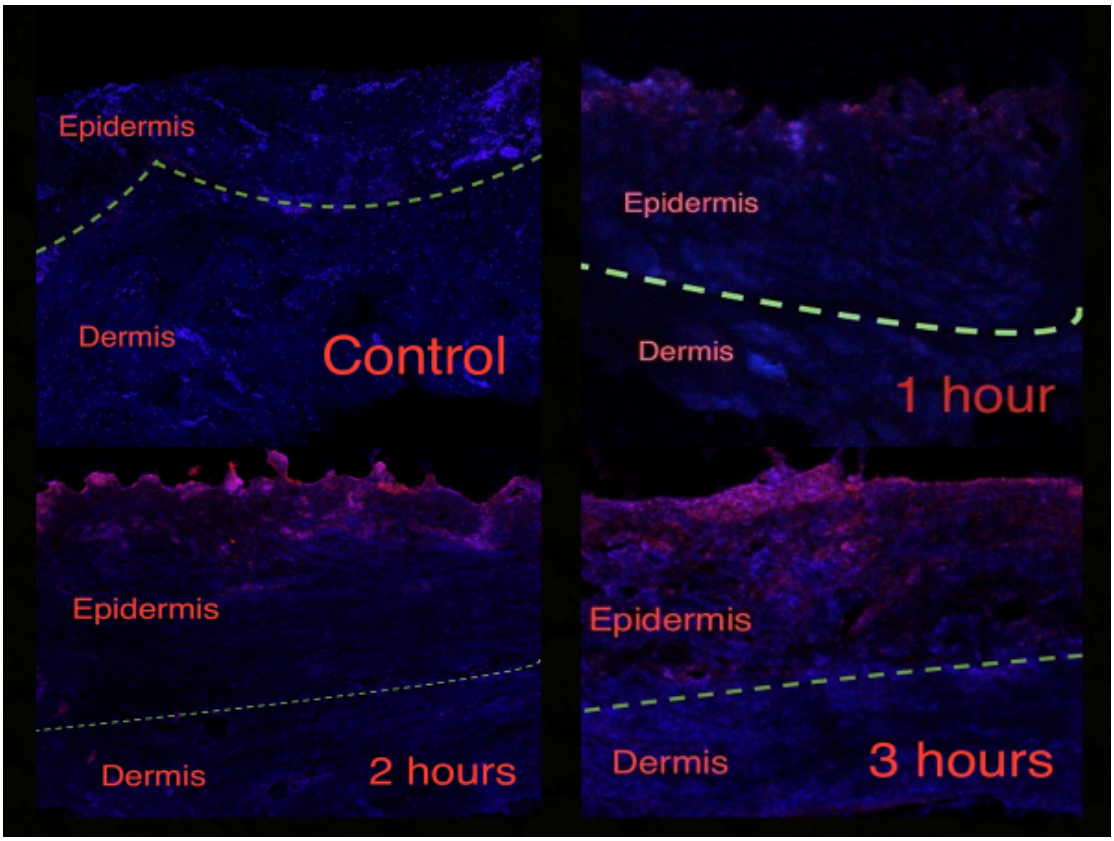

Figure 31. Topical delivery of ELPC formulation overtime

In the CLSM pictures, a red color was utilized to indicate the fluorescent labeling agent Nile Red within the self-assembled nano emulsion generated from the ELPC; a blue color was utilized to indicate the fluorescent dye DAPI to visualize the cells and tissues of the pigskin. The accumulation and migration of ELPC generated formulation was clearly observed. For the first two hours, the formulations start to accumulate to higher and higher amount in the stratum corneum around the top area of epidermis without apparent penetration. At the time of three hours, the distribution of Nile Red could be observed throughout the epidermis, which means the carnosic acid loaded formulation reached the basal cell layer where the melanocytes existed. At six hours of the topical delivery process, the accumulation of Nile Red in the epidermis was apparently less than that of the three hours. Nevertheless, this phenomenon was due to further penetration of the carnosic acid loaded formulation into the dermis layer of the

`

skin, which could be observed in the last picture. A lot of detail information in topical delivery status demonstrated was revealed by CLSM imaging, which was unable to be determined only by quantifying the total carnosic accumulation in the skin.

3.3.5 MTT assay for carnosic acid

In the above section, CLSM examination proved that ELPC was able to bring the carnosic acid formulation to the area of melanocytes. As a result, the final imperative step for the active compound to take effect as a skin-whitening agent was to be able to enter the melanocytes. In order to substantiate this process, an *in vitro* cellular uptake study was designed. Before the evaluation of cellular uptake efficacy, a MTT assay was prerequisite to find out the safe dosage for applying the active compound without significantly inhibiting cell growth (>90% cell viability). Moreover, in most situations, the growth speed of normal cell lines is fairly slow. Therefore, their corresponding cancer cell-lines are frequently utilized to investigate the safe dosage. In this research, B16F10 mice melanoma cell line was adopted to investigate the safety dosage of carnosic acid.

Nevertheless, carnosic acid has a unique mechanism that interrupts the growth of B16F10 melanoma cells. It was reported that carnosic acid interfered the process of melanoma cell adhesion by suppressing the production of vascular cell adhesion protein (VCAM-1).[99] As a consequence, the MTT assay data shown below demonstrated very limited cell viability against pure carnosic acid.

`

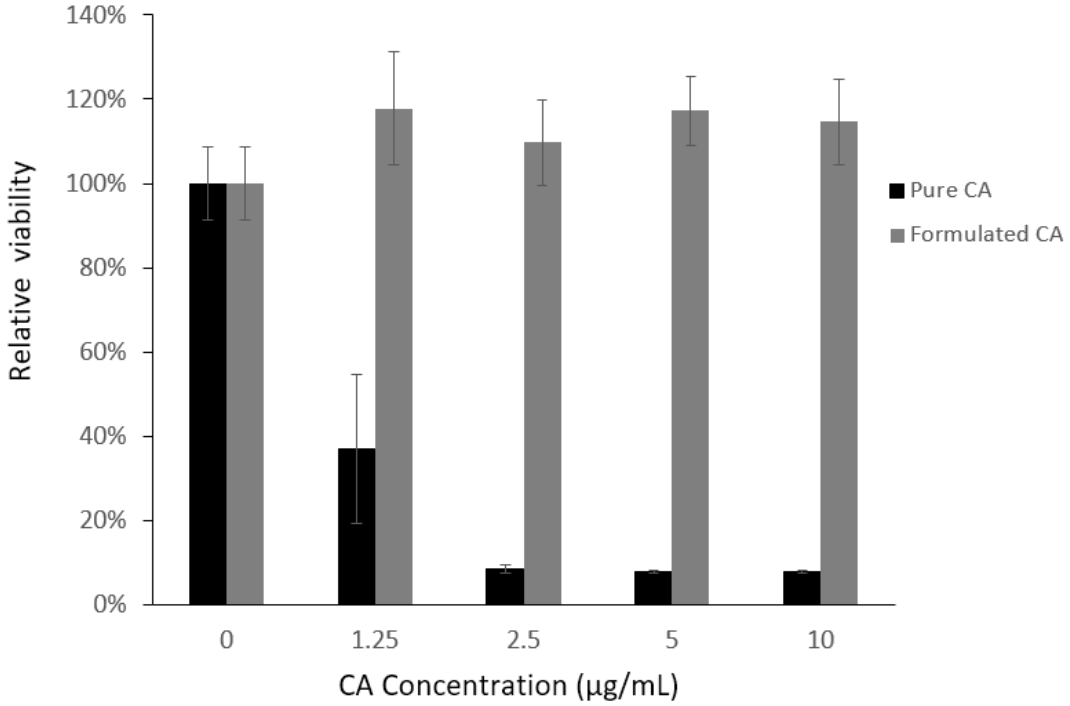

Figure 32. MTT assay for pure CA and formulated CA

But fortunately, when carnosic acid was loaded in the self-assembled nano emulsion generated from ELPC, its effect on interrupting melanoma cell attachment was not discernable. This is demonstrated by the MTT assay for formulated carnosic acid in figure 32. This may be possibly due to the formulation concealed the carnosic acid molecules from the VCAM-1 signaling proteins thus the normal melanoma cell growth was not interrupted.[100] As a result, formulated carnosic acid up to 10 µg /mL was confirmed safe for the cellular uptake study that mimics the real situations in human skin.

`

3.3.6 B16F10 melanoma cellular uptake

After confirming the safety dosage range by the MTT assay above, a carnosic acid-loaded self-assembled nano emulsion generated from ELPC with fluorescent dye was diluted to 1.25 μg/mL to ensure a safe cellular uptake process. ELPC nano emulsion was added to B16F10 melanoma cells for a series of time period generally in accord with the time arrangement for Franz-cell pigskin diffusion assay. In order to create comparable CLSM images, capturing parameters were carefully tuned and kept the same throughout the whole imaging process. 405nm and 458nm laser beams were adopted for exciting and visualization of DAPI and coumarin-6 dyes independently without interfering or bleeding through. Laser power of 405nm was set to 0.03 while for 458nm it was set to 0.025 for more balanced visualization and less noise. Pinhole was set to 64.2 units to scan 17.9μm of section. For the DAPI channel, gain was set to 575 units while for the Nile Red channel the gain was 776. The captured images were displayed as below.

`

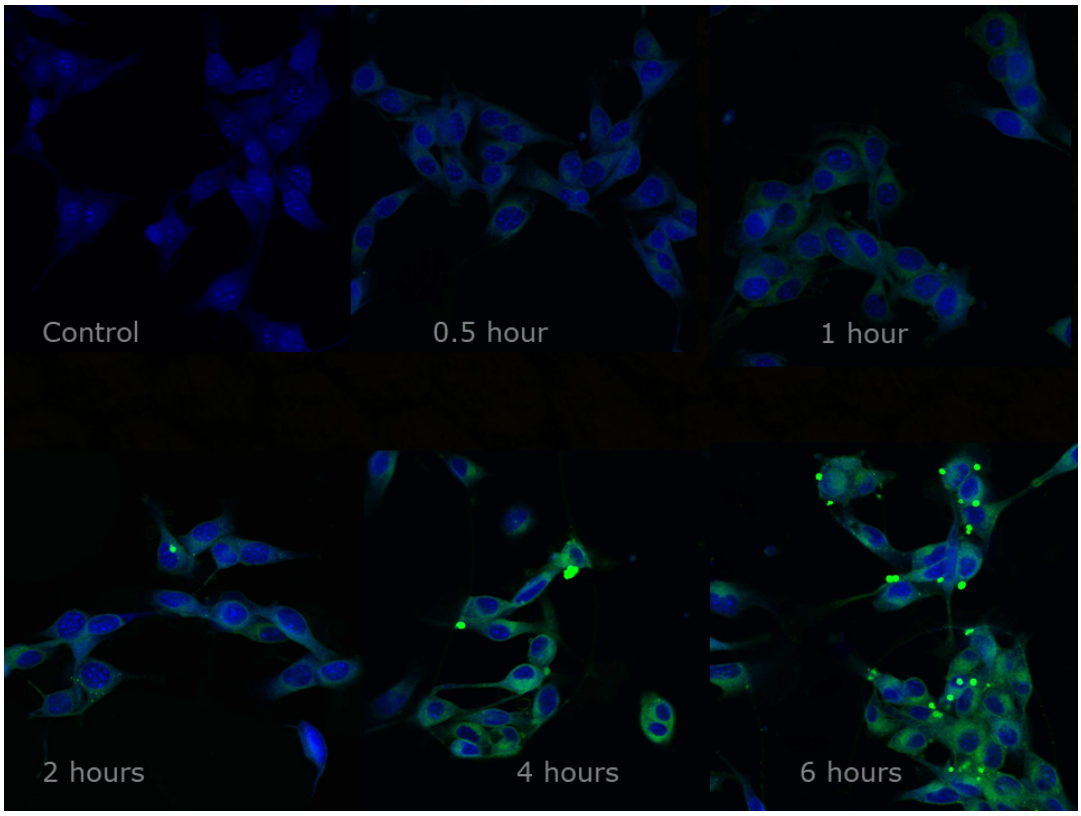

Figure 33. CLSM image for B16M10 cellular uptake of formulation at each time point

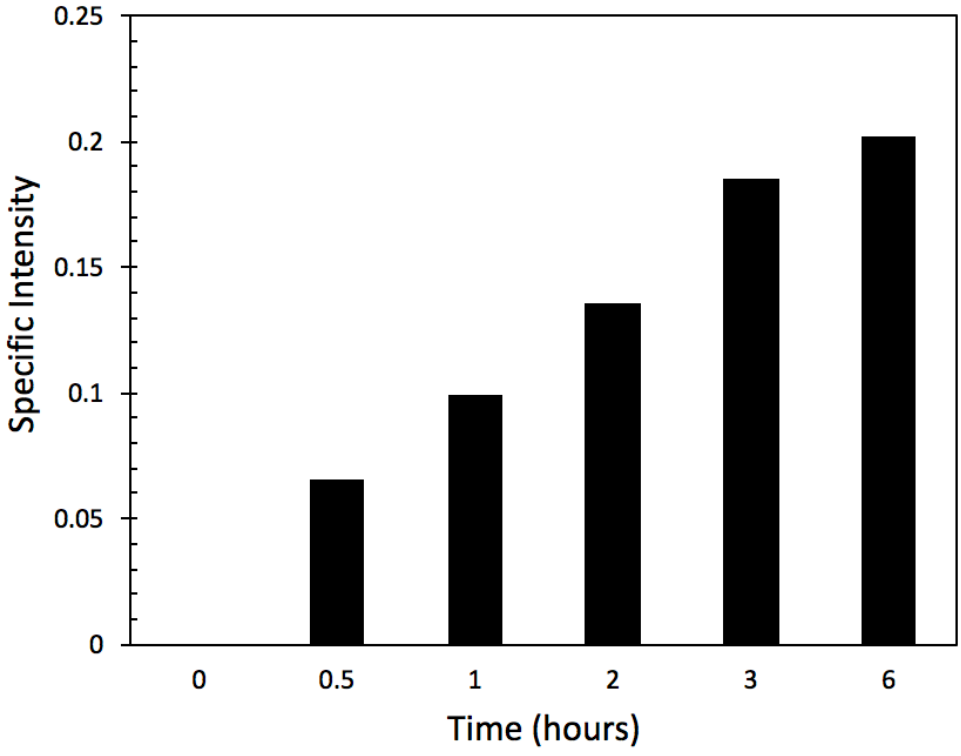

Figure 34. Accumulation of formulation over time

`

The CLSM images demonstrated the B16F10 cellular uptake in high resolution. Accumulation of carnosic acid formulation was clearly observed to exist in the cytoplasm of each melanoma cell. From the beginning to three hours of uptake experiment, increase in the accumulation of the formulation was fairly visible as the green channel of coumarin-6 became brighter and brighter. At three hours of experiment, crystallization of the formulation began to appear right at the boundary area of the cell membranes, indicating the melanoma cells cellular uptake reached equilibrium. It was highly possible that the crystals were formed by cell exocytosis but not by breaking of the formulation because these crystals only exist at the membrane of the cells. The picture of uptake at six hours verified the assumption that the cells were already saturated with the formulation because the green channel had almost the same intensity as displayed in the three-hour uptake picture. Besides, apparently more crystals appeared at the cell membrane area indicating cell exocytosis was becoming more active over time. To summarize, melanoma cellular uptake for the carnosic acid loaded formulation generated by ELPC was successful and in a fast pace, it took only around three hours to reach the equilibrium level of uptake.

In addition, the actual accumulation amount of carnosic acid loaded formulation from ELPC was semiquantitatively analyzed by Fiji software. Firstly, coumarin-6 channel was used in determination of the total fluorescence intensity. Images of coumarin-6 channel for each time interval were firstly subtracted background and then measured the fluorescence intensity in the whole canvas. Then, the DAPI channel was utilized to count the number of nuclei which equals to the number of living cells. Specific fluorescence intensity was determined as total intensity divided by number of cells, which semiquantitatively measured the amount of formulation went into the cytoplasm of the B16F10 melanoma cells.

`

4. Conclusion

In this project, a novel type of lipid delivery system called electrosprayed lipid-polymer complex was established for the first time. It was substantiated to be capable of achieving topical delivery of carnosic acid, a water-insoluble active phytochemical with the ability of anti-oxidation and tyrosinase inhibition, to the area in between epidermis and dermis (basal cell layer) where the melanocytes located, to achieve skin-whitening effects. SEM characterization of ELPC found the addition of lecithin and MCT oil in varied concentrations had highly diverse effects on the appearance and diameters of the nanoparticles. CLSM results proved the self-assembled nano emulsion generated from ELPC could reach particle sizes as small as around 200nm. X-ray diffraction discovered some structural information of the oil phase existing within the ELPC, which was in a status in between amorphous and crystalline. FTIR spectrums of the ELPC implied that hydrogen bonding was not the major interaction within ELPC components. Their detail special distribution and interactions remained valuable to be further researched. ORAC anti-oxidative value assay confirmed the free-radical scavenging power of carnosic acid which supported the theory of its tyrosinase inhibition activities. A key step in evaluating the skin-whitening potential of a compound, the tyrosinase inhibition assay was carried out against carnosic acid. It was found that carnosic acid could inhibit tyrosinase with an IC50 value of 1.532mM which was higher than the kojic acid (0.376mM) as a widely accepted skin whitening agent. A Lineweaver-Burk plot further implied that the inhibition belonged to competitive type. Carnosic acid was proved to interrupt the secondary structure of tyrosinase by reducing alpha helixes of the tyrosinase and increasing the more unordered structures by circular dichroism analysis. Franz-cell diffusion assay for the carnosic acid loaded ELPC was performed against pig shoulder skin. It substantiated that ELPC was highly

`

capable of delivering carnosic acid in the topical route which was significantly outperformed the oil solution of carnosic acid at the same quantity. Cryo-slicing and CLSM imaging further substantiated that the formulated carnosic acid reached the target site of delivery—basal cell layer where melanocytes attached in just three hours. Cellular uptake CLSM images visualized the formulation within the cytoplasm of melanoma cells, which was the final key step to substantiate that ELPC was potent in assisting topical delivery of carnosic acid and achieving skin-whitening effects.

`

Chapter III: Studies on a GRAS Electrospun Lipid Gelatin Complex Encapsulated with Tetrahydrocurcumin

1. Background

Electrospun lipid-polymer complex (ELPC) was a novel type of delivery system generated by electrospinning/spraying in a one-step process. It combines structural polymers, various types of triglycerides, surfactants and active compounds together and, because it was atomized to down to nano scale, it was capable of generating self-assembling nano emulsions once it contacts with water. Therefore, it has high potential in becoming a popular industrial processing technique and delivery system for overcoming the shortcomings of many flavonoids and beneficial phytochemicals, including limited water solubility, bioaccessibility and bioavailability prone to environmental impacts like oxidation. Other than encapsulating active compounds to be made into dietary supplements or functional foods, ELPC could also encapsulate flavor chemicals and was capable of instantly emulsifying itself into beverages, pastes and even some solids like soft gelatin candies with various kinds of flavors. The fully natural-originated food grade ELPC discussed here in this research project utilizes all GRAS material during the fabrication process, including gelatin as the structural polymer, lecithin PC75 as the surfactant, medium chain triglycerides (MCT) as the oil phase and tetrahydrocurcumin as the GRAS active phytochemical. Environmental friendly and non-toxic solvents were utilized in the electrospinning process, currently limited to acetic acid and water. The residue amount of acetic acid was extremely low and was certainly safe for human consumption and met the FDA requirements.

Preparation of ELPC requires a high voltage electric field (15,000V~20,000V) in order to squeeze the polymer blend solution into ultrafine strands of fluids and

`

evaporate the solvents. Nevertheless, the electric current is very low during the fabrication process so in fact electrospinning does not consume high energy and generate large amount of heat like the other types of atomization techniques (spray-drying, high pressure processing, etc.) do. The efficiency of ELPC production have a great potential in benefiting the current food, cosmetic and other emulsion production related industry by reducing their energy and time cost during production. For example, when fabricating gelatin soft candies, manufacturers have to apply high heat and shear to completely dissolve their gelatin and other polymeric raw materials. After that, the gelatin solution has to be cooled down to some degree to avoid degrading the flavor and other additives of the candies during mixing and molding. This cooling process is time consuming and delayed the production speed. Nevertheless, if the manufacturer changed to use ELPC to produce the candies, it saves them a lot of time, efforts and most importantly, lowering the cost. ELPC utilizes glacial acetic acid as solvent, therefore it dissolves gelatin much faster and require much less heating (60 degree Celsius is enough). Many compatible key additives, like pigments and flavors could be added to the ELPC before electrospinning. More importantly, the candy manufacturers don't need to prepare ELPC by themselves. ELPC can be fabricated by stand-alone formulation factories and store in dry film conditions by simple vacuum packaging processing. The candy manufacturers just need to purchase the ELPC films and readily dissolve them in water and then a solution of gelatin with emulsified flavors, pigments and other additives is prepared in a one-step process. The high cost on heating and dissolving gelatin and other related cost are significantly reduced and profits will be elevated by increased efficiency in production processing. ELPC could also defines a sub category in formulation production industry and which has high economic potential to boost the whole food industry.

`

Tetrahydrocurcumin (THC) is a white color curcuminoid partially reduced from curcumin and is one of the major curcumin metabolite detected in the intestine and liver area within human and rat under hepatic, intestinal or colon bacterial metabolisms (related with NADPH-dependent curcumin reductase).[101] In detail, C. R. Ireson et al. studied and discussed on curcumin metabolism fate against subcellular fractions (cytosol and microsome) from human tissues and also intact rat intestines, which was one of the very first researches on curcumin biotransformation. They detected bio-reduced metabolites of curcumin including sulfates, tetrahydro- and hexahydro-curcumin in the cytosol and glucuronide conjugated metabolites in the microsome. In addition, sulfating metabolic activity of curcumin majorly occurred in the liver tissue while glucuronide conjugation mainly happened in the intestine, especially the colon.[102]

THC is a curcuminoid compound with multiple bioactivities especially the anti-oxidative property. It is the most potent antioxidant in the family of curcumin derivatives substantiated by a series of anti-oxidative assays including linoleic acid autoxidation, rabbit erythrocyte membrane ghosts peroxidation and rat liver microsome peroxidation.[103] Other bioactivities include but not limited to protection from hepatoxicity,[104] inhibition of cervical tumor,[105] recovering the functions of the carbohydrate metabolism related enzymes and restoring the normal blood glucose level for diabetic rats,[106] osteoarthritis relieving and reduce pro-inflammatory cytokines,[107] anti-inflammation and anti-cancer,[108] etc.

`

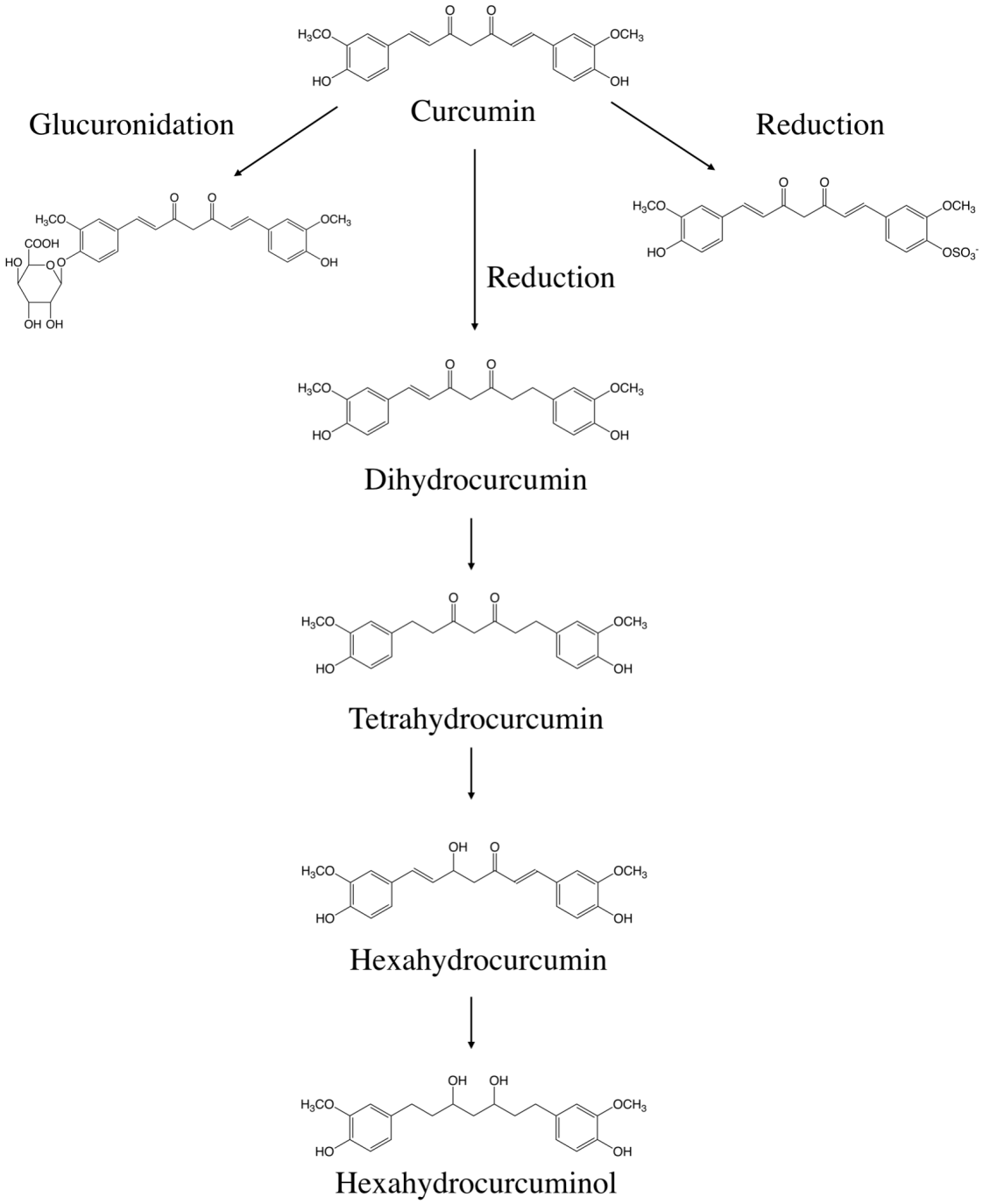

Figure 35. Typical curcumin metabolites

Comparing to curcumin, which was highly unstable under physiological and higher pH environment (90% lost at pH 7.2 in half an hour),[109] THC was much more

`

compatible with physiological environment (stable for 48 hours at pH 7.0) and even more harsh environment (about 68% retention after 48 hours).[110] This property should benefit the absorption, bioaccessibility and bioavailability of THC. However, the aqueous solubility of THC is rather limited and the major part of the orally consumed THC was unable to contact with bile juice and digestive enzymes thus achieving very low bioaccessibility.

In this research, THC, gelatin, MCT, lecithin was mixed in acetic acid in a stable and feasible ratio to be fabricated into ELPC by electrospinning. Gelatin was chosen as the backbone polymer of the ELPC involved in this research due to several advantages it possesses. Firstly, gelatin is a common seen food polymer that is readily and largely available in the market with low cost. Secondly, it is a highly electrospinnable food grade polymer with decent water solubility. Many food polymers with high solubility belong to carbohydrates. However, difficulties frequently appear in electrospinning the carbohydrates compounds. Even for the electrospinnable carbohydrates, most of them require toxic organic solvents to electrospin thus the solvent residue becomes an issue. Another large category of electrospinnable food polymer is the food grade protein. Nevertheless, plenty of them are hydrophobic proteins. In the few electrospinnable hydrophilic food grade proteins, gelatin should be the easiest one to electrospin. The plain flavor and color nature of gelatin also let the ELPC to be more acceptable by consumers. MCT oil and lecithin were incorporated in order to grant the ELPC an advantage of self-assembling nano emulsion generation. Polyunsaturated lipids like various types of vegetable oils were found difficult to be blend into the polymer solution in the trial experiments. As the formulation of the food grade ELPC was established, a series of characterizations were carried out upon this ELPC to understand the physical situations and bioactive functions.

`

2. Experimental

2.1 Materials

Gelatin (from bovine skin, Type B, ~225 Bloom), pancreatin (from porcine, P7545) and glacial acetic acid were products of Sigma Aldrich (MO, USA). Tetrahydrocurcumin was requested from Sabinsa Corporation (NJ, USA). Medium Chain Triglyceride was a kind gift from Stepan® Company (Neobee 1053). Lecithin PC75 was purchased from American Lecithin Company.

2.2 Fabrication of the Electrosprayed Lipid-Polymer Composite

Gelatin 16% (w/v), MCT 5.5% (w/v), PC-75 lecithin 5.5% (w/v) and 1.5%(w/v) THC were weighed before preparing the polymer blend. Gelatin need to be dissolved in glacial acetic acid at the very first step since it required heating to dissolve (60-100°C). After the gelatin-acetic acid solution was cooled down, MCT, lecithin and THC were mixed into the solution all together and vortex thoroughly to create a polymer blend for electrospinning.

The polymer blend was loaded into 3ml syringes and installed onto a syringe pump. Feeding rate of the solution was set at 1ml/hour. An electric source was applied to both the syringe tips (positive end) and a piece of aluminum foil (negative end). The distance between the foil and the tips was 20cm and the electric field was set at 18KV. The electrospun ELPC film products were placed in the fume hood for 12 hours to evaporate the solvent residues and then kept within desiccators to avoid contact with moisture before further characterizations.

`

2.3. Morphology and Physical Characterizations

The morphology of the electrospun ELPC fiber films (n>200) were captured by CLSM, and average ELPC fiber diameters were measured with FIJI (Fiji Is Just ImageJ) software.[82] DLS system was adopted to examine the hydrodynamic droplet diameter of the self-assembled emulsions generated from the ELPCs. The emulsion-gel formed by the ELPC self-assembled nano emulsion was again characterized with CLSM to examine the 3D structure of the emulsion-gel matrix. Fourier transform infrared spectroscopy (FTIR) systems were adopted to examine molecular interaction within the ELPC.

2.4. Functional characterizations

2.4.1 Dissolution profile assay for the ELPC with USP 4 apparatus

The gelatin ELPC is capable of generating a self-assembled nano emulsion when it is orally consumed and meet the stomach hydrochloric acid environment. As a result, the first step that the ELPC encapsulated THC become bio-accessed, is the release of THC from the self-assembled nano emulsion into the stomach acid environment. During stomach digestion, a lot of stomach muscle movement like cramping, grinding is involved which changed the flow of the food mixture. In addition, bile acid secreted from the liver serves as a strong emulsifier that facilitates the absorption of many water insoluble compounds. These factors were all important for the consideration of bioaccessibility evaluations. Therefore, a USP type 4 apparatus (CE 7 smart manual closed loop) was adopted as the dissolution testing device for mimicking and analyzing of the release of ELPC in the stomach. This dissolution tester contains sample cells with ruby and glass beads which modify the motion of the flowing medium to mimics the

`

movements of food solution inside the stomach; It also features a temperature control system that maintains the whole dissolution compartment at 37°C throughout the assay. The dissolution medium was designed as 900mL 0.1N HCl (pH=1, mimicking stomach juice acidity) at the first two hours and brought up to pH 6.8 by adding 100ml basic buffered supplement (6.805g/L KH2PO4 + 0.896g/L NaOH) at the later hours to mimic the emptying of stomach and filling of colon.[111] The medium contain 1% tween 80 which was in accord with the FDA guideline for dissolution medium design. The dissolution assay was carried out for 6 hours totally. At the time intervals including 15 minutes, 0.5, 1, 2, 3, 4, 6 hours. 0.5mL of the dissolution medium was pipetted and mixed with 0.5mL ethanol to break the emulsion encapsulated THC for thoroughly detection. The 1mL sample was then send to HPLC to assay the THC concentration and plot the dissolution profile curve for the ELPC.

2.4.2 HPLC detection of THC

Quantification of the THC amount in the dissolution samples was being carried out with HPLC. A reverse phase C18 column was utilized for the separation and identification of THC. The mobile phase was designed to run isocratically at 1 mL/minute with the composition of 60% acetonitrile and 40% of deionized-water with 0.1% of phosphoric acid added for reduction of tailing and better elution. The injection volume was 10 μL and the samples were filtered by 13mm 0.22μm Nylon Syringe filters (ArkBio Group Inc.) before HPLC sampling. The examination UV wavelength was set at 280nm. 425nm was also detected in the Caco-2 monolayer transport section as an internal standard.

`

2.4.3 Lipolysis

The very first step of digestion of a phytochemical, is to interrupt and disintegrate its crystalline status in the food matrix then solubilize it into our digestive juice. Then, the phytochemical could be biologically available for the intestine to absorb, enter the blood stream and varied organs to exert its health beneficial bioactive functions.[112-113] As a result, it is with great significance to investigate the bioaccessibility of THC when it is encapsulated in the ELPC. There various methods capable of determining the bioaccessibility or getting related information for bioactive compounds. These methods were divided into four categories of models as below.[113] Within these categories, the *in vitro* models and *in vivo* models were the most frequently utilized models for studying bioaccessibility of bioactive phytochemicals. It is usually more reasonable and cost-effective to run in vitro models to get a general idea of bioaccessibility and related estimation then go further for in vivo models that more accurately define bioaccessibility and even bioavailability of phytochemicals. In this research, in vitro models including lipolysis and caco-2 membrane transport were adopted to evaluate the accessibility and related information on THC loaded ELPC.

`

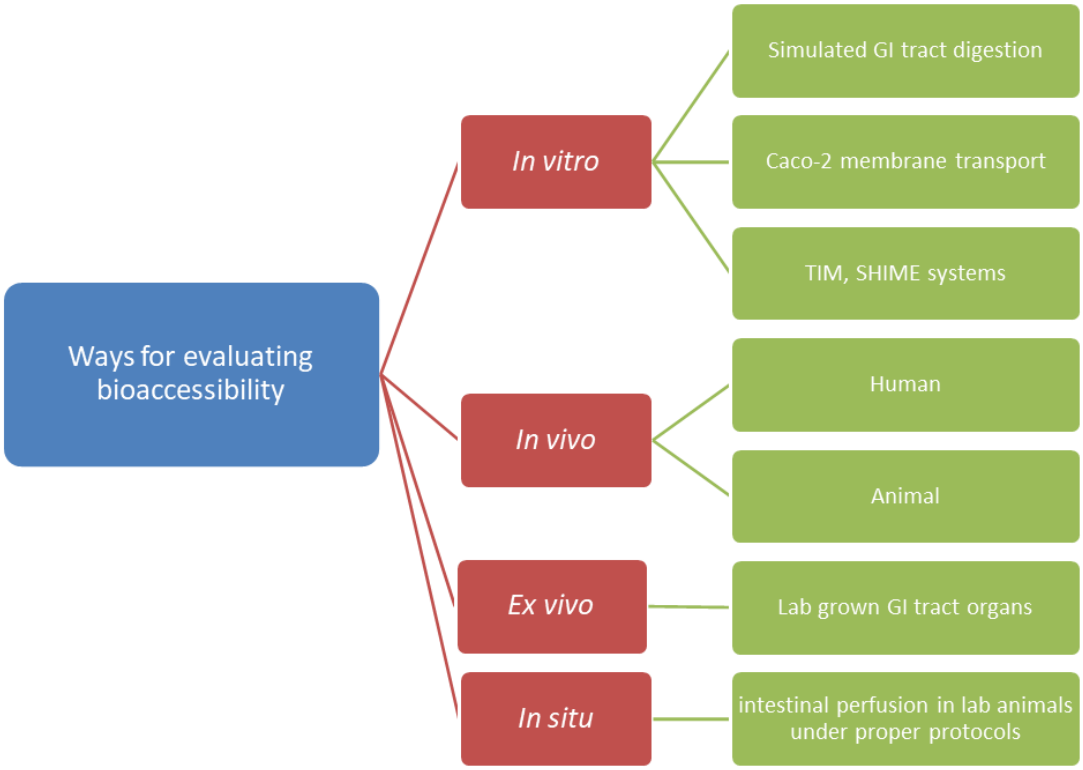

Figure 36. Schematic of bioaccessibility evaluation models modified from previous report[113]

In this research, the lipolysis experiment was designed to mimic the empty and after meal state of stomach juice to evaluate lipid digestion and THC bioaccessibility. The is achieved by preparing two types of buffering system as shown in the table below.

	Fasted	Fed
Tris Maleate	11.86	11.86
NaCl	8.7664	8.7664
$CaCl_2 \cdot 2H_2O$	0.7351	0.7351
NaTDC (sodium taurodeoxycholate, bile salts)	2.6084	10.4336
Phosphatidylcholine	0.9501	3.8004

Table 3. Recipe for Fed and Fasted state buffer system, measured in gram/liter.

`

The detail procedures of lipolysis experiment in this project are described as follows. Firstly, 1g of pancreatin was dissolved in 5mL of lipolysis buffer which heated to 37 °C and kept stirring for 15minutes for thorough suspending. Then, centrifuge the pancreatin suspension at 2000rpm for another 15 minutes to separate the undissolved sediments. The supernatant, which was the pancreatin solution would be transferred to clean containers and chilled on ice for later use. Now, 1.316g ELPC sample containing 250mg of MCT oil fraction, 250mg lecithin and 0.066g THC was added to 9mL of lipolysis buffer and kept agitating at 37 °C for 10 minutes. Adjust the pH of the mix to 7.5 with 0.25M sodium hydroxide solution drop by drop carefully and record the amount of NaOH added all the time. When the pH reaches 7.5, quickly add 1mL of the pancreatin buffered solution prepared before and then start the titration experiment using 0.25M sodium hydroxide solution drop by drop carefully. Under the effect of the catalyzer pancreatin, triglycerides would be broken down in to free fatty acids and the THC will be released and forming micelles with the surfactants in the matrix to become bioaccessible. During this process, the free fatty acid would keep dropping the pH of the system. As a result, titration of the free fatty acid could assay the amount of oil that was digested. The pH during titration experiment was maintained at 7.5±0.02 for totally two hours as the end of the experiment. After that, the titrated mixture was chilled on ice and preparing for centrifugation. The parameter for ultracentrifugation was 50,000rpm for 40 minutes at 4°C. As the ultracentrifugation finished, the middle layer in the tubes was transferred out and filtered with 0.2μm filter. 200μL of the filtered sample was then mixed well with 400μL methanol and then brought to HPLC for detection of final THC concentration.

In this section, both the lipolysis extent and bioaccessbility of THC from the ELPC was analyzed according to the previous reports.[114] For the extent of lipolysis, it was

`

calculated as: Total NaOH used in titration / Maximum amount of NaOH the lipid react with (2 x molarity of lipids) x 100%, assuming the reaction molarity ratio of NaOH and lipid molecule is two to one according to the enzyme properties. And the bioaccessbility was yielded by free released THC content in the centrifuged supernatant / total THC loaded in the sample x 100%. Besides, because the molecular weight of the MCT was not readily determined, it could also be estimated by saponification value, which is 334 for MCT. Then the Molecular weight of the MCT could be calculated as 3 x 1000 x Mw KOH / 334 which is about 504.

2.4.3 Caco-2 cell culturing

To study the interaction between formulated THC and human GI tract, multiple cell studies utilizing colon cancer cell line Caco-2 (ATCC HTB-37) would carried out, including Caco-2 membrane transport for bioaccessibility evaluation, Caco-2 cytotoxicity assay and cellular uptake studies. The cells were from Dr. J. Storch in Department of Nutrition, Rutgers University as a generous gift. They were cultured in DMEM with 10% fetal bovine serum and 100 IU/ml of penicillin and 100 mg/ml of streptomycin (Gibco™, Thermo Fisher Scientific, USA) at 37◦C with 5% CO_2. Culturing medium was changed twice a week.

2.4.4 Caco-2 monolayer membrane transport assay

The design of research procedures followed the order of gastrointestinal tract digestion. The lipolysis assay carried out above represented the digestive reactions occurred in the stomach. When the food matrix was transferred to the intestinal area, the absorption of most types of nutrients began to occur. In this section, the Caco-2 membrane transport experiment was adopted to investigate the permeation and

`

absorption of THC from the stomach-digested fluid in the intestinal area of human. The Caco-2 cell monolayer membrane was generated from the uncontrolled proliferation and aggregation of Caco-2 cancer cells. This aggregated monolayer membrane resembled the key features of a real intestinal membrane like the tight junctions existing between intestinal cells, the villi on the inner surface of the intestine and it also produce proteins and enzymes related to the transport of nutrients. Therefore, the Caco-2 monolayer membrane was a suitable model to evaluate the permeation and absorption of bioactive phytochemicals *in vitro*.

In order to form the monolayer membrane, the Caco-2 cells were transferred to the wells in 12-well plates with specially designed inserts with 0.45μM filters (Corning). Each insert was filled with 0.5mL of cell suspension with a density of 0.6×10^6 cells / mL . Each well was filled with 1.5mL culture media mentioned in the previous section and the media was changed every other one day for both the inserts and the wells. The Caco-2 cells were cultured for about 21 days to reach an appropriate thickness for the transport assay of THC loaded ELPC samples. At the time that the Caco-2 was fully grown for the transport experiment, the media above and below the membrane was carefully removed from the edge of the container. Then, the membrane was cleaned by Hank's balanced salt solution (HBSS) plus 25mM HEPES (4-(2-hydroxyethyl)-1-piperazineethanesulfonic acid, a zwitterionic buffer) for three times. After washing, the top insert was filled with 0.5mL the same HBSS+HEPES while the bottom was filled with 1.5mL and maintained at 37 ° C for half an hour before addition of the lipolyzed formulation. Now, transepithelial electrical resistance (TEER) was utilized to evaluate the quality of the monolayer related to its thickness and integrity. The TEER value was measured by EVOM2 Epithelial Voltohmmeter (World Precision Instruments). The appropriate thickness was defined as the TEER reading result about 300 Ω. As long as

`

the resistance reading was appropriate, sample could be added to the compartment and started the transport experiment. [115]

After electrical resistance evaluation was passed, 5μL of the sample (lipolyzed THC nano emulsion self-assembled from ELPC) was added in the top insert. In this experiment, only fed state lipolyzed formulation was applied because sodium taurodeoxycholate was toxic to the Caco-2 cells and may cause monolayer membrane to be damaged or even leaked. Samples were diluted about 100 times before application. For the control, THC solution in DMSO was prepared and adjusted to a concentration similar to the diluted lipolyzed THC formulation. Transport experiment was designed to run for 20, 40, 60, 80, 100, 120 minutes. At each time interval, medium from the top insert and below was transferred to 2mL centrifuge tubes. They were extracted with 1mL ethyl acetate for 5 minutes by three times and finally re-dissolved with 0.1mL methanol to be detected by HPLC.

Intestinal membrane permeation and absorption was evaluated by apparent permeation rate (P_{app}). Which is calculated as:

$$P_{app} = \left(\frac{dQ}{dt}\right)\left(\frac{1}{AC_0}\right)$$

Where Q was the quantity of permeated substance, t was the interval, A as the permeation contact area=1.1cm^2 and C_0 was the concentration of substance at the beginning. [116]

`

2.4.5 Cytotoxicity evaluation

To estimate the safety dosage of THC and THC-loaded self-assembled ELPC nano emulsion in the intestine, cytotoxicity of Caco-2 cells against these substances was examined. As previously mentioned, an MTT cell viability assay was conducted against the Caco-2 cells in a 96-well plate. 1×10^4 cells in the DMEM medium was seeded in each well and kept at 37◦C for a whole day. On the next day, DMEM was discarded and cleaned with PBS 1X for three times then filled with empty medium again. Then, 100μL 0.5% DMSO solution of THC with concentration gradients were added to the wells. The control background was pure 0.5% DMSO 100uL. The whole plate was then incubated in the environment same as above for another 24 hours and then discarded the medium and washed by PBS for three times. After this, 100 μL MTT 0.5 mg/mL solution (in RPMI 1640) was applied to all the experiments then incubate at 37◦C for 2 hours, then the solution was all discarded and washed for three times. 100 μL DMSO was then added to dissolve formazan generated by normal functioning cells. Finally, the plate was fed to the microplate reader (Bio-Tek) to shake for 20 minutes and read the absorbance at 570nm (490nm as reference). Experiments were carried out in triplicates. Cell viability was defined as the percentage of the sample's absorbance result divided by that of the control (background deducted).

2.4.6 Cellular uptake of formulated THC visualized by CLSM

In order to substantiate that the THC loaded formulation was capable of entering the cells in the intestine as a final step of phytochemical absorption, a cellular uptake study was performed against the Caco-2 cell line. They were seeded on 20mm round cover glasses (CELLTREAT® SCIENTIFIC PRODUCTS) with quantity of $1*10^5$ cells/ml and placed into 12-well plates. To visualize and semi-quantify the uptake situation for

`

the formulated THC, the ELPC formulation was incorporated with 0.01% coumarin-6 dye as a fluorescence indicator. 0.1g of this fluorescent ELPC was put into 0.9mL of cell culture medium to self-emulsify. This emulsion was further diluted with culture medium by 500 times to ensure the coumarin-6 and THC amount are safe for the melanoma cells. Then the diluted emulsion-medium was added to the wells for 0.5, 1, 2, 4, 6 hours to gradually observe the cellular uptake process. Another fluorescent dye, DAPI (10μg/mL) was utilized for staining the nuclei area of the Caco-2 cells. At each time interval, medium in the wells were removed and DAPI solution was utilized to stain for 30 minutes. After that, DAPI was cleaned with PBS buffer for three times to avoid over staining. The seeded glasses treated with emulsion and dyes were then brought to CLSM for examination. Addition of emulsion-medium to the cells should follow a reverse chronological order to let all the time interval finish at the same moment, which facilitated CLSM examination.

2.4.6 Statistical analysis

Data presented were carried out in duplicates or triplicates. Origin® 2016 and Microsoft Office 2016 were applied to calculate the averages and standard deviations. Average values were compared and statistical significance was considered at confidence level <0.05 with IBM SPSS software.

`

3. Results and discussions

3.1 Physical characterizations

3.1.1 Overall appearances of ELPC

Figure 37. Film and flake appearance of the THC loaded ELPC product

`

3.1.2 ELPC Morphology examined by CLSM and fiber diameter distributions

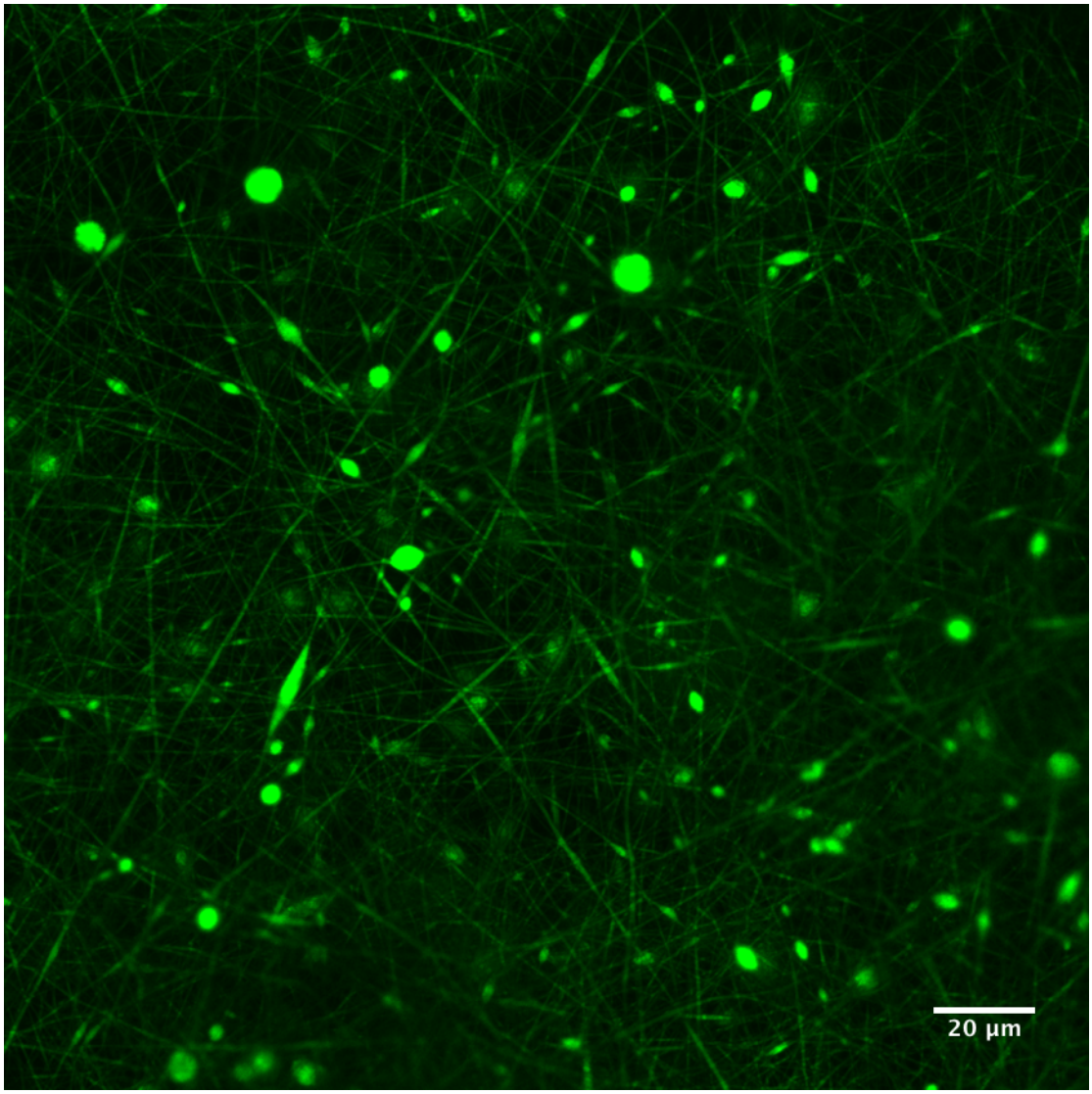

Figure 38. CLSM pictures of the THC loaded ELPC fibers dyed with coumarin-6

The morphology of the electrospun complex was displayed in figure 38. A post-processed green color was applied to indicate the strength of fluorescence of the fibers. In the image, both ultrafine fibers and small particle were observed. This information implied that the fabrication process was somewhere between electrospinning (fiber forming) and electrospraying (particle forming). The more the process approaching to the fiber forming, the higher the fiber diameter could be and usually stronger fiber films

`

will be formed. The more approaching to particle forming, the lower the particle size could be reached and the product would be more disintegrated, fragile and finally became a powder. The fragile flake like film appearance in figure 38. also agree with this theory.

3.1.2 Fiber diameter distribution of the ELPC

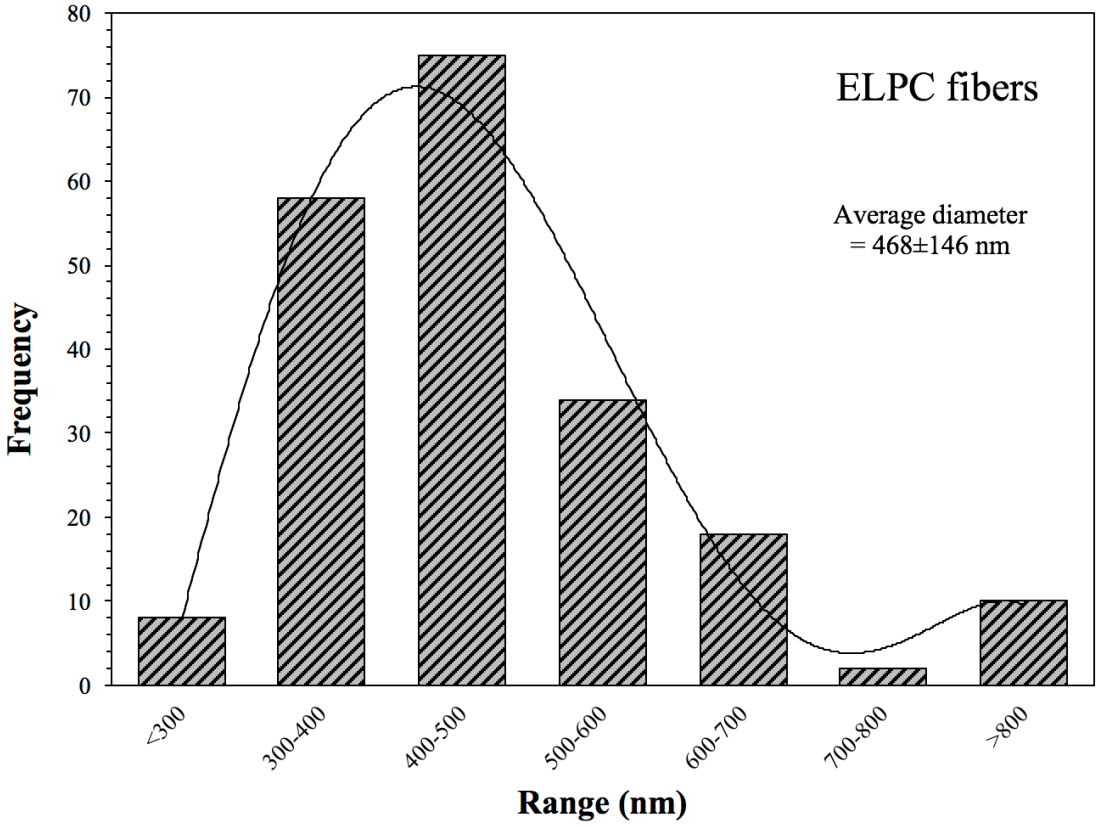

Figure 39. Diameter information of the THC loaded ELPC fibers

From the fluorescent image of the ELPC fibers, it could be observed that the fiber diameter distribution was relatively even. From the diameter information chart in figure 56, the fibers had relatively focused diameter distribution in a range from 300 to 700 nanometers. 67% of the fibers were 300-500nm thick and the average diameter of all fibers was 468±146nm.

`

3.1.2 Hydrodynamic radius of the ELPC generated self-assembled emulsion

The whole piece of ELPC was able to turn into a self-assembled emulsion at the moment when ELPC contacted with water. The emulsion was a mixture of gelatin molecules, fine droplets of MCT oil, lecithin micelles and complexes of one or more of these components. This emulsion was prepared by dissolving 10% ELPC (w/w) in water and then diluted 5000 times and before the DLS for particle size examination. The diluted emulsion was placed into cuvettes (1cm path) detected by DLS system with 658nm laser set at 90° scattering angle at the temperature of 20°C. DLS results demonstrated that the fitted autocorrelation function has an R^2 of 0.9999 and the droplet size was yielded as 410nm.

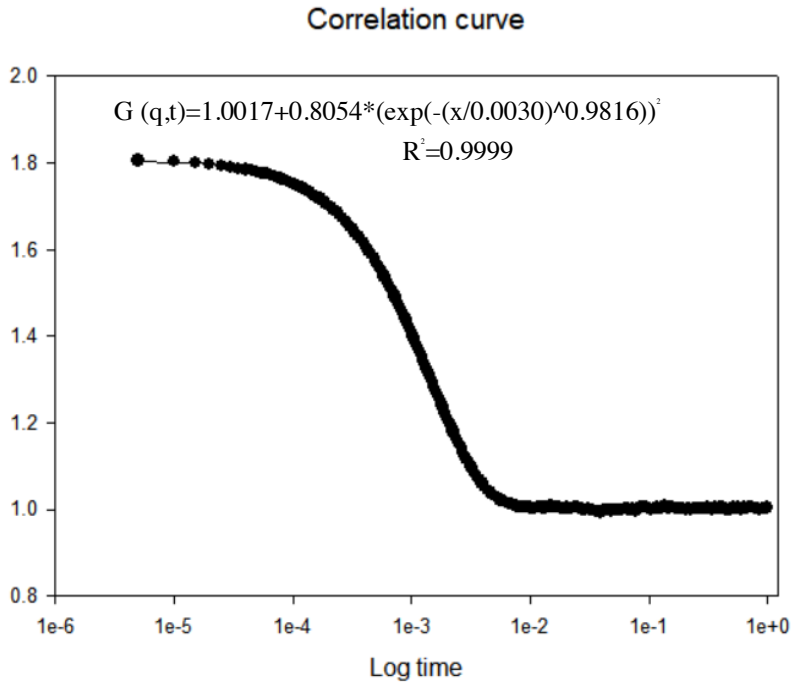

Figure 40. Autocorrelation curve and fitted function

`

3.1.3 Structure of the ELPC generated self-assembled emulsion-gel examined by CLSM

Because the ELPC was in fact an ultrafine fiber network of gelatin, lecithin, MCT oil and small amount of THC. All the components within the ELPC were highly atomized that it could immediately disintegrate and forming a self-assembled emulsion once it was contacted with water. Due to the nature of gelatin, this self-assembled emulsion was able to set and become a gel when the ELPC concentration was high enough (tested >4% by weight) and kept at room temperature or below. This gel could be defined as an emulsion-gel since it fell into both categories. It has a dispersed phase (MCT+ lecithin+ THC) existing in a grand continuous phase matrix (gelatin+ water). At the same time, the continuous phase formed a stable three-dimensional cross-linked network that made the system stationary. Nevertheless, the detail distribution of the hydrophilic hydrogel network and the hydrophobic components were not being studied before and it had significance in understanding the emulsion-gel structural mechanisms and interactions between different phases. As a result, in this section, the ELPC was fluorescently dyed with coumarin-6 as mentioned before and put into deionized water pre-dissolved with another hydrophilic fluorescent dye rhodamine-6G. By this means, the distribution and interactions between varied components within the special emulsion-gel could be defined.

`

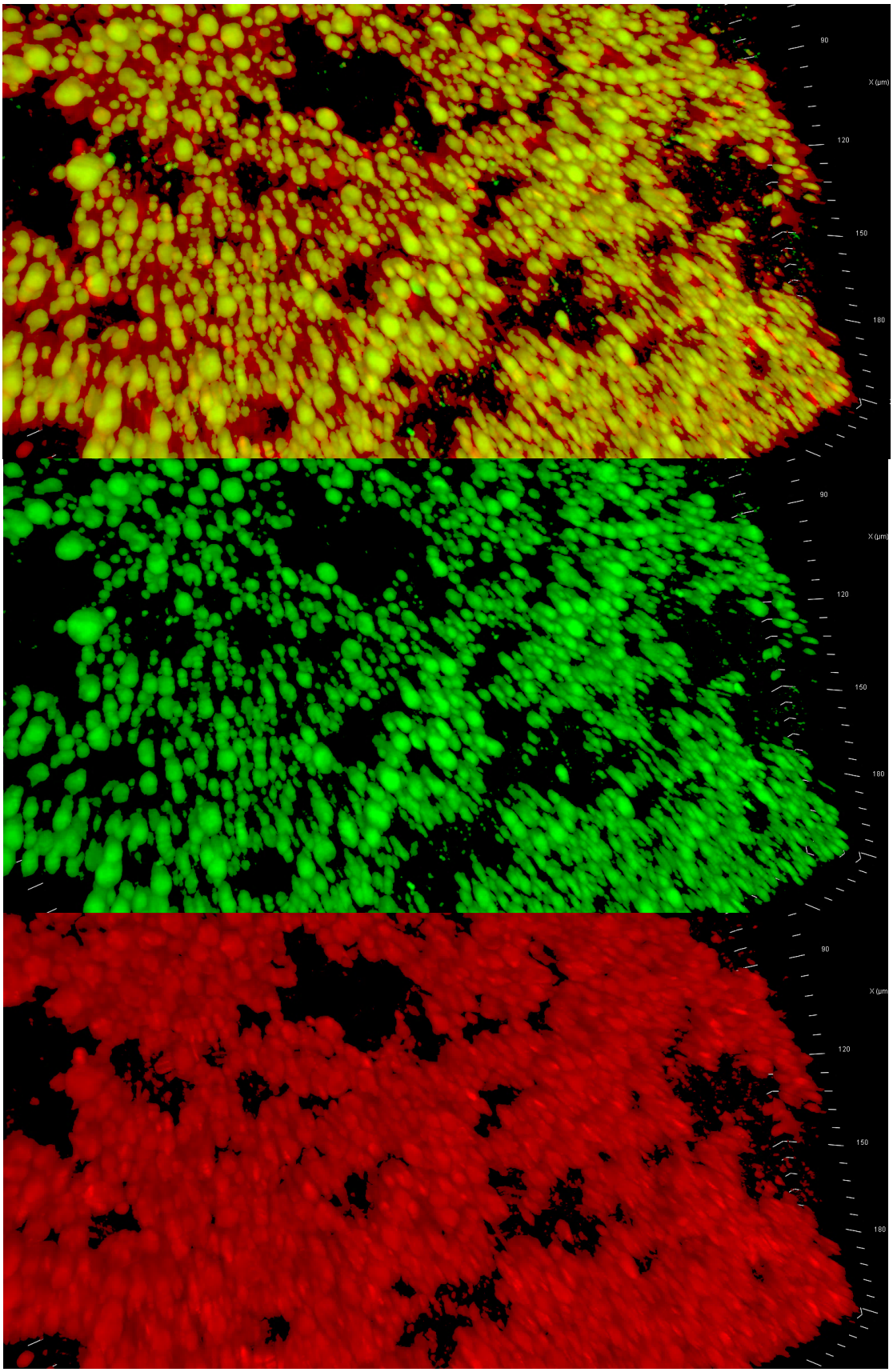

Figure 41. CLSM images of the ELPC emulsion-gel. Rhodamine-6G channel was labeled in red while coumarin-6 was labeled in green.

`

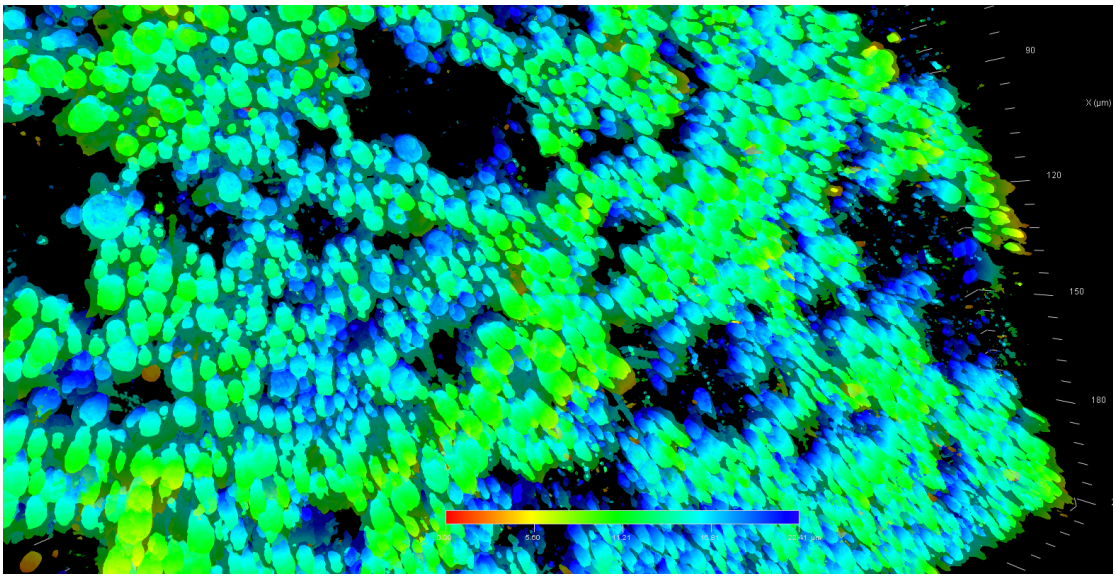

Figure 42. Phase image of the emulsion gel. Gel depth was about 22.41µm.

As figure 41 depicted, the gel framework had a massive clustered structure build with capsule-like units. According to the 3-D scale bar and the phase image, the capsule like units were about three to six microns in diameter and up to 22.41 in height. The lipophilic phase was embedded within each "capsules" instead of entrapped in the hollow areas inside the clustered gel matrix. The reason why the lipophilic and hydrophilic phase existed in such a form that closely contacting each other should be the effect of lecithin as a surfactant that reduced interfacial surface energy between the two phases, which means the thermodynamic theories for emulsions was still applicable to the emulsion-gel system. The lipid phase embedded within the clusters appeared to be rounded beads or little rods. The mechanism behind the rounded appearance of the embedded lipid phase should be the same as lipids in the emulsions. Beads and rods have no edges therefore they were the forms with lowest contacting surface area, lowest surface energy and highest stability to exist within the hydrophilic gelatin framework.

`

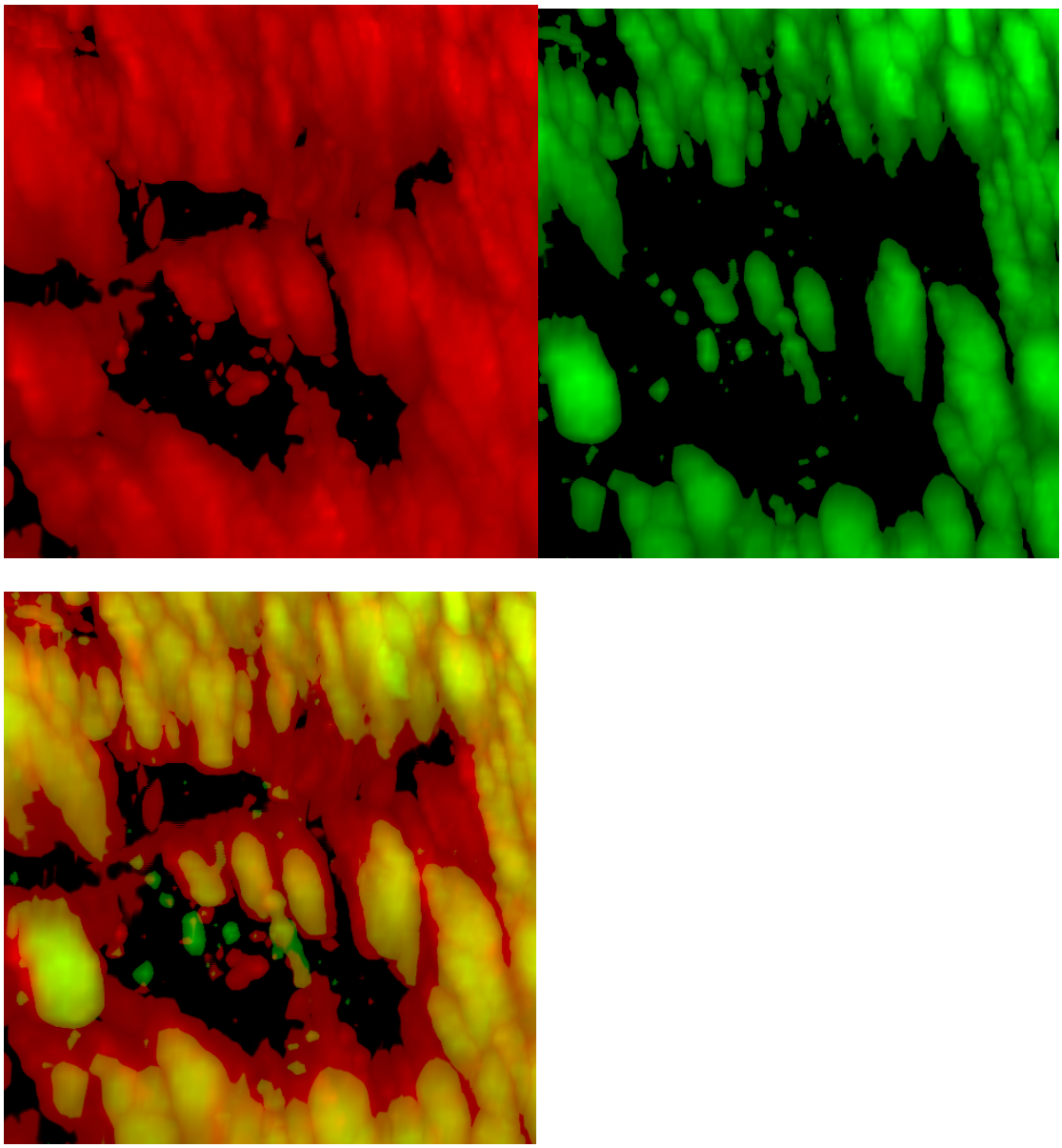

Figure 43. Enlarged CLSM images of the emulsion gel “capsules”

`

3.1.4 FTIR examination

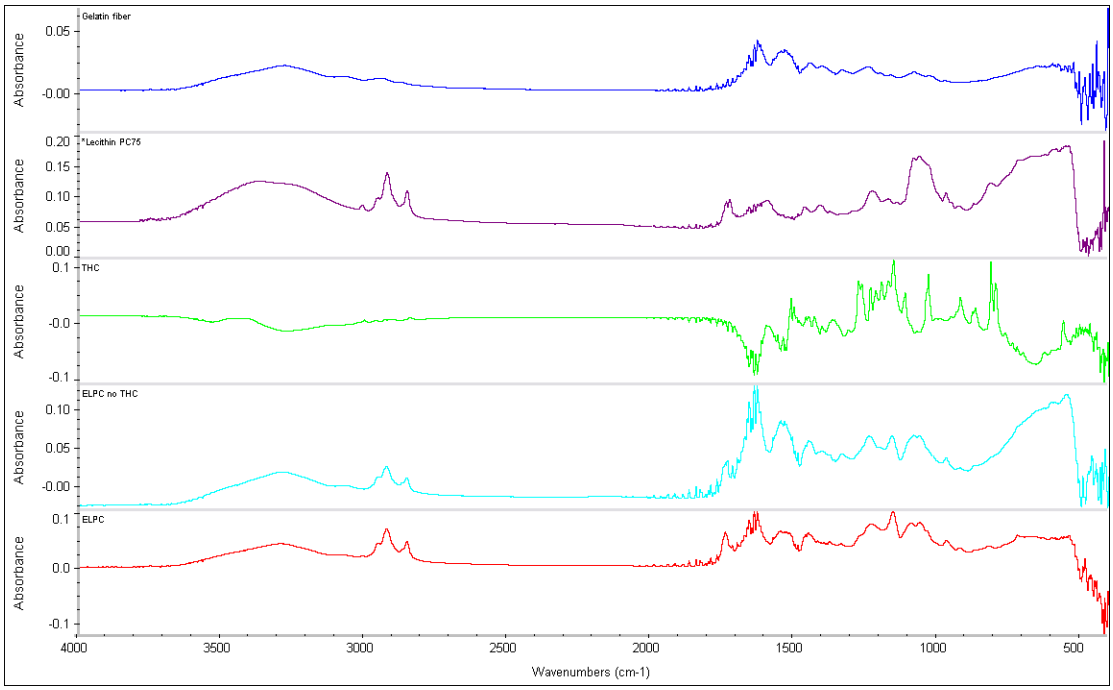

Figure 44. FTIR charts of ELPC with varied oil content

Functional groups interaction situations for the ELPC was assayed by FTIR. THC acid crystal has a fingerprint pattern region at the wavenumber range from 500 - 1600 cm^{-1}. Nevertheless, these fingerprint signals disappeared in the both the ELPC with or without THC, which was in accord with previous reports.[90-91] IR peaks at 2923 and 2852 cm^{-1} for the alkyl C-H stretch on the spectrum represented the hydrocarbons in the alkyl chain of lecithin and MCT oil.[92] These C-H stretch signals were found in the THC loaded ELPC with lecithin and ELPC with lecithin plus MCT oil. In addition, strong C-O stretch at wavenumber of 1150 from the ester bond of the large amount of MCT oil was detected in the ELPC with MCT, which was not observed in the FTIR spectrum of pure gelatin. These clues were potentially correlated with the fact that the lipids in the ELPC existed in some degree of crystalline form. Strong and broad hydrogen bonded O-H stretch at the wavenumber 3200 - 3600 cm^{-1} was displayed in the IR spectrum for lecithin PC75. However, this signal was significantly reduced when

`

lecithin was incorporated within ELPC, implying that intermolecular hydrogen bonding of lecithin was disrupted and it was not a major interaction mechanism between the components within the ELPC. Hydrophobic interactions and Van der Waals forces were dominant interactions inside the massive ELPC matrix.

3.2 Functional characterizations

3.2.1 Dissolution of ELPC

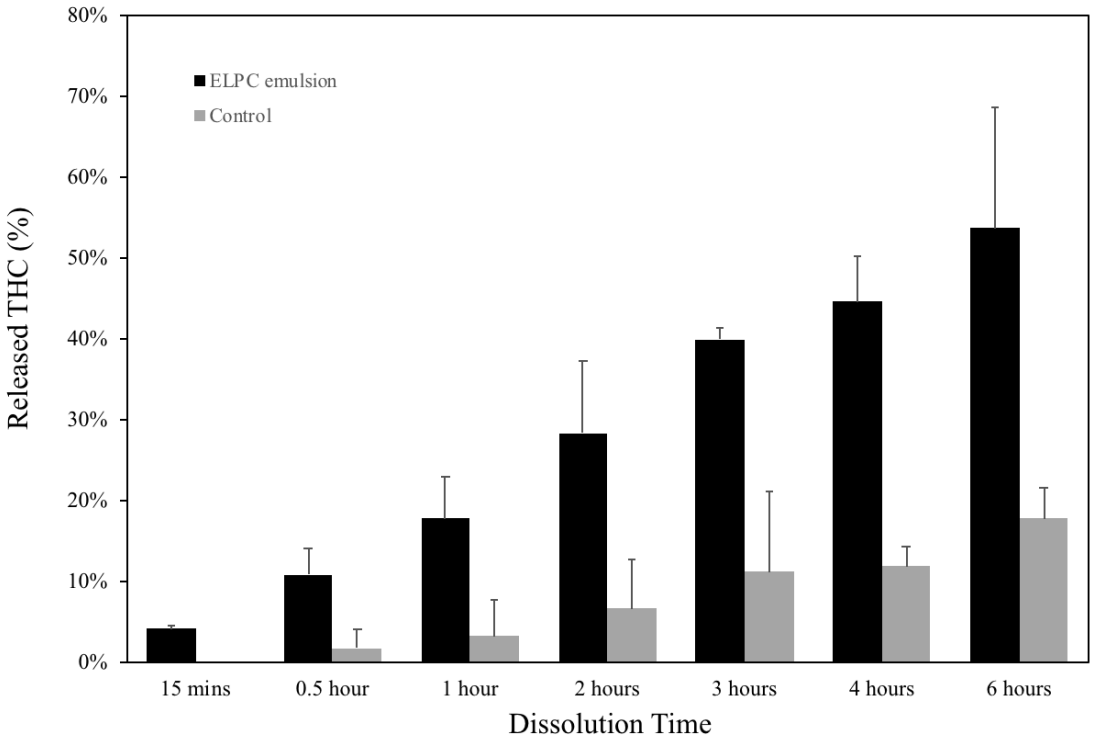

Figure 45. Dissolution profiles for ELPC emulsion and the control suspension

Dissolution profiles of the THC loaded self-assembled emulsion versus the control THC suspension is displayed in figure 45. Both the emulsion and the suspension contained 5mg of THC and thus the released quantity of THC in the dissolution medium was divided by 5mg as the percentage of THC released from emulsion or suspension. Over the experimental time mimicking 6 hours of human GI tract digestion, the release

`

of THC dissolution was in a trend of gentle increase. For the first two hours, the dissolution power of the ELPC emulsion was 3 to 4.6 times higher than the suspension; for the later four hours, ELPC still outperform the suspension for 2.1 to 2.6 folds. The preponderance of ELPC was reduced in the later stage was related to the THC solubility in the medium. Because this was a closed system USP-4 apparatus, sink condition could not be achieve especially in the medium with only 1% tween 80 with limited solubility for THC. Considering this limitation, if the ELPC was consumed in reality situations, it's dissolution potential should be higher with the large flow of gastric fluid and high amount of surface-active bile juice was involved.

To further analyze the dissolution pattern of the ELPC, the profile was being fitted with several classic mathematical models for drug diffusion and dissolution. Comparing the correlation fitting curve of various models, the Higuchi model was found to be the best fit for the ELPC dissolution activity with the highest R^2 of 0.9932.

Kinetic models	**Fitted equations**	**R^2**
Zero order	$Q_{\%}=0.0855t+0.0009$	0.9379
First order	$\ln Q_{\%}=0.377t-2.4424$	0.7276
Hixon-Crowell	$(1-Q_{\%})^{1/3}=-0.0369t+0.977$	0.9641
Higuchi	$\mathbf{Q_{\%}=0.2592t^{1/2-0.079}}$	**0.9932**
Korsemeyer-Peppas	$Q\%=0.1549t^{0.7868}$	0.97

Table 4. Fitted models for the dissolution profile of ELPC loaded with THC

`

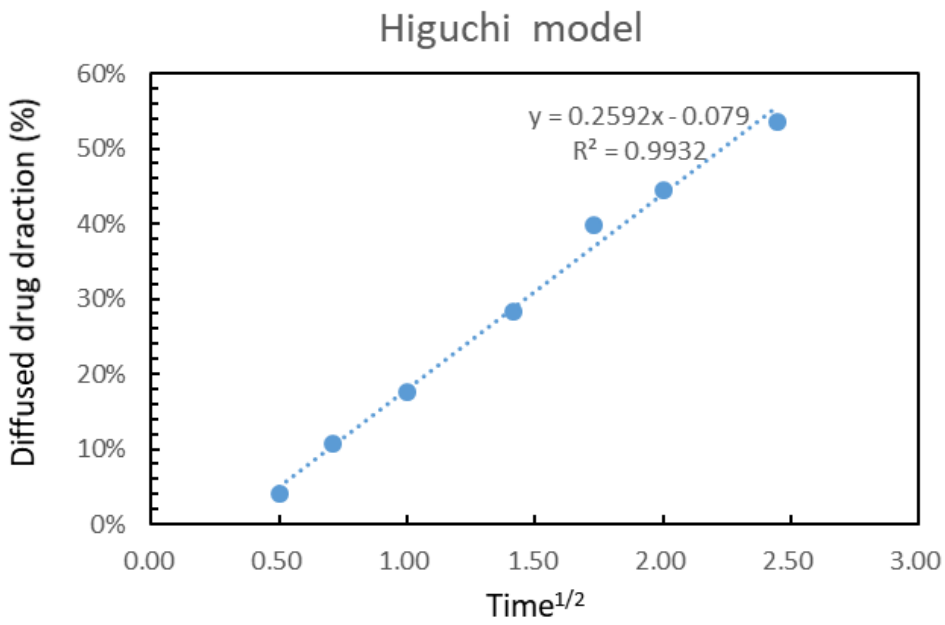

Figure 46. THC release from ELPC absent the square root of time, fitted with Higuchi model of drug diffusion

Higuchi model hypothesizes that the drug concentration in the formulation (ELPC self-assembled emulsion in this case) is much higher than the release medium solubility with perfect sink condition. It was also limited to the situations that the drug diffusivity is constant and the conformational transformations (like swelling, disassembling) of the formulation matrix is negligible. These requirements were met for the ELPC dissolution environment. Since the Higuchi equation was a highly simplified form derived from Fick's law, it suggested that the ELPC dissolution process is a Fickian diffusion driven process, which was suitable and already applied in multiple drug delivery system studies.[117-119] With the Higuchi rate constant assayed from the correlation curve as 0.259 and a high r^2 of 0.9932, it is promising to adopt this modeled function to predict the ELPC dissolution release within the whole stomach digestion process.

`

3.2.1 Lipolysis

From the lipid digestion profile displayed in the figure below, it was apparent that the speed of digestion at the first several minutes was very high. The "log phase" for the fed state digestion last about 6.75 minutes while for the fasted state the rapid digestion last about 3.35 minutes. During the log phase of digestion, the fed state situation digested 65% of the total lipolyzed lipids; for the fasted state, 72% total lipolyzed lipids was consumed. Both curves indicated that atomization was a highly efficient technique to accelerate lipid digestion thus increase the speed of active compound release.

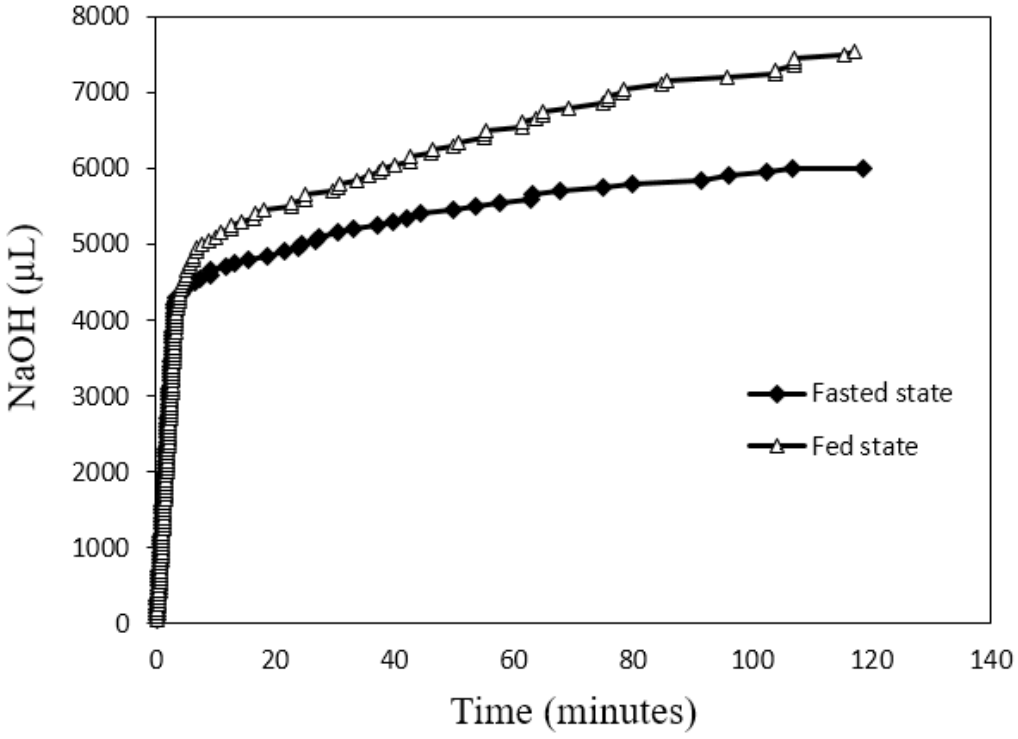

Figure 47. Lipolysis profiles comparison between fasted state and fed state situations

`

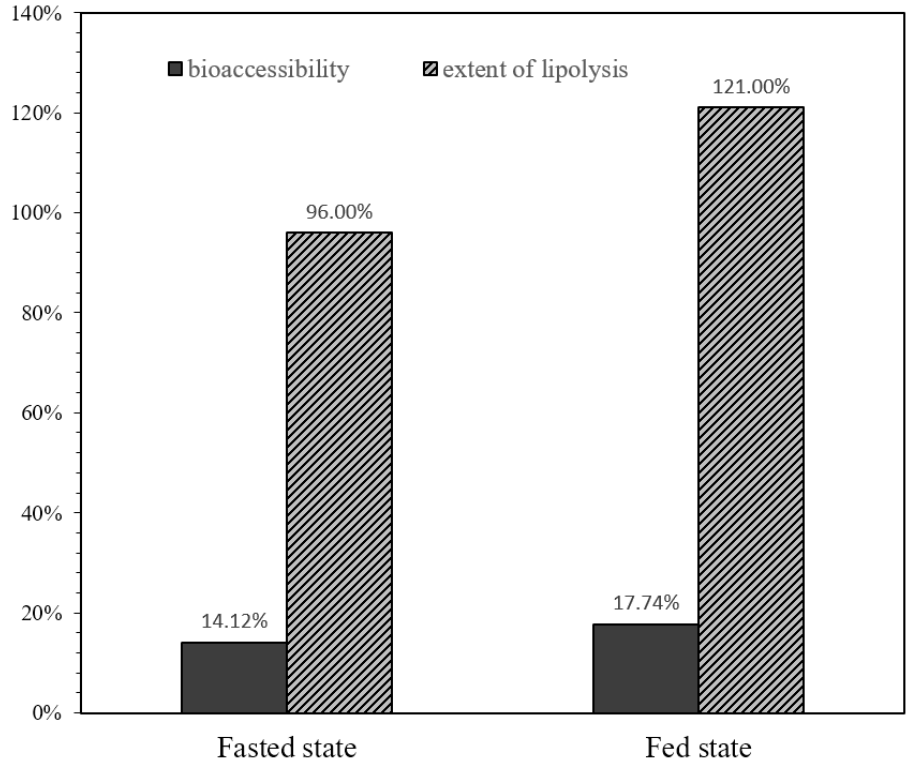

Figure 48. Bioaccessibility and ELPC lipolysis situations in varied situations

The chart in figure 48 displayed both the calculated bioaccessibility and degree of lipolysis for empty and after meal situations. In fed state situation, lipid would be digested more completely and higher amount of the active compound THC could be released. This observation agreed with previous report,[120] indicating that ELPC would perform better if consumed after meal. However, the bioaccessibility of the ELPC was relatively low regarding the results (about 10% THC was accessible). It was possible that there was still certain amount of entangled ELPC complex wasn't fully emulsified in the buffer system which concealed considerable amount of THC from releasing. Another possible explanation could be that the interaction between THC and gelatin was strong enough to keep THC from releasing. Nevertheless, ELPC could easily reach high loading to 10% which was much higher than conventional emulsions. Therefore, ELPC could still outperform in the total absorbed amount of active compounds.

`

3.2.2 Caco-2 monolayer membrane transport assay

The Caco-2 monolayer membrane transportation data was shown in the figure 49. below. Transport direction was found to be the major factor that affect the quantity and speed of the Caco-2 membrane transport. The upward transport activity was about 4 times over the upward for the THC in digested ELPC while about 3 times over the upward transport for the THC dissolved in DMSO. During downward transport, the sample would firstly contact the microvilli of the monolayer. The microvilli provided a huge surface contacting area, which could possess capturing and filtering effects for the THC thus retarded the drug transport for both the lipolyzed ELPC and THC DMSO solution. In addition, from both upward and downward transport profiles for the THC DMSO solution, it could be observed that the general trend of delivery was firstly increase then decrease from 80 minutes of experiment. Considering the diffusion mechanism, decrease in THC delivery was not reasonable since it was a closed system. It was highly possible that the Caco-2 cells were starting to uptake the THC from around 80 minutes of treatment thus consumed the transported amount of THC. In comparison, the THC transport profile of digested ELPC appear to reach an equilibrium quantity from about 40-60 minutes of treatment. To further describe the diffusion process of the Caco-2 transport, the apparent permeation rates (P_{app}) were calculated. For the THC DMSO solution transport, the P_{app} was 6.35×10^{-5} cm/s upwards and 7.18×10-5 cm/s downwards, with the efflux ratio value of 0.88. For the digested ELPC transport, the P_{app} was 3.19×10^{-5} cm/s upwards and 3.08×10-5 cm/s downwards, with the efflux of 1.04. The Efflux of both the control and the digested ELPC was less than 2, a common cut-off to suggest an active efflux. Therefore, the caco-2 membrane transport for both were belonged to passive diffusion.

`

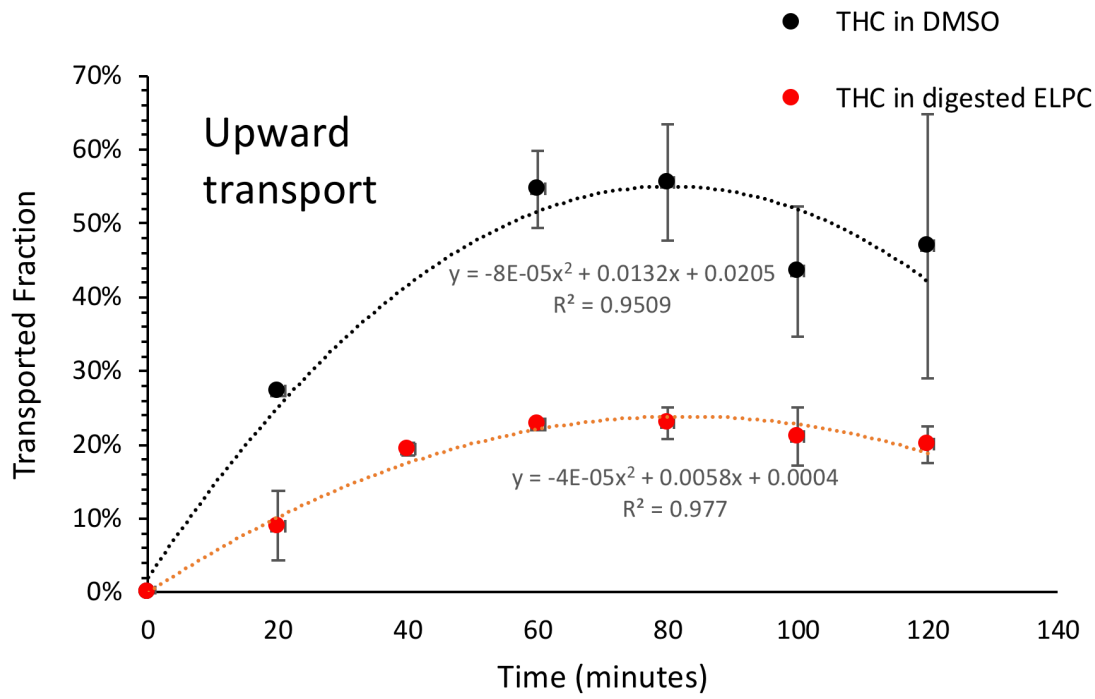

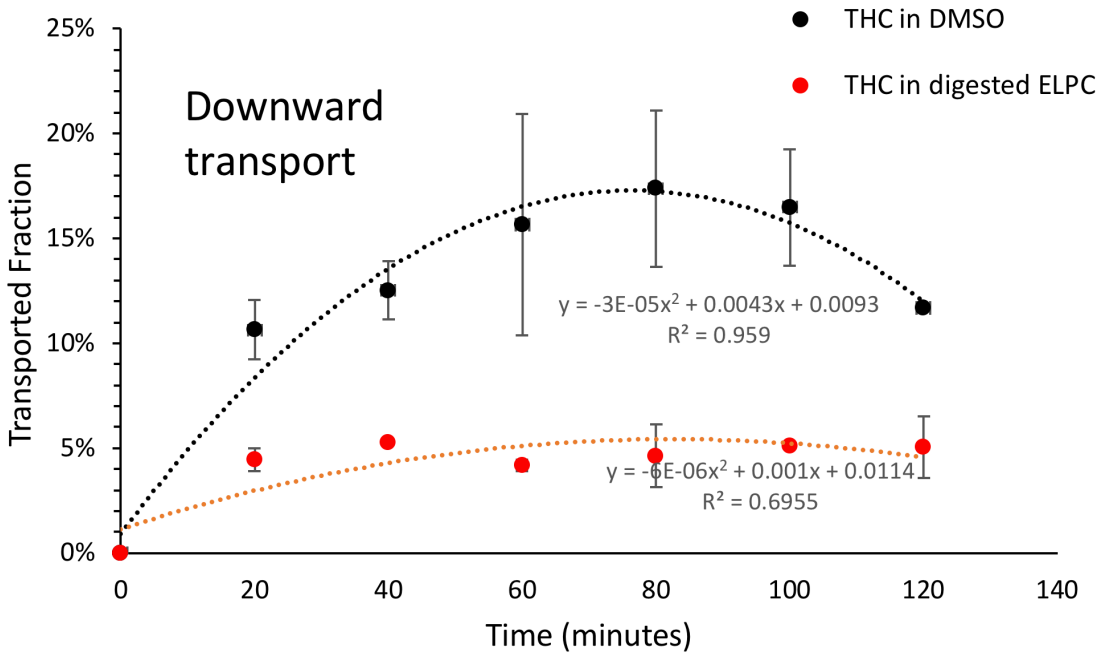

Figure 49. Upward and Downward Transportation situation for THC in DMSO solution and THC in lipolyzed ELPC

3.2.3 MTT assay for THC and THC loaded ELPC emulsion

The above functional characterizations had proved that ELPC was able to release the THC and finally being absorbed in the intestinal area. Besides permeation through the intestinal membrane, another important indicator for the active compound absorption was to be able to enter the intestine cells. To substantiate this process, cellular uptake study against Caco-2 cell line was arranged. Before the uptake experiment, to ensure active compound was safe for the cells, a MTT assay was done to find out the range of phytochemical concentration without hurting the cells apparently (>90% cell viability).

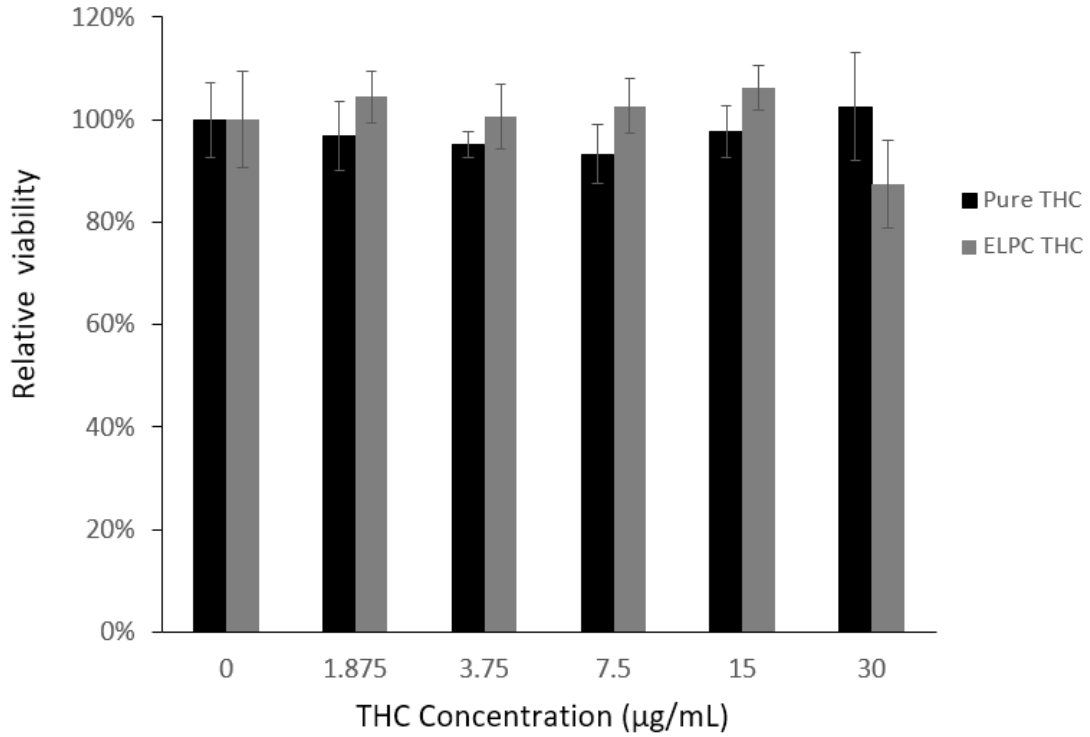

Figure 50. MTT assay for pure THC and ELPC emulsion THC

As demonstrated in figure 50, the overall cytotoxicity of THC against Caco-2 cells was low. All the designed THC concentrations from 0 to 30µg/mL were considered non-toxic to Caco-2 cells (viability>90%). For the THC loaded in the ELPC self-assembled emulsions, they were also non-toxic and even sort of promote the growth of

`

the cells, except the 30μg/mL concentration where the cytotoxicity was right around safety line (88%). As a result, THC in ELPC emulsions up to 15 μg /mL was confirmed safe for the following cellular uptake study.

3.3.6 Cellular uptake against THC in ELPC emulsions

By the safety dosage determined in the above MTT experiment, an ELPC with proper concentration of THC was fabricated loaded with coumarin-6 as a fluorescent indicator for cellular uptake visualization. To capture images that could semi-quantify the accumulated active compounds within the cells, CLSM was dedicatedly tuned and configured with the same set of parameters throughout the whole imaging process. 405nm laser was for the visualization of DAPI while 458nm beam was for exciting coumarin-6. Laser intensity of 405nm was set to 0.03 and 0.025 for 458nmfor the best visual effects. Pinhole was set to 64.2 units to scan 17.9μm of section. For the DAPI channel, gain was set to 575 units while for the Nile Red channel the gain was 776.

`

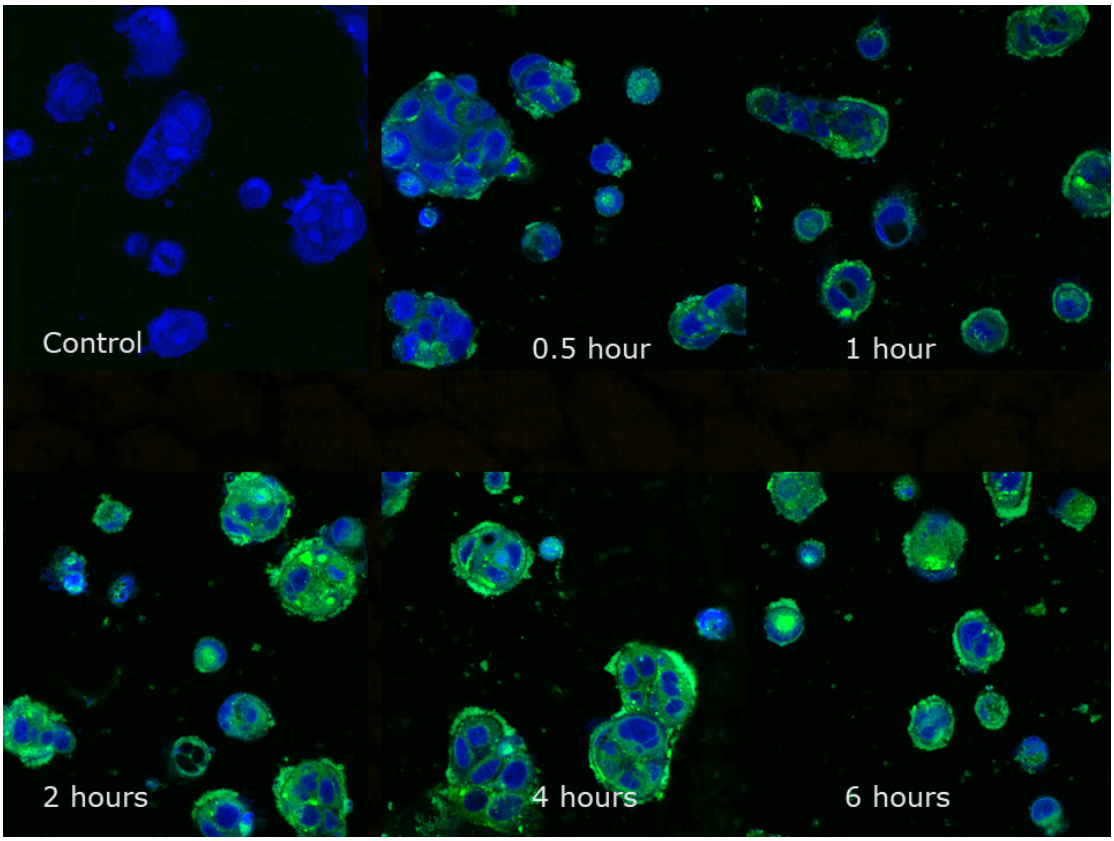

Figure 51. CLSM image of ELPC emulsion THC cellular uptake

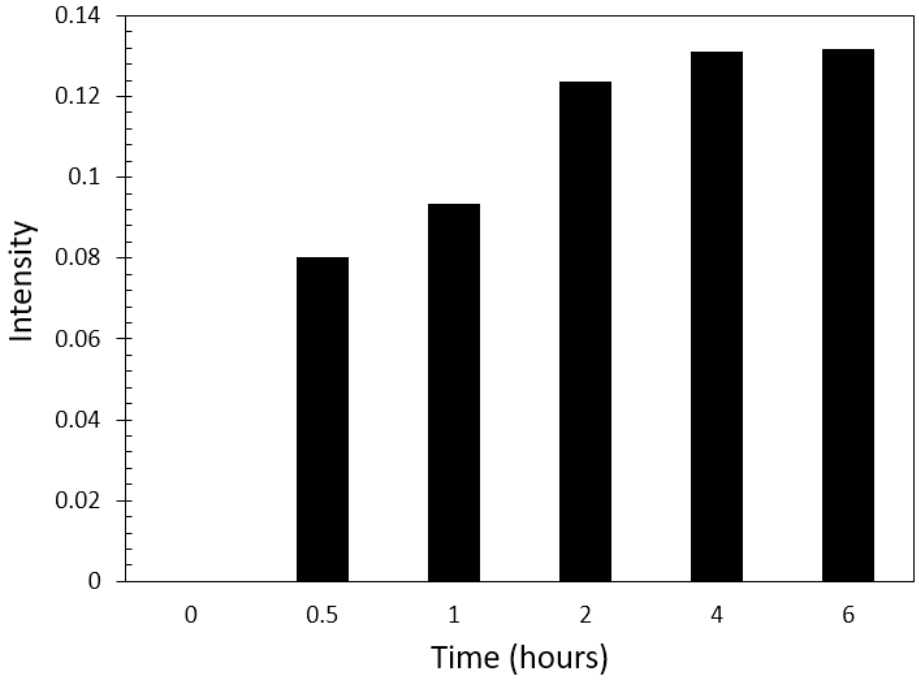

Figure 52. Semi-quantification of ELPC emulsion THC cellular uptake

`

From the CLSM images in figure 51, Caco-2 cellular uptake was clearly observed as the accumulation of the green channel color throughout the designed range of time intervals. It could also be observed that the ELPC emulsion accumulate throughout the cytoplasm and especially higher amount seen in the edges of the cells and cell aggregates. The uptake process was relatively rapid. From the semi-quantification chart demonstrated in figure 52., it can be concluded that it just took 30 minutes for the Caco-2 cells to absorb about 61% of the equilibrium level of THC uptake. From two hours on, the uptake process appeared to be reaching the equilibrium, which was indicated by both the CLSM pictures and the semi-quantification chart.

4. Conclusion

In this research, a electrospun lipid-polymer complex delivery system with GRAS level of high safety was announced for the first time in the bio-degradable electrospinning material research field. Through a series of physical and functional characterizations, the ability for ELPC to deliver active compound THC to our human body was evaluated with satisfying outcomes. CLSM examination of this ELPC found that it had a structure between electrospun fibers and electrosprayed fine particles, which provided a decent formulation stability throughout the electrospinning process without phase separation. The fibers were fabricated evenly whose diameter mostly focused at 300-500nm with an average of 468±146nm. CLSM also captured the self-assembled emulsion formed by ELPC with average droplet size around 675±314nm, which was almost a half larger than the fiber that the emulsion originated from. This phenomenon might indicate that the self-assembled emulsion still contained large amount of aggregated ELPC. Further tuning of the formulation might have a great potential in reducing the mean diameter of the self-assembled emulsion and increase

`

the bioaccessibility of the encapsulated THC. Due to the gel forming property of gelatin, this self-assembled emulsion could further be turned into a solid gel if the temperature was no higher than room temperature and critical gelling concentration was met. This gel was examined by CLSM and was found that the gel matrix was constructed with numerous capsule-like units clustered together. The lipid phase, instead of existing in hollow area inside the clustered gelatin network, they were visualized to be encapsulated right inside each "capsules" with rod shape to reduce its surface energy. FTIR spectrums of the ELPC could not substantiate whether hydrogen bonding was the major interaction between different ELPC components. Fingerprint spectrum of THC was concealed in the ELPC however the hydrocarbon stretch from the incorporated lipids were still found. Detailed interactions and physical status of various components inside ELPC remained to be researched. USP-4 Dissolution profiles substantiated that the ELPC had high performance in delivering THC to the stomach, which was 2.1 to 4.6 folds comparing to THC crystals. A lipolysis assay was carried out to investigate the digestion situations of the ELPC. It was proved that the lipid inside ELPC was digested in a very fast pace. For the fed state digestion, it took just 6.75 minutes to digest 65% of the total lipolyzed lipids. For the fasted state only 3.35 minutes was used to digest 72% total lipolyzed lipids. However, the bioaccessibility of ELPC was relatively low, this result might be related to the insufficient self-emulsifying of the ELPC that formed aggregates with low bioaccessibility. This phenomenon was in accord with the relatively large droplet size of the self-assembled ELPC emulsion. A Caco-2 monolayer membrane transport experiment was applied to finally confirm the intestinal THC delivery from the ELPC. In upward transport direction, ELPC appeared with high transport ability that outperformed the THC DMSO solution. Nevertheless, this advantage was not seen in downward transport situation, which might due to

`

microvilli filtration. Cellular uptake results demonstrated a rapid THC delivery to the Caco-2 cells by ELPC, which indicated the potent delivery efficiency of the ELPC delivery system. The fast absorption of THC into the Caco-2 cells might be an explanation to the decrease in total permeated THC at later stage of Caco-2 monolayer transport.

In a word, ELPC as a novel and high safety complex material has high potential to be a potent delivery system for active compounds, flavors and many others. It could also save a lot of the production energy spend in the emulsion-related industries. Researches to further study and tune the ELPC are attractive to achieve broader and better applications for the ELPC.

`

Appendices

UV	Ultraviolet
ELPC	Electrosprayed Lipid-Polymer Complex
USP	United States Pharmacopoeia
SC	Stratum Corneum
E-spun	Electrospun
ROS	Reactive Oxidative Species
EGCG	Epigallocatechin Gallate
DNA	Deoxyribonucleic Acid
NF-kB	Nuclear Factor-κB
AP-1	Activator Protein 1
DMSO	Dimethyl Sulfoxide
CA	Cellulose Acetate
SEM	Scanning Electron Microscope
XRD	X-Ray Diffraction
FTIR	Fourier Transform Infrared spectroscopy
PBS	Phosphate Buffered Saline
HPLC	High Performance Liquid Chromatography
MCT	Medium Train Triglyceride
PC	Phosphatidylcholine
KV	Kilo-Volts
DLS	Dynamic Light Scattering system
AAPH	2,2′-Azobis (2-amidinopropane) dihydrochloride

`

ORAC	Oxygen Radical Absorbance Capacity
DOPA	3,4-dihydroxyphenylalanine
OD	Optical Density
CD	Circular Dichroism
DAD	Diode Array Detector
CLSM	Confocal Laser Scanning Microscopy
O.C.T compound	Optimal Cutting Temperature Embedding Medium
DAPI	4',6-diamidino-2-phenylindole
ATCC	American Type Culture Collection
DMEM	Dulbecco's Modified Eagle's Medium
MTT	Methyl Thiazol Tetrazolium bromide
VCAM-1	Vascular Cell Adhesion protein 1
GRAS	Generally Recognized As Safe
THC	Tetrahydrocurcumin
NADPH	Nicotinamide adenine dinucleotide phosphate
HBSS	Hank's Balanced Salt Solution
HEPES	4-(2-hydroxyethyl)-1-piperazineethanesulfonic acid
TEER	Transepithelial Electrical Resistance
RPMI	Roswell Park Memorial Institute medium
P_{app}	apparent permeation rates

`

Reference

1. Nasri, H.; Baradaran, A.; Shirzad, H.; Rafieian-Kopaei, M., New Concepts in Nutraceuticals as Alternative for Pharmaceuticals. *International Journal of Preventive Medicine* **2014,** *5* (12), 1487-1499.
2. Auner, B. G.; Wirth, M.; Valenta, C., Antioxidative activity and cytotoxicity of four different flavonoids for dermal applications. *Journal of Drug Delivery Science and Technology* **2005,** *15* (3), 227-232.
3. Georgetti, S. R.; Casagrande, R. b.; Mambro, V. r. M. D.; Azzolini, A. E.; Fonseca, M. J., Evaluation of the antioxidant activity of different flavonoids by the chemiluminescence method. *AAPS PharmSci* **2003,** *5* (2), 111-115.
4. Anunciato, T. P.; Filho, P. A. d. R., Carotenoids and polyphenols in nutricosmetics, nutraceuticals, and cosmeceuticals. *Journal of Cosmetic Dermatology,* **2012,** *11* (1), 51-54.
5. PETO, R.; DOLL, R.; BUCKLEY, J. D.; SPORN, M. B., Can dietary beta-carotene materially reduce human cancer rates? *Nature* **1981,** *290*, 201-208.
6. Hassanpour, H.; Moghaddam, A. Z.; Yazdani, A.; Bashi, M. C., Evaluation of intestinal morphology and nitric oxide metabolites in broiler chickens supplemented by green tea. *Comparative clinical pathology* **2010,** *19* (1), 43-47.
7. Xu, Y.; Ho, C.-T.; Amin, S. G.; Han, C.; Chung, F.-L., Inhibition of tobacco-specific nitrosamine-induced lung tumorigenesis in A/J mice by green tea and its major polyphenol as antioxidants. *Cancer Research* **1992,** *52* (14), 3875-3879.
8. Lin, J.-K.; Chen, P.-C.; Ho, C.-T.; Lin-Shiau, S.-Y., Inhibition of xanthine oxidase and suppression of intracellular reactive oxygen species in HL-60 cells by theaflavin-3, 3'-digallate,(-)-epigallocatechin-3-gallate, and propyl gallate. *Journal of Agricultural and Food Chemistry* **2000,** *48* (7), 2736-2743.
9. Hong, J.; Smith, T. J.; Ho, C.-T.; August, D. A.; Yang, C. S., Effects of purified green and black tea polyphenols on cyclooxygenase-and lipoxygenase-dependent metabolism of arachidonic acid in human colon mucosa and colon tumor tissues. *Biochemical pharmacology* **2001,** *62* (9), 1175-1183.
10. Yang, C. S.; Chung, J. Y.; Yang, G. Y.; Li, C.; Meng, X.; Lee, M. J., Mechanisms of inhibition of carcinogenesis by tea. *Biofactors* **2000,** *13* (1-4), 73-79.
11. Crespy, V.; Williamson, G., A review of the health effects of green tea catechins in in vivo animal models. *The Journal of nutrition* **2004,** *134* (12), 3431S-3440S.
12. Koo, M. W.; Cho, C. H., Pharmacological effects of green tea on the gastrointestinal system. *European journal of pharmacology* **2004,** *500* (1), 177-185.
13. Sueoka, N.; Suganuma, M.; Sueoka, E.; Okabe, S.; Matsuyama, S.; Imai, K.; Nakachi, K.; Fujiki, H., A New Function of Green Tea: Prevention of Lifestyle-related Diseases. *Annals of the New York Academy of Sciences* **2001,** *928* (1), 274-280.
14. Babu, P. V. A.; Sabitha, K. E.; Shyamaladevi, C. S., Therapeutic effect of green tea extract on oxidative stress in aorta and heart of streptozotocin diabetic rats. *Chemico-biological interactions* **2006,** *162* (2), 114-120.
15. Tsuneki, H.; Ishizuka, M.; Terasawa, M.; Wu, J.-B.; Sasaoka, T.; Kimura, I., Effect of green tea on blood glucose levels and serum proteomic patterns in diabetic (db/db) mice and on glucose metabolism in healthy humans. *BMC pharmacology* **2004,** *4* (1), 18.
16. Raederstorff, D. G.; Schlachter, M. F.; Elste, V.; Weber, P., Effect of EGCG on lipid absorption and plasma lipid levels in rats. *The Journal of nutritional biochemistry* **2003,** *14* (6), 326-332.

`

17. Haqqi, T. M.; Anthony, D. D.; Gupta, S.; Ahmad, N.; Lee, M.-S.; Kumar, G. K.; Mukhtar, H., Prevention of collagen-induced arthritis in mice by a polyphenolic fraction from green tea. *Proceedings of the National Academy of Sciences* **1999,** *96* (8), 4524-4529.
18. Roccaro, A. S.; Blanco, A. R.; Giuliano, F.; Rusciano, D.; Enea, V., Epigallocatechin-gallate enhances the activity of tetracycline in staphylococci by inhibiting its efflux from bacterial cells. *Antimicrobial Agents and Chemotherapy* **2004,** *48* (6), 1968-1973.
19. Donà, M.; Dell'Aica, I.; Calabrese, F.; Benelli, R.; Morini, M.; Albini, A.; Garbisa, S., Neutrophil restraint by green tea: inhibition of inflammation, associated angiogenesis, and pulmonary fibrosis. *The Journal of Immunology* **2003,** *170* (8), 4335-4341.
20. Weber, J. M.; Ruzindana-Umunyana, A.; Imbeault, L.; Sircar, S., Inhibition of adenovirus infection and adenain by green tea catechins. *Antiviral research* **2003,** *58* (2), 167-173.
21. Hirasawa, M.; Takada, K., Multiple effects of green tea catechin on the antifungal activity of antimycotics against Candida albicans. *Journal of Antimicrobial Chemotherapy* **2004,** *53* (2), 225-229.
22. Weinreb, O.; Mandel, S.; Amit, T.; Youdim, M. B., Neurological mechanisms of green tea polyphenols in Alzheimer's and Parkinson's diseases. *The Journal of nutritional biochemistry* **2004,** *15* (9), 506-516.
23. Unno, K.; Takabayashi, F.; Yoshida, H.; Choba, D.; Fukutomi, R.; Kikunaga, N.; Kishido, T.; Oku, N.; Hoshino, M., Daily consumption of green tea catechin delays memory regression in aged mice. *Biogerontology* **2007,** *8* (2), 89-95.
24. K.Katiyar, S.; Afaq, F.; Perez, A.; Mukhtar, H., Green tea polyphenol (–)-epigallocatechin-3-gallate treatment of human skin inhibits ultraviolet radiation-induced oxidative stress. *Carcinogenesis* **2001,** *22* (2), 287-294.
25. Kim, J.; Hwang, J. S.; Cho, Y. K.; Han, Y.; Jeon, Y. J.; Yang, K. H., Protective effects of (-)-epigallocatechin-3-gallate on UVA- and UVB-induced skin damage. *Skin Pharmacol Appl Skin Physiol* **2001,** *14* (1), 11-9.
26. Wach, A.; Pyrzyńska, K.; Biesaga, M., Quercetin content in some food and herbal samples. *Food Chemistry* **2007,** *100* (2), 699-704.
27. Rice-Evans, C. A.; Miller, N. J.; Paganga, G., Structure-antioxidant activity relationships of flavonoids and phenolic acids. *Free radical biology and medicine* **1996,** *20* (7), 933-956.
28. Morel, I.; Lescoat, G.; Cogrel, P.; Sergent, O.; Pasdeloup, N.; Brissot, P.; Cillard, P.; Cillard, J., Antioxidant and iron-chelating activities of the flavonoids catechin, quercetin and diosmetin on iron-loaded rat hepatocyte cultures. *Biochemical pharmacology* **1993,** *45* (1), 13-19.
29. Hertog, M. G.; Feskens, E. J.; Kromhout, D.; Hollman, P.; Katan, M., Dietary antioxidant flavonoids and risk of coronary heart disease: the Zutphen Elderly Study. *The Lancet* **1993,** *342* (8878), 1007-1011.
30. Kaul, T. N.; Middleton, E.; Ogra, P. L., Antiviral effect of flavonoids on human viruses. *Journal of medical virology* **1985,** *15* (1), 71-79.
31. Lamson, D. W.; Brignall, M. S., Antioxidants and cancer, part 3: quercetin. *Alternative medicine review: a journal of clinical therapeutic* **2000,** *5* (3), 196-208.
32. Landolfi, R.; Mower, R. L.; Steiner, M., Modification of platelet function and arachidonic acid metabolism by bioflavonoids: structure-activity relations. *Biochemical pharmacology* **1984,** *33* (9), 1525-1530.

`

33. Comalada, M.; Camuesco, D.; Sierra, S.; Ballester, I.; Xaus, J.; Gálvez, J.; Zarzuelo, A., In vivo quercitrin anti-inflammatory effect involves release of quercetin, which inhibits inflammation through down-regulation of the NF-κB pathway. *European journal of immunology* **2005,** *35* (2), 584-592.
34. Guardia, T.; Rotelli, A. E.; Juarez, A. O.; Pelzer, L. E., Anti-inflammatory properties of plant flavonoids. Effects of rutin, quercetin and hesperidin on adjuvant arthritis in rat. *Il farmaco* **2001,** *56* (9), 683-687.
35. Vicentini, F. T.; He, T.; Shao, Y.; Fonseca, M. J.; Verri, W. A.; Fisher, G. J.; Xu, Y., Quercetin inhibits UV irradiation-induced inflammatory cytokine production in primary human keratinocytes by suppressing NF-κB pathway. *Journal of dermatological science* **2011,** *61* (3), 162-168.
36. Bonina, F.; Lanza, M.; Montenegro, L.; Puglisi, C.; Tomaino, A.; Trombetta, D.; Castelli, F.; Saija, A., Flavonoids as potential protective agents against photo-oxidative skin damage. *International Journal of Pharmaceutics* **1996,** *145* (1), 87-94.
37. Casagrande, R.; Georgetti, S. R.; Verri, W. A.; Dorta, D. J.; dos Santos, A. C.; Fonseca, M. J., Protective effect of topical formulations containing quercetin against UVB-induced oxidative stress in hairless mice. *Journal of Photochemistry and Photobiology B: Biology* **2006,** *84* (1), 21-27.
38. Montenegro, L.; Carbone, C.; Maniscalco, C.; Lambusta, D.; Nicolosi, G.; Ventura, C. A.; Puglisi, G., In vitro evaluation of quercetin-3-O-acyl esters as topical prodrugs. *Int J Pharm* **2007,** *336* (2), 257-62.
39. Rothwell, J. A.; Day, A. J.; Morgan, M. R., Experimental determination of octanol-water partition coefficients of quercetin and related flavonoids. *Journal of agricultural and food chemistry* **2005,** *53* (11), 4355-4360.
40. Kitagawa, S.; Tanaka, Y.; Tanaka, M.; Endo, K.; Yoshii, A., Enhanced skin delivery of quercetin by microemulsion. *Journal of Pharmacy and Pharmacology* **2009,** *61* (7), 855-860.
41. Saija, A.; Tomaino, A.; Trombetta, D.; Giacchi, M.; De Pasquale, A.; Bonina, F., Influence of different penetration enhancers on in vitro skin permeation and in vivo photoprotective effect of flavonoids. *International Journal of Pharmaceutics* **1998,** *175* (1), 85-94.
42. Montagna, W., *The Structure and Function of Skin 3E*. Elsevier: 2012.
43. Torin Huzil, J.; Sivaloganathan, S.; Kohandel, M.; Foldvari, M., Drug delivery through the skin: molecular simulations of barrier lipids to design more effective noninvasive dermal and transdermal delivery systems for small molecules, biologics, and cosmetics. *Wiley Interdisciplinary Reviews: Nanomedicine and Nanobiotechnology* **2011,** *3* (5), 449-462.
44. Tojo, K., Random brick model for drug transport across stratum corneum. *Journal of pharmaceutical sciences* **1987,** *76* (12), 889-891.
45. Förster, M.; Bolzinger, M.-A.; Fessi, H.; Briançon, S., Topical delivery of cosmetics and drugs. Molecular aspects of percutaneous absorption and delivery. *European Journal of Dermatology* **2009,** *19* (4), 309-323.
46. Nakpiban, C. Skin Structure and Function. http://cosbiology.pbworks.com/w/page/11556260/LESSON%206-01%20–%20Skin%20Structure%20and%20Function.
47. Prausnitz, M. R.; Elias, P. M.; Franz, T. J.; Schmuth, M.; Tsai, J.-C.; Menon, G. K.; Holleran, W. M.; Feingold, K. R., Skin barrier and transdermal drug delivery. *Dermatology* **2012**, 2065-2073.

`

48. de Gruijl, F. R., Photocarcinogenesis: UVA vs. UVB radiation. *Skin Pharmacology and Physiology* **2002,** *15* (5), 316-320.
49. Scharffetter–Kochanek, K.; Brenneisen, P.; Wenk, J.; Herrmann, G.; Ma, W.; Kuhr, L.; Meewes, C.; Wlaschek, M., Photoaging of the skin from phenotype to mechanisms. *Experimental Gerontology* **2000,** *35* (3), 307-316.
50. Sander, C. S.; Chang, H.; Salzmann, S.; Müller, C. S.; Ekanayake-Mudiyanselage, S.; Elsner, P.; Thiele, J. J., Photoaging is associated with protein oxidation in human skin in vivo. *Journal of Investigative Dermatology* **2002,** *118* (4), 618-625.
51. Berneburg, M.; Plettenberg, H.; Krutmann, J., Photoaging of human skin. *Photodermatology, photoimmunology & photomedicine* **2000,** *16* (6), 239-244.
52. Speiser, P. P., Nanoparticles and liposomes: a state of the art. *Methods and findings in experimental and clinical pharmacology* **1991,** *13* (5), 337-342.
53. Baroli, B., Penetration of nanoparticles and nanomaterials in the skin: fiction or reality? *Journal of pharmaceutical sciences* **2010,** *99* (1), 21-50.
54. Montenegro, L.; Lai, F.; Offerta, A.; Sarpietro, M. G.; Micicchè, L.; Maccioni, A. M.; Valenti, D.; Fadda, A. M., From nanoemulsions to nanostructured lipid carriers: A relevant development in dermal delivery of drugs and cosmetics. *Journal of Drug Delivery Science and Technology* **2015**.
55. Baji, A.; Mai, Y.-W.; Wong, S.-C.; Abtahi, M.; Chen, P., Electrospinning of polymer nanofibers: effects on oriented morphology, structures and tensile properties. *Composites science and technology* **2010,** *70* (5), 703-718.
56. Han, S. O.; Youk, J. H.; Min, K. D.; Kang, Y. O.; Park, W. H., Electrospinning of cellulose acetate nanofibers using a mixed solvent of acetic acid/water: Effects of solvent composition on the fiber diameter. *Materials Letters* **2008,** *62* (4), 759-762.
57. Li, C.; Wang, Z.-H.; Yu, D.-G., Higher quality quercetin sustained release ethyl cellulose nanofibers fabricated using a spinneret with a Teflon nozzle. *Colloids and Surfaces B: Biointerfaces* **2014,** *114*, 404-409.
58. Brewer, M. S., Natural Antioxidants: Sources, Compounds, Mechanisms of Action, and Potential Applications. *Compr Rev Food Sci F* **2011,** *10* (4), 221-247.
59. Birtic, S.; Dussort, P.; Pierre, F. X.; Bily, A. C.; Roller, M., Carnosic acid. *Phytochemistry* **2015,** *115*, 9-19.
60. Hidalgo, P. J.; Ubera, J. L.; Tena, M. T.; Valcarcel, M., Determination of the carnosic acid content in wild and cultivated Rosmarinus officinalis. *Journal of Agricultural and Food Chemistry* **1998,** *46* (7), 2624-2627.
61. del Bano, M. J.; Lorente, J.; Castillo, J.; Benavente-Garcia, O.; del Rio, J. A.; Ortuno, A.; Quirin, K. W.; Gerard, D., Phenolic diterpenes, flavones, and rosmarinic acid distribution during the development of leaves, flowers, stems, and roots of Rosmarinus officinalis. Antioxidant activity. *Journal of Agricultural and Food Chemistry* **2003,** *51* (15), 4247-4253.
62. Hawthorne, S. B.; Krieger, M. S.; Miller, D. J., Analysis of Flavor and Fragrance Compounds Using Supercritical Fluid Extraction Coupled with Gas-Chromatography. *Anal Chem* **1988,** *60* (5), 472-477.
63. Rao, L. J.; Singh, M.; Raghavan, B.; Abraham, K. O., Rosemary (Rosmarinus officinalis L.): Impact of drying on its flavor quality. *J Food Quality* **1998,** *21* (2), 107-115.
64. Zhang, Y.; Yang, L.; Zu, Y. G.; Chen, X. Q.; Wang, F. J.; Liu, F., Oxidative stability of sunflower oil supplemented with carnosic acid compared with synthetic antioxidants during accelerated storage. *Food Chemistry* **2010,** *118* (3), 656-662.

`

65. Wang, H.; Liu, F.; Yang, L.; Zu, Y. G.; Wang, H.; Qu, S. Z.; Zhang, Y., Oxidative stability of fish oil supplemented with carnosic acid compared with synthetic antioxidants during long-term storage. *Food Chemistry* **2011,** *128* (1), 93-99.
66. Moran, L.; Giraldez, F. J.; Panseri, S.; Aldai, N.; Jordan, M. J.; Chiesa, L. M.; Andres, S., Effect of dietary carnosic acid on the fatty acid profile and flavour stability of meat from fattening lambs. *Food Chemistry* **2013,** *138* (4), 2407-2414.
67. Frutos, M. J.; Hernandez-Herrero, J. A., Effects of rosemary extract (Rosmarinus officinalis) on the stability of bread with an oil, garlic and parsley dressing. *Lwt-Food Science and Technology* **2005,** *38* (6), 651-655.
68. Inatani, R.; Nakatani, N.; Fuwa, H., Antioxidative effect of the constituents of rosemary (Rosmarinus officinalis L.) and their derivatives. *Agricultural and biological chemistry* **1983,** *47* (3), 521-528.
69. Zhao, Y. T.; Sedighi, R.; Wang, P.; Chen, H. D.; Zhu, Y. D.; Sang, S. M., Carnosic Acid as a Major Bioactive Component in Rosemary Extract Ameliorates High-Fat-Diet-Induced Obesity and Metabolic Syndrome in Mice. *Journal of Agricultural and Food Chemistry* **2015,** *63* (19), 4843-4852.
70. Park, M. Y.; Mun, S. T., Dietary carnosic acid suppresses hepatic steatosis formation via regulation of hepatic fatty acid metabolism in high-fat diet-fed mice. *Nutr Res Pract* **2013,** *7* (4), 294-301.
71. Ibarra, A.; Cases, J.; Roller, M.; Chiralt-Boix, A.; Coussaert, A.; Ripoll, C., Carnosic acid-rich rosemary (Rosmarinus officinalis L.) leaf extract limits weight gain and improves cholesterol levels and glycaemia in mice on a high-fat diet. *Brit J Nutr* **2011,** *106* (8), 1182-1189.
72. Ninomiya, K.; Matsuda, H.; Shimoda, H.; Norihisa, N.; Kasajima, N.; Yoshino, T.; Morikawa, T.; Yoshikawa, M., Carnosic acid, a new class of lipid absorption inhibitor from sage. *Bioorg Med Chem Lett* **2004,** *14* (8), 1943-1946.
73. Harach, T.; Aprikian, O.; Monnard, I.; Moulin, J.; Membrez, M.; Beolor, J. C.; Raab, T.; Mace, K.; Darimont, C., Rosemary (Rosmarinus officinalis L.) Leaf Extract Limits Weight Gain and Liver Steatosis in Mice Fed a High-Fat Diet. *Planta Med* **2010,** *76* (6), 566-571.
74. Barni, M. V.; Carlini, M. J.; Cafferata, E. G.; Puricelli, L.; Moreno, S., Carnosic acid inhibits the proliferation and migration capacity of human colorectal cancer cells. *Oncol Rep* **2012,** *27* (4), 1041-8.
75. Steiner, M.; Priel, I.; Giat, J.; Levy, J.; Sharoni, Y.; Danilenko, M., Carnosic acid inhibits proliferation and augments differentiation of human leukemic cells induced by 1,25-dihydroxyvitamin D3 and retinoic acid. *Nutr Cancer* **2001,** *41* (1-2), 135-44.
76. Einbond, L. S.; Wu, H. A.; Kashiwazaki, R.; He, K.; Roller, M.; Su, T.; Wang, X.; Goldsberry, S., Carnosic acid inhibits the growth of ER-negative human breast cancer cells and synergizes with curcumin. *Fitoterapia* **2012,** *83* (7), 1160-8.
77. Gao, Q.; Liu, H.; Yao, Y.; Geng, L.; Zhang, X.; Jiang, L.; Shi, B.; Yang, F., Carnosic acid induces autophagic cell death through inhibition of the Akt/mTOR pathway in human hepatoma cells. *J Appl Toxicol* **2015,** *35* (5), 485-492.
78. Kocak, C.; Kocak, F. E.; Akcilar, R.; Isiklar, O. O.; Kocak, H.; Bayat, Z.; Simsek, H.; Taser, F.; Altuntas, I., Molecular and biochemical evidence on the protective effects of embelin and carnosic acid in isoproterenol-induced acute myocardial injury in rats. *Life Sci* **2016,** *147*, 15-23.
79. Satoh, T.; Kosaka, K.; Itoh, K.; Kobayashi, A.; Yamamoto, M.; Shimojo, Y.; Kitajima, C.; Cui, J.; Kamins, J.; Okamoto, S. i., Carnosic acid, a catechol-type electrophilic compound, protects neurons both in vitro and in vivo through activation

`

of the Keap1/Nrf2 pathway via S-alkylation of targeted cysteines on Keap1. *J Neurochem* **2008,** *104* (4), 1116-1131.
80. Azad, N.; Rasoolijazi, H.; Joghataie, M. T.; Soleimani, S., Neuroprotective effects of carnosic Acid in an experimental model of Alzheimer's disease in rats. *Cell J* **2011,** *13* (1), 39-44.
81. Poeckel, D.; Greiner, C.; Verhoff, M.; Rau, O.; Tausch, L.; Hörnig, C.; Steinhilber, D.; Schubert-Zsilavecz, M.; Werz, O., Carnosic acid and carnosol potently inhibit human 5-lipoxygenase and suppress pro-inflammatory responses of stimulated human polymorphonuclear leukocytes. *Biochemical pharmacology* **2008,** *76* (1), 91-97.
82. Schindelin, J.; Arganda-Carreras, I.; Frise, E.; Kaynig, V.; Longair, M.; Pietzsch, T.; Preibisch, S.; Rueden, C.; Saalfeld, S.; Schmid, B., Fiji: an open-source platform for biological-image analysis. *Nature methods* **2012,** *9* (7), 676-682.
83. Ou, B.; Hampsch-Woodill, M.; Prior, R. L., Development and validation of an improved oxygen radical absorbance capacity assay using fluorescein as the fluorescent probe. *Journal of agricultural and food chemistry* **2001,** *49* (10), 4619-4626.
84. XU Jie-kun, Y. X.-s., Hiroshi Kurihara, Oxygen radical absorbance capacity assay and its application. *Chinese Pharmacological Bulletin* **2006,** *22* (8), 1015~21.
85. Liu, S.-H.; Pan, I.-H.; Chu, I.-M., Inhibitory effect of p-hydroxybenzyl alcohol on tyrosinase activity and melanogenesis. *Biological and Pharmaceutical Bulletin* **2007,** *30* (6), 1135-1139.
86. Yusoff, A.; Murray, B. S., Modified starch granules as particle-stabilizers of oil-in-water emulsions. *Food Hydrocolloids* **2011,** *25* (1), 42-55.
87. Chan, Y. Y.; Kim, K. H.; Cheah, S. H., Inhibitory effects of Sargassum polycystum on tyrosinase activity and melanin formation in B16F10 murine melanoma cells. *J Ethnopharmacol* **2011,** *137* (3), 1183-8.
88. Berridge, M. V.; Herst, P. M.; Tan, A. S., Tetrazolium dyes as tools in cell biology: new insights into their cellular reduction. *Biotechnology annual review* **2005,** *11*, 127-152.
89. Mosmann, T., Rapid colorimetric assay for cellular growth and survival: application to proliferation and cytotoxicity assays. *J Immunol Methods* **1983,** *65* (1-2), 55-63.
90. Li, C.; Wang, Z. H.; Yu, D. G., Higher quality quercetin sustained release ethyl cellulose nanofibers fabricated using a spinneret with a Teflon nozzle. *Colloids and surfaces. B, Biointerfaces* **2014,** *114*, 404-9.
91. Li, X. Y.; Li, Y. C.; Yu, D. G.; Liao, Y. Z.; Wang, X., Fast disintegrating quercetin-loaded drug delivery systems fabricated using coaxial electrospinning. *International journal of molecular sciences* **2013,** *14* (11), 21647-59.
92. Arshad, M.; Saied, S.; Ullah, A., PEG-lipid telechelics incorporating fatty acids from canola oil: synthesis, characterization and solution self-assembly. *Rsc Adv* **2014,** *4* (50), 26439-26446.
93. Rashtbari, S.; Dehghan, G.; Yekta, R.; Jouyban, A.; Iranshahi, M., Effects of Resveratrol on the Structure and Catalytic Function of Bovine Liver catalase (BLC): Spectroscopic and Theoretical Studies. *Adv Pharm Bull* **2017,** *7* (3), 349-357.
94. Whitmore, L.; Wallace, B. A., DICHROWEB, an online server for protein secondary structure analyses from circular dichroism spectroscopic data. *Nucleic Acids Res* **2004,** *32* (Web Server issue), W668-73.
95. Whitmore, L.; Wallace, B. A., Protein secondary structure analyses from circular dichroism spectroscopy: methods and reference databases. *Biopolymers* **2008,** *89* (5), 392-400.

`

96. Sreerama, N.; Woody, R. W., Estimation of protein secondary structure from circular dichroism spectra: Comparison of CONTIN, SELCON, and CDSSTR methods with an expanded reference set. *Anal Biochem* **2000,** *287* (2), 252-260.
97. Higuchi, T., Rate of release of medicaments from ointment bases containing drugs in suspension. *J Pharm Sci* **1961,** *50*, 874-5.
98. Siepmann, J.; Peppas, N. A., Higuchi equation: Derivation, applications, use and misuse. *International Journal of Pharmaceutics* **2011,** *418* (1), 6-12.
99. Park, S. Y.; Song, H.; Sung, M. K.; Kang, Y. H.; Lee, K. W.; Park, J. H., Carnosic acid inhibits the epithelial-mesenchymal transition in B16F10 melanoma cells: a possible mechanism for the inhibition of cell migration. *International journal of molecular sciences* **2014,** *15* (7), 12698-713.
100. Park, S. Y.; Song, H.; Sung, M.-K.; Kang, Y.-H.; Lee, K. W.; Park, J. H. Y., Carnosic acid inhibits the epithelial-mesenchymal transition in B16F10 melanoma cells: A possible mechanism for the inhibition of cell migration. *International journal of molecular sciences* **2014,** *15* (7), 12698-12713.
101. Heath, D. D.; Pruitt, M. A.; Brenner, D. E.; Begum, A. N.; Frautschy, S. A.; Rock, C. L., Tetrahydrocurcumin in plasma and urine: Quantitation by high performance liquid chromatography. *J Chromatogr B* **2005,** *824* (1-2), 206-212.
102. Ireson, C. R.; Jones, D. J.; Orr, S.; Coughtrie, M. W.; Boocock, D. J.; Williams, M. L.; Farmer, P. B.; Steward, W. P.; Gescher, A. J., Metabolism of the cancer chemopreventive agent curcumin in human and rat intestine. *Cancer Epidemiol Biomarkers Prev* **2002,** *11* (1), 105-11.
103. Osawa, T.; Sugiyama, Y.; Inayoshi, M.; Kawakishi, S., Antioxidative activity of tetrahydrocurcuminoids. *Biosci Biotechnol Biochem* **1995,** *59* (9), 1609-12.
104. Pari, L.; Amali, D. R., Protective role of tetrahydrocurcumin (THC) an active principle of turmeric on chloroquine induced hepatotoxicity in rats. *J Pharm Pharm Sci* **2005,** *8* (1), 115-123.
105. Yoysungnoen, B.; Bhattarakosol, P.; Changtam, C.; Patumraj, S., Effects of Tetrahydrocurcumin on Tumor Growth and Cellular Signaling in Cervical Cancer Xenografts in Nude Mice. *Biomed Res Int* **2016**.
106. Pari, L.; Murugan, P., Effect of tetrahydrocurcumin on blood glucose, plasma insulin and hepatic key enzymes in streptozotocin induced diabetic rats. *J Basic Clin Physiol Pharmacol* **2005,** *16* (4), 257-74.
107. Park, S.; Lee, L. R.; Seo, J. H.; Kang, S., Curcumin and tetrahydrocurcumin both prevent osteoarthritis symptoms and decrease the expressions of pro-inflammatory cytokines in estrogen-deficient rats. *Genes Nutr* **2016,** *11*.
108. Sandur, S. K.; Pandey, M. K.; Sung, B.; Ahn, K. S.; Murakami, A.; Sethi, G.; Limtrakul, P.; Badmaev, V.; Aggarwal, B. B., Curcumin, demethoxycurcumin, bisdemethoxycurcumin, tetrahydrocurcumin and turmerones differentially regulate anti-inflammatory and anti-proliferative responses through a ROS-independent mechanism. *Carcinogenesis* **2007,** *28* (8), 1765-1773.
109. Wang, Y. J.; Pan, M. H.; Cheng, A. L.; Lin, L. I.; Ho, Y. S.; Hsieh, C. Y.; Lin, J. K., Stability of curcumin in buffer solutions and characterization of its degradation products. *J Pharm Biomed Anal* **1997,** *15* (12), 1867-76.
110. Sneharani, A. H.; Singh, S. A.; Srinivas, P.; Rao, A. G. A., Inhibition of lipoxygenase-1 by tetrahydrocurcumin. *Eur Food Res Technol* **2011,** *233* (4), 561-568.
111. Mannina, P.; Segale, L.; Giovannelli, L.; Bonda, A. F.; Pattarino, F., Self-emulsifying excipient platform for improving technological properties of alginate-hydroxypropylcellulose pellets. *International Journal of Pharmaceutics* **2016,** *499* (1-2), 74-80.

`

112. Fernandez-Garcia, E.; Carvajal-Lerida, I.; Perez-Galvez, A., In vitro bioaccessibility assessment as a prediction tool of nutritional efficiency. *Nutr Res* **2009,** *29* (11), 751-760.
113. Carbonell-Capella, J. M.; Buniowska, M.; Barba, F. J.; Esteve, M. J.; Frigola, A., Analytical Methods for Determining Bioavailability and Bioaccessibility of Bioactive Compounds from Fruits and Vegetables: A Review. *Compr Rev Food Sci F* **2014,** *13* (2), 155-171.
114. Yu, H. L.; Shi, K.; Liu, D.; Huang, Q. R., Development of a food-grade organogel with high bioaccessibility and loading of curcuminoids. *Food Chemistry* **2012,** *131* (1), 48-54.
115. Yu, H.; Huang, Q., Investigation of the cytotoxicity of food-grade nanoemulsions in Caco-2 cell monolayers and HepG2 cells. *Food Chem* **2013,** *141* (1), 29-33.
116. Yu, H.; Huang, Q., Improving the oral bioavailability of curcumin using novel organogel-based nanoemulsions. *Journal of agricultural and food chemistry* **2012,** *60* (21), 5373-5379.
117. Gouda, R.; Baishya, H.; Qing, Z., Application of Mathematical Models in Drug Release Kinetics of Carbidopa and Levodopa ER Tablets. *J Develop Drugs* **2017,** *6* (171), 2.
118. Thakkar, V. T.; Shah, P. A.; Soni, T. G.; Parmar, M. Y.; Gohel, M. C.; Gandhi, T. R., Goodness-of-Fit Model-Dependent Approach for Release Kinetics of Levofloxacin Hemihydrates Floating Tablet. *Dissolut Technol* **2009,** *16* (1), 35-39.
119. Costa, P.; Lobo, J. M. S., Modeling and comparison of dissolution profiles. *European journal of pharmaceutical sciences* **2001,** *13* (2), 123-133.
120. Ting, Y.; Li, C. C.; Pan, M. H.; Ho, C. T.; Huang, Q., Effect of a labile methyl donor on the transformation of 5-demethyltangeretin and the related implication on bioactivity. *J Agric Food Chem* **2013,** *61* (34), 8090-7.

`